

Soil respiration phenology improves modeled phase of terrestrial net ecosystem exchange in northern hemisphere

K. Arthur Endsley¹, John Kimball², and Rolf H Reichle³

¹Numerical Terradynamic Simulation Group (NTSG), WA Franke College of Forestry and Conservation, University of Montana

²University of Montana

³NASA Goddard Space Flight Center

November 23, 2022

Abstract

In the northern hemisphere, terrestrial ecosystems transition from net sources of CO₂ to the atmosphere in winter to net ecosystem carbon sinks during spring. The timing (or phase) of this transition, determined by the balance between ecosystem respiration (RECO) and primary production, is key to estimating the amplitude of the terrestrial carbon sink. We diagnose an apparent phase bias in the RECO and net ecosystem exchange (NEE) seasonal cycles estimated by the Terrestrial Carbon Flux (TCF) model framework and investigate its link to soil respiration mechanisms. Satellite observations of vegetation canopy conditions, surface meteorology, and soil moisture from the NASA SMAP Level 4 Soil Moisture product are used to model a daily carbon budget for a global network of eddy covariance flux towers. Proposed modifications to TCF include: the inhibition of foliar respiration in the light (the Kok effect); a seasonally varying litterfall phenology; an O₂ diffusion limitation on heterotrophic respiration (RH); and a vertically resolved soil decomposition model. We find that RECO phase bias can result from bias in RECO magnitude and that mechanisms which reduce northern spring RECO, like substrate and O₂ diffusion limitations, can mitigate the phase bias. A vertically resolved soil decomposition model mitigates this bias by temporally segmenting and lagging RH throughout the growing season. Applying these model enhancements at Continuous Soil Respiration (COSORE) sites verifies their improvement of RECO and NEE skill compared to in situ observations (up to $\Delta \text{RMSE} = -0.76 \text{ g C m}^{-2} \text{ d}^{-1}$). Ultimately, these mechanisms can improve prior estimates of NEE for atmospheric inversion studies.

1 **Soil respiration phenology improves modeled phase of**
2 **terrestrial net ecosystem exchange in northern**
3 **hemisphere**

4 **K. Arthur Endsley¹, John S. Kimball¹, Rolf H. Reichle²**

5 ¹Numerical Terradynamic Simulation Group (NTSG), W.A. Franke College of Forestry and Conservation,
6 University of Montana, Missoula, MT

7 ²Global Modeling and Assimilation Office, NASA Goddard Space Flight Center, Greenbelt, Maryland,
8 USA

9 **Key Points:**

- 10 • A bias in the seasonal cycle of net ecosystem exchange at high northern latitudes
11 is identified in a first-order soil decomposition model
12 • Soil respiration processes that reduce or delay respiration during spring mitigate
13 this phase bias and improve modeling skill
14 • In situ chamber measurements of soil respiration provide validation and verifica-
15 tion of model enhancements

Abstract

In the northern hemisphere, terrestrial ecosystems transition from net sources of CO₂ to the atmosphere in winter to net ecosystem carbon sinks during spring. The timing (or phase) of this transition, determined by the balance between ecosystem respiration (RECO) and primary production, is key to estimating the amplitude of the terrestrial carbon sink. We diagnose an apparent phase bias in the RECO and net ecosystem exchange (NEE) seasonal cycles estimated by the Terrestrial Carbon Flux (TCF) model framework and investigate its link to soil respiration mechanisms. Satellite observations of vegetation canopy conditions, surface meteorology, and soil moisture from the NASA SMAP Level 4 Soil Moisture product are used to model a daily carbon budget for a global network of eddy covariance flux towers. Proposed modifications to TCF include: the inhibition of foliar respiration in the light (the Kok effect); a seasonally varying litterfall phenology; an O₂ diffusion limitation on heterotrophic respiration (RH); and a vertically resolved soil decomposition model. We find that RECO phase bias can result from bias in RECO magnitude and that mechanisms which reduce northern spring RECO, like substrate and O₂ diffusion limitations, can mitigate the phase bias. A vertically resolved soil decomposition model mitigates this bias by temporally segmenting and lagging RH throughout the growing season. Applying these model enhancements at Continuous Soil Respiration (COSORE) sites verifies their improvement of RECO and NEE skill compared to in situ observations (up to $\Delta\text{RMSE} = -0.76 \text{ g C m}^{-2} \text{ d}^{-1}$). Ultimately, these mechanisms can improve prior estimates of NEE for atmospheric inversion studies.

Plain Language Summary

In the northern hemisphere, the plants and the soil respond to warming temperatures and increasing day lengths in spring and begin to store more carbon than they release to the atmosphere, on average. The timing of this change is very important for accurately modeling how much carbon is stored or released to the atmosphere. We found that a commonly used model of plants and soil has delayed predictions of the timing of this seasonal cycle of carbon. We studied different potential changes to the model, including changes to: how carbon inputs to the soil from plant roots, dead leaves, and down wood are added over time; how soil microbes respond to high levels of soil moisture; whether the soil is represented by a single layer or by multiple layers at different depths; and how the release of carbon by plants varies with solar radiation. We found that multiple different changes resulted in similar corrections to the seasonal cycle of carbon so long as they reduced or delayed the amount of carbon released during the spring season. We discuss why that is and how it impacts the model's performance and its importance for other modeling studies.

1 Introduction

In northern hemisphere temperate, boreal, and tundra regions, the spring season is marked by an increase in temperature and day length, stimulating vegetation photosynthesis and growth. A result of this increased primary production is that northern ecosystems transition from net sources of CO₂ to the atmosphere during the winter to net ecosystem carbon sinks during spring. The timing of this transition is determined by the balance between ecosystem respiration (RECO) and primary production (Chapin et al., 2006; Noormets et al., 2009). The northern land sink dominates the global, terrestrial carbon sink and its seasonal amplitude has been increasing for decades (Graven et al., 2013; Forkel et al., 2016; Ciais et al., 2019).

At high northern latitudes ($\geq 40N$) where there is strong seasonal variation in conditions that support soil decomposition and plant growth, the timing of soil respiration phenology is key to accurately estimating the amplitude of the terrestrial carbon sink (Zhao & Zeng, 2014; Migliavacca et al., 2015; Parazoo et al., 2018). Changes in the on-

66 set of the growing season, such as an earlier start of spring or delayed start of autumn,
 67 may lead to a longer carbon uptake period (Wu et al., 2013; Keenan et al., 2014) pro-
 68 vided that concurrent increases in RECO are smaller (Richardson et al., 2010); i.e., that
 69 the carbon flux to plants and the soil is larger than the respired CO₂ flux to the atmo-
 70 sphere. Thus, the northern hemisphere (NH) seasonal cycle of carbon uptake is an emer-
 71 gent property (Birch et al., 2021) that depends upon the timing and relative magnitudes
 72 of multiple component ecosystem sources and sinks. Shifts in the modeled seasonal car-
 73 bon uptake period, relative to atmospheric inversion data or multi-model means, can be
 74 substantial and generally point to significant model biases (Forkel et al., 2014; Ito et al.,
 75 2016; Zhao et al., 2016).

76 Models are, necessarily, simplified representations of complex ecosystem processes
 77 and direct observation of some CO₂ fluxes is infeasible at large scales (Bond-Lamberty
 78 et al., 2016). However, satellite observations of vegetation provide a strong constraint
 79 on canopy phenology and on net (NPP) and gross primary productivity (GPP). In north-
 80 ern ecosystems, they are also a strong constraint on net ecosystem CO₂ exchange (NEE)
 81 due to the tight link between plant productivity and the seasonal increase in CO₂ up-
 82 take (Järveoja et al., 2018). Models without direct observations of canopy conditions tend
 83 to have biases in simulated GPP that propagate to other modeled fluxes (e.g., Thum et
 84 al., 2020). The ability to directly observe canopy changes has previously been used to
 85 diagnose model biases in northern ecosystem GPP (Peng et al., 2015; Shi et al., 2020;
 86 Birch et al., 2021).

87 Here, we diagnose an apparent bias in the NH seasonal cycle of RECO in the Ter-
 88 restrial Carbon Flux (TCF) model framework (Kimball et al., 2009), which combines a
 89 satellite data-driven light-use efficiency (LUE) model with a first-order soil decomposi-
 90 tion model to estimate a daily carbon budget. The TCF framework has been used to in-
 91 fer climate impacts on northern ecosystems’ productivity and soil carbon (Yi et al., 2013;
 92 Watts et al., 2014) and is part of the NASA Soil Moisture Active Passive (SMAP) mis-
 93 sion Level 4 Carbon (L4C) operational product (Entekhabi et al., 2010; Jones et al., 2017;
 94 Endsley et al., 2020). A bias in the timing of the RECO seasonal cycle or its components,
 95 heterotrophic respiration (R_H) and autotrophic respiration (R_A), can result in a bias in
 96 the seasonal cycle of NEE (Noormets et al., 2009; Alexandrov, 2014) and limits the use
 97 of data-driven terrestrial carbon flux estimates as priors in atmospheric inversion stud-
 98 ies (Byrne et al., 2018). Identifying and mitigating such biases can generate insight into
 99 the biotic and abiotic factors that influence CO₂ exchange between the land and atmo-
 100 sphere, informing future model developments. Whereas previous studies of potential bi-
 101 ases in carbon flux estimates have tended to focus on GPP (e.g., Zhao & Zeng, 2014; Migli-
 102 avacca et al., 2015; Parazoo et al., 2018), here, we examine the role of model processes
 103 for estimating RECO.

104 Compared to eddy covariance (EC) flux tower and atmospheric inversion datasets,
 105 the timing of the seasonal change in NEE as modeled by TCF is delayed (Figure 1), likely
 106 as a result of an advanced RECO cycle. The temporal advance in the modeled RECO
 107 seasonal cycle suggests that canopy respiration or soil respiration are high-biased early
 108 in the growing season (NH spring). We also note that the NH summer NEE amplitude
 109 is under-estimated in TCF. This bias is common among terrestrial biosphere models (Peng
 110 et al., 2014). A similar NEE phase difference can be seen between the Carnegie-Ames
 111 Stanford Approach (CASA) and Simple Biosphere 3 (SiB3) models (Byrne et al., 2018).
 112 Our study aims to diagnose this issue and answer the broader questions:

- 113 1. Does a seasonally varying adjustment of RECO or its components, R_H and R_A ,
 114 improve the fit in modeled NEE phase compared to observed NH ecosystem CO₂
 115 fluxes from a global network of EC flux towers? This adjustment might take the
 116 form of either an explicit phenology model or a seasonally varying climatic response.

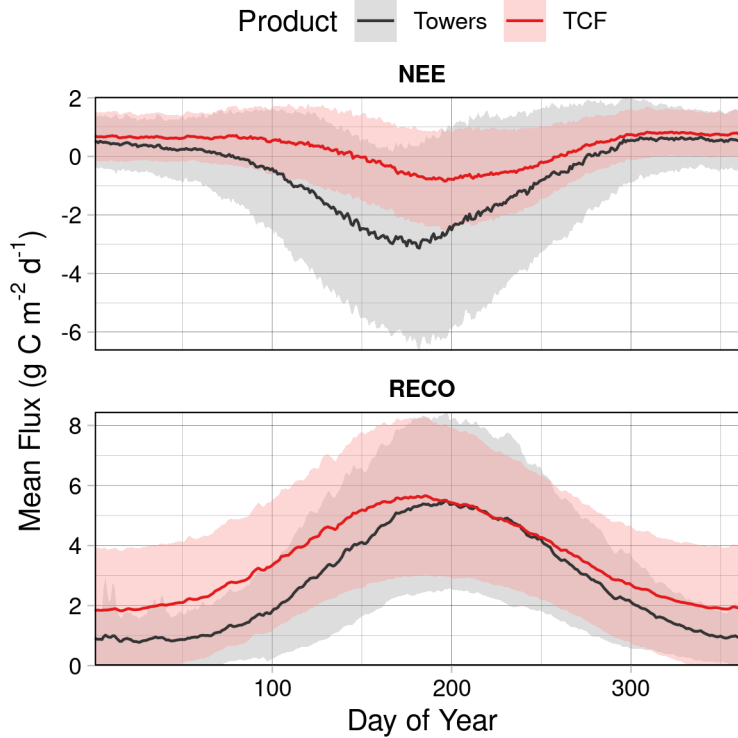


Figure 1. NEE and RECO mean seasonal cycles, as measured by EC flux towers (“Towers”) or modeled by TCF, for tower sites north of 40 degrees N latitude. Shaded area represents one spatial standard deviation. TCF data are from the L4C Nature Run v8.3 simulation.

- 117 2. What is the impact of alternative R_H or R_A models on the mean RECO phase
 118 and estimation skill, validated against flux data measured at towers and *in situ*
 119 chamber sites?

120 We identified potential improvements to the TCF model based on mechanisms hy-
 121 pothesized to affect the timing of RECO components that are missing or inadequately
 122 represented in the current framework. Potential improvements should be consistent with
 123 an operational, data-driven, and low-latency daily model such as SMAP L4C. We did
 124 not consider refinements to the LUE model or GPP parameters in this study because
 125 GPP in TCF is constrained by satellite-observed vegetation phenology.

126 Specifically, we hypothesized that one or a combination of processes might be crit-
 127 ical to the correct timing of the RECO seasonal cycle in the NH: seasonally varying lit-
 128 terfall inputs to SOC, which would enhance an R_H phenology; an upper limit on the re-
 129 sponse of R_H to soil moisture (SM) due to limited O_2 diffusion at near-saturating SM
 130 conditions, which may occur seasonally; and the slow diffusion of heat and moisture across
 131 vertically stratified soil layers, which can result in temporally lagged R_H flux. The RECO
 132 seasonal cycle could also be adjusted by changes to the R_A component; for example, through
 133 modeling of the inhibition of leaf R_A in the light (Wehr et al., 2016; Keenan et al., 2019),
 134 also known as the Kok effect, which could reduce the high RECO bias during the NH
 135 spring (Heskel et al., 2013; Byrne et al., 2018), as the TCF framework lumps above- and
 136 below-ground R_A together. Other potential modifications to the R_A model not inves-
 137 tigated here include increased construction respiration during spring leaf-out (Papale &

138 Valentini, 2003) or increased respiration associated with the maintenance of photosyn-
 139 thetic rates (Migliavacca et al., 2015)

140 These hypotheses have support in the literature. The Kok effect is well-known, de-
 141 spite uncertainty regarding the cellular mechanism(s) responsible (Heskel et al., 2013).
 142 A seasonally varying litterfall scheme is intuitive and consistent with observations of soil
 143 respiration in the NH fall season (Davidson et al., 2006) and experimental manipulations
 144 of litter inputs (Leitner et al., 2016; Nielsen et al., 2019). A looser coupling of litterfall
 145 and GPP is also consistent with the finding that peak below- and above-ground respi-
 146 ration are temporally separated (Davidson et al., 2006; Giasson et al., 2013). An O₂ dif-
 147 fusion limitation has been implemented in other terrestrial carbon flux models (David-
 148 son et al., 2012; Sihi et al., 2018) and has some experimental support. For instance, Järveoja
 149 et al. found that the temperature sensitivity of R_H in northern peatlands is enhanced
 150 in dry periods, possibly due to increased O₂ supply to heterotrophs. It has also been found
 151 to improve RECO estimation at wetland sites (Sulman et al., 2012) and where snowmelt
 152 also leads to an increase in soil water content in spring (Oikawa et al., 2014; Winnick et
 153 al., 2020). A vertically stratified soil column has been adopted in land models (Tao et
 154 al., 2017; dos Santos et al., 2021). The mechanics of heat diffusion suggest that surface
 155 layers of the soil will warm before deeper layers, inducing lagged respiration through-
 156 out the soil column. This time lag, most evident in the spring and fall, has been asso-
 157 ciated with changes in the share of ecosystem respiration from the soil (Davidson et al.,
 158 2006). Vertical variation in soil temperature, in particular, has been shown to substan-
 159 tially improve soil carbon stock estimates at high latitudes (Koven et al., 2017; Yi et al.,
 160 2020).

161 2 Data and Methods

162 We modified the open-source TCF source code (Endsley, 2021a) to support the res-
 163 piration processes hypothesized to affect the timing of the NEE and RECO seasonal cycles.
 164 In TCF, soil decomposition proceeds according to first-order kinetics as a function
 165 of litterfall inputs and the total SOC substrate (Jones et al., 2017; Endsley et al., 2020).
 166 The base rates of decomposition, or (inverse) turnover times, are modified by environ-
 167 mental constraint functions. Surface SM is used to model the response of R_H to substrate
 168 availability; i.e., liquid water in the soil pore spaces allows microbes to access organic
 169 carbon substrates, the decomposition of which produces a CO₂ flux (R_H). Soil temper-
 170 ature in the top 5 cm also promotes soil decomposition, modeled by an Arrhenius tem-
 171 perature function. Daily litterfall is computed as a constant daily fraction of annual NPP.

172 The response of R_H to surface SM and temperature is calibrated against a repre-
 173 sentative, global set of EC flux towers, separately, for towers representing different Plant
 174 Functional Types (PFTs), using constrained non-linear least squares optimization. The
 175 global distribution of up to eight PFT classes are defined from the MODIS MOD12Q1
 176 (Type 5) land-cover classification (Friedl et al., 2010): Evergreen Needleleaf Forest (ENF),
 177 Evergreen Broadleaf Forest (EBF), Deciduous Needleleaf Forest (DNF), Deciduous Broadleaf
 178 Forest (DBF), Shrubland (SHB), Grassland (GRS), Cereal Crop (CCR), and Broadleaf
 179 Crop (BCR).

180 In this study, the L4C Nature Run version 8.3 (NRv8.3), a model-only version of
 181 L4C uninformed by SMAP satellite brightness temperatures, is used as the baseline ver-
 182 sion of TCF against which potential model enhancements are evaluated. L4C NRv8.3
 183 is, in turn, based on soil moisture and temperature data from the SMAP Level 4 Soil Mois-
 184 ture (L4SM) Nature Run version 8.3, a model-only version of the operational SMAP L4SM
 185 product (Reichle et al., 2019, 2017). Both the operational SMAP L4C Version 5 and L4C
 186 NRv8.3 have the same model logic, with NEE computed as the residual difference be-
 187 tween GPP and RECO. L4C NRv8.3 and the modified versions of TCF use the same daily
 188 surface meteorological driver data for the period January 1, 2000 through December 31,

189 2017. For each modification to TCF, a full, daily carbon budget was calculated at 356
 190 EC flux tower sites from the FLUXNET La Thuille Collection (Baldocchi, 2008). The
 191 modeled fluxes are site-scale, representing a 9-km area centered on each EC tower site;
 192 model processing occurs at 1-km spatial resolution within that footprint.

193 The GPP model of L4C NRv8.3 is unchanged throughout this study; each exper-
 194 iment uses the same minimum air temperature, vapor pressure deficit (VPD), and pho-
 195 tosynthetically active radiation (PAR) data from the Modern Era Retrospective Re-analysis
 196 (MERRA-2, Gelaro et al., 2017). Similarly, the fraction of PAR absorbed by the canopy
 197 (fPAR) is derived from the Moderate Resolution Imaging Spectroradiometer (MODIS)
 198 MCD15A2H product (Myneni et al., 2015) and is used as a model input to compute iden-
 199 tical GPP estimates in each experiment. The environmental responses for each PFT in
 200 L4C NRv8.3 and subsequent experiments were calibrated against observed GPP and RECO
 201 fluxes partitioned from daily NEE using the night-time method at representative tower
 202 sites (Keenan et al., 2019). In every experiment, the three SOC pools (stratified by base
 203 decomposition rates) were brought to steady-state conditions through an analytical spin-
 204 up followed by a numerical spin-up, consisting of repeated cycling of annual climatolo-
 205 gies until the annual NEE balance is within $\pm 1 \text{ g C m}^{-2} \text{ d}^{-1}$.

206 2.1 Litterfall Phenology

The timing of litterfall allocation to SOC pools could have a profound effect on the
 seasonal cycle of R_H . Randerson et al. tested litterfall allocation schemes based on re-
 motely sensed leaf-area index (LAI) and selected the best-performing scheme for the CASA
 model. The CASA litterfall scheme, as implemented in the modified TCF framework,
 changes litterfall input, \mathcal{L} , from a constant daily fraction of NPP to a moving-window
 function of LAI:

$$\mathcal{L}(t) = \text{NPP} \times (f_E \delta t + f_L(t)) \quad \text{where} \quad f_E = \frac{\min(\text{LAI})}{\text{mean}(\text{LAI})}, \quad t \in [1, 365] \quad (1)$$

Where t is the day-of-year; δt is the time step in years (1/365); f_E is the evergreen
 fraction, an estimate of the proportion of the canopy that is evergreen; and f_L is the lit-
 terfall fraction in excess of a constant daily fraction (1/365):

$$f_L(t) = \frac{L_{loss}(t)}{\sum L_{loss}(t)} (1 - f_E) \quad (2)$$

207 f_L is normalized by the annual sum of L_{loss} , the leaf-loss function. L_{loss} is a tri-
 208 angular moving window centered on the current time step, amounting to the difference
 209 between lagged and leading LAI. Here, satellite-observed LAI inputs to the TCF model
 210 are obtained from the MODIS MCD15A2H product (Myneni et al., 2015). Unlike Ran-
 211 derson et al., we re-calculate f_E each year, allowing for potential changes in the canopy
 212 species composition. We also used the full MODIS MCD15A2H record, down-scaled to
 213 daily time steps by forward-filling values, over the 2000-2017 period. The approach re-
 214 quires two leading values from MCD15A2H (two 8-day MCD15A2H composites), which
 215 would introduce a ca. 16-day latency. For an operational algorithm aiming for low la-
 216 tency, like SMAP L4C, a static 365-day LAI climatology could be used instead.

217 2.2 O₂ Diffusion Limitation

218 If O₂ diffusion becomes limiting at high SM, this could explain the apparent RECO
 219 high bias in TCF during the spring season. We verified that high SM conditions exist
 220 in the NH spring at multiple U.S. Surface Climate Observing Reference Networks (USCRN)
 221 (Diamond et al., 2013) and Soil Climate Analysis Network (SCAN) (Schaefer et al., 2007)
 222 *in situ* monitoring sites in the contiguous United States (CONUS) north of 40 degrees

223 latitude. An annual SM climatology, compiled for each sensor depth, based on these sites
 224 suggests that shallow soil layers, in particular, experience an increase in SM anomaly dur-
 225 ing the NH spring (Figure S1).

To model an O₂ diffusion limit at high SM conditions, we adopted a Michaelis-Menten (MM) function of soil volumetric water content (Davidson et al., 2012) as an additional constraint on R_H . Currently in TCF (NRv8.3), R_H from pool i is a function of the base decomposition, k_i , the amount of SOC, C_i , an Arrhenius function of soil temperature, $f(T)$, and a linear ramp function of soil wetness (volumetric percent of pore space occupied by liquid water), $g(\theta\%)$, representing substrate diffusion. In the modified TCF R_H function, $g(\theta\%)$ is replaced by the minimum of itself and the O₂ diffusion limit term, a function of the volumetric O₂ concentration, $[O_2]$, and the MM or half-saturation constant, $k_{M_{O_2}}$:

$$R_H = \sum_{i=1}^3 k_i \times C_i \times f(T) \times \min \left(g(\theta\%), \frac{[O_2]}{k_{M_{O_2}} + [O_2]} \right) \quad (3)$$

In taking the minimum of these two constraints, we assume they are equally limiting for soil heterotrophs. We calculate the O₂ concentration based on the diffusion coefficient of O₂ in the air, d_{gas} , the air fraction of O₂ (0.209 L L^{-1}), the porosity of the soil, ϕ , and the volumetric soil moisture, θ . In our approach, no new fit parameters are required, as the constants $k_{M_{O_2}}$ and d_{gas} can be identified based on the soil moisture distribution observed among sites with the same PFT. First, following Davidson et al., we assume that when soil moisture is very low (below 5th percentile), the O₂ concentration in the soil pore spaces is the same as in the air, leading to:

$$[O_2] = 0.209 d_{gas} (\phi - \theta)^{4/3} \quad \longrightarrow \quad d_{gas} = \lim_{\theta \rightarrow 0} (\phi - \theta)^{-4/3} \quad (4)$$

226 Second, we set $k_{M_{O_2}} \equiv [O_2]$, calculated using this inferred value of d_{gas} and the
 227 median soil moisture. As in NRv8.3, soil moisture and porosity are derived from the SMAP
 228 L4SM (Reichle et al., 2019) and GEOS-5 Catchment Land Model (Koster et al., 2000;
 229 Tao et al., 2017), respectively.

230 **2.3 Vertically Resolved Soil Decomposition Model**

231 The original TCF framework is not vertically stratified: soil decomposition and R_H
 232 flux are considered to occur near the surface in a single soil layer of arbitrary thickness.
 233 The SMAP L4SM product estimates soil temperatures in seven layers with interfaces at
 234 5, 15, 35, 75, 150, and 300 cm depth, accounting for bedrock. However, because of the
 235 particular structure of the Catchment model, L4SM only reports SM in three nested lay-
 236 ers: the surface layer (0-5 cm), the root-zone (approximately 0-100 cm), and the soil pro-
 237 file (0 cm to bedrock depth). In order to obtain vertically resolved estimates of soil wa-
 238 ter content, we developed a simple physical model of soil water infiltration, diffusion, and
 239 lateral drainage (Endsley, 2021b) based on the modified Richards' equation and which
 240 is fully described in Appendix A. The corresponding, vertically stratified soil decompo-
 241 sition model is driven with these estimates of the soil water profile, which depend on sur-
 242 face infiltration estimates from L4SM, while L4C NRv8.3 is driven using L4SM surface
 243 soil moisture.

The multi-layer soil profile modification to TCF includes modifications of the SOC and R_H sub-models. The new, vertically resolved SOC model is similar to that of Yi et al.:

$$\frac{\partial}{\partial t} C_i(z) = \mathcal{R}_i(z) - k_i C_i(z) + \frac{\partial}{\partial z} \left(D(z) \frac{\partial C_i}{\partial z} \right) \quad (5)$$

Where $\mathcal{R}_i(z)$ represents inputs (and transfers) to SOC pool i at depth z and $D(z)$ is the vertical diffusivity of SOC. Diffusivity is taken to be $2 \times 10^{-4} \text{ m}^2 \text{ yr}^{-1}$, after Yi

et al. for non-permafrost soils. Each soil layer or depth, z , contains the same three SOC pools, which are the same pools in the baseline NRv8.3 and the other experiments. Litterfall input is now a function of depth:

$$\mathcal{R}_i(z) = \mathcal{L}_i(z) + f_{ji} \quad \text{where} \quad \mathcal{L}_i(z) = \mathcal{L}_i \times \exp\left(-\frac{z}{z_e}\right) \quad (6)$$

244 Where $\mathcal{L}_i(z)$ is the litterfall input to SOC pool i at depth z , an exponentially de-
 245 clining function of depth, after Koven et al., which estimated the e -folding depth, z_e , to
 246 be equal to 10 cm. \mathcal{L}_i , the total daily litterfall input across the soil profile, is estimated
 247 as in NRv8.3 as a constant daily fraction of NPP. f_{ji} is the transfer function defining
 248 carbon (C) transfers from pool j to pool i .

Finally, R_H is calculated similar to the baseline TCF model, NRv8.3, with envi-
 ronmental modifiers soil moisture and temperature, but as a composite sum of the R_H
 in each soil layer and with an additional rate modifier, $h(z)$, which accounts for the ex-
 tinction of R_H with depth due to factors *other than* soil moisture or temperature (Koven
 et al., 2013):

$$R_H = \sum_{z=1}^Z \sum_{i=1}^3 k_i C_{i,z} f(T_z) g(\theta_z) h(z) \quad \text{where} \quad h(z) = \exp\left(-\frac{z}{z_k}\right) \quad (7)$$

249 z_k , the depth at which environmentally-constrained R_H declines by a factor of e
 250 (due to, e.g., mineral protection, aggregation, etc.), is a free parameter that is fit in cal-
 251 ibration against the observed RECO flux.

2.4 The Kok Effect

252 To simulate the inhibition of R_A by light (the Kok effect), prior modeling studies
 have modulated maximum light-use efficiency (LUE) according to irradiance (Turner et
 al., 2006) or adjusted R_A directly as a function of irradiance, solar elevation, and the leaf
 angle distribution (Wohlfahrt et al., 2005). In TCF, however, a potential inhibition of
 R_A implicates both the calibration and forward modeling through plant carbon use ef-
 ficiency (CUE), or the fraction of GPP that is not respired. During calibration, CUE is
 used to compute R_H for fitting against EC flux tower observations. In this experiment,
 CUE now varies with PAR:

$$R_H = \text{RECO} - R_A \quad (8)$$

$$= \text{RECO} - (1 - \text{CUE} \times g(\text{PAR})) \times \text{GPP} \quad (9)$$

Where $g(\text{PAR})$ is a linear ramp function that monotonically increases with increas-
 ing PAR:

$$g(x) = \begin{cases} 1 & \text{if } x \geq x_{max} \\ 0 & \text{if } x \leq x_{min} \\ \frac{x - x_{min}}{x_{max} - x_{min}} & \text{otherwise} \end{cases} \quad (10)$$

253 Where x_{min} and x_{max} are the lower and upper bounds of the ramp function. In
 254 the experiment NRv8.3 + Kok Effect, x_{min} and x_{max} are fit parameters. In the base-
 255 line TCF NRv8.3, CUE does not vary with PAR (i.e., $g(\text{PAR}) \equiv 1$).

During forward modeling, CUE is key to computing NEE as the residual between
 RECO and GPP or, equivalently, between R_H and NPP:

$$\text{NEE} = R_H - \text{NPP} \quad (11)$$

$$= R_H - [\text{CUE} \times g(\text{PAR}) \times \text{GPP}] \quad (12)$$

2.5 Verification and Validation against Flux Tower Observations

The mean seasonal cycle at the 356 EC tower sites was used as a within-sample check on the experimental results, as it is observed that the mean seasonal cycle of the calibrated model does not match that of the underlying calibration data for high northern latitudes (Figure 1); i.e., does the modified TCF model display better fidelity to NH seasonal cycles in the calibration dataset? In addition to this model verification, we validated RECO and NEE modeling skill, in carbon terms, against the L4C Core Validation Sites (CVS) (Jones et al., 2017).

We also validated the TCF mean seasonal cycles against that of the FLUXCOM up-scaled tower fluxes dataset (Jung et al., 2020), which is based on the random forest method with combined remote sensing and meteorology drivers (RS+METEO). Like FLUXCOM, TCF-based models (e.g., SMAP L4C) extrapolate to the global land domain the site-level relationships between environmental drivers and carbon fluxes, based on a representative set of EC flux towers. Though not entirely independent of the FLUXNET towers used to calibrate TCF, the additional driver datasets and larger spatial extent of FLUXCOM motivate our comparison of the aggregate, mean NEE and RECO seasonal cycles. Unlike the EC tower data, FLUXCOM provides gridded data over land; we subset the data to all pixels ≥ 40 N latitude. As the global network of 356 EC towers used to calibrate TCF are assumed to be sufficiently representative for inferring relationships at global scale, we compared the aggregated mean seasonal cycle from FLUXCOM's larger spatial extent to that of our site-level modeled results.

Two techniques were used to quantify the effect of each TCF modification on the modeled NEE and RECO seasonal cycles. First, we applied a low-pass filter (smoother) to the mean seasonal cycle, aggregated across all towers matching each PFT or across the FLUXCOM time series. We chose a 7-day moving window for the filter based on visual inspection of the filtered results. Second, we used Fourier regression to quantify the phase shift, in days, of a harmonic function fit to the FLUXCOM time series or the complete time series of all tower sites within each PFT group. Specifically, with smoothing, we aggregated the mean seasonal cycle prior to applying the filter; with Fourier regression, the raw time series data were used to estimate model parameters. Fourier regression provides a standard error for the phase offset across PFTs; the low-pass filter provides an estimate of the location of minimum NEE or maximum RECO.

2.6 Validation against Chamber Data

We used data from the Community Soil Respiration (COSORE) database (Bond-Lamberty et al., 2020), a collection of *in situ* chamber studies, to investigate the relative advantage of each TCF modification and validate the modeled RECO fluxes. As TCF does not distinguish between above-ground and below-ground respiration and calculates R_A as a constant fraction of GPP, we assume that TCF RECO is roughly proportional to soil respiration (R_S) at daily time scales. R_S should be the largest component of RECO and they generally show similar dynamics (Bond-Lamberty et al., 2018; Barba et al., 2018). Using the Soil Respiration Database (SRDB) version 5 (Jian et al., 2021), we extracted $R_H:R_S$ ratios averaged by PFT and used these to calculate the R_H fraction of COSORE-reported R_S , based on matching PFT classes. Those ratios are consistent with the analysis of Bond-Lamberty et al. (Table S6). COSORE datasets that reported negative SM or $SM < 0.02 \text{ m}^3 \text{ m}^{-3}$ were excluded from the analysis. Few COSORE sites report the depth of collar insertion; all have recorded depths ≤ 10 cm. We computed the median R_S flux, converted from $\mu\text{mol CO}_2 \text{ m}^{-2} \text{ s}^{-1}$ to $g \text{ C m}^{-2} \text{ s}^{-1}$ using the molar mass of carbon, across ports.

After filtering COSORE datasets on these criteria, we split them into two groups. In the first group, 13 COSORE datasets (Chang et al., 2008; Carbone et al., 2011, 2013; Ataka et al., 2014; Sánchez-Cañete et al., 2016; Vargas et al., 2018) reported concurrent,

307 daily SM, temperature, and R_S flux values (Table S1). These *in situ* SM and temper-
 308 ature data are most appropriate for modeling at COSORE sites given the relatively coarse
 309 scale of TCF input datasets. Soil texture and porosity data were obtained for these sites
 310 from the Catchment model. We computed a 365-day GPP climatology from SMAP L4C
 311 Version 5 dataset (2015-2019) at each COSORE location. Use of a GPP climatology elim-
 312 inates canopy changes, real or spurious, that may not be reflected in the respiration mea-
 313 surements from COSORE chamber studies due to the scale mismatch. For experiments
 314 that included a CASA litterfall phenology, the daily litterfall fraction was computed as
 315 the average across EC tower sites for each PFT class.

316 A key issue arises with using COSORE-reported driver data in TCF models cali-
 317 brated on L4SM, as SM values generated by one model (or measured in the field) are
 318 generally not comparable with those derived from another (Koster et al., 2009). The small
 319 number of relevant COSORE datasets precludes re-calibration of TCF using COSORE
 320 observations. Instead, we applied a bias correction, using an affine statistical transforma-
 321 tion to re-scale COSORE moisture and temperature values to match the L4SM data
 322 based on within-PFT means. The coefficients from a linear regression of rank-ordered
 323 L4SM values on rank-ordered COSORE values were applied to transform the COSORE
 324 values of sites based on their PFT (i.e., slope parameter varying with PFT). We mapped
 325 the COSORE-reported biome to MOD12Q1 PFTs, which were often identical. To ob-
 326 tain a continuous record of soil moisture and temperature (required for TCF model op-
 327 eration), a daily COSORE climatology, by PFT, was used to fill-in missing values.

328 The second group of COSORE datasets consists of 12 other sites (Curtis et al., 2005;
 329 Baldocchi et al., 2006; Jassal et al., 2008; Noormets et al., 2010; Detto et al., 2013; Gaumont-
 330 Guay et al., 2014; Zhang et al., 2018; Ueyama et al., 2018) located within 9 km of a FLUXNET
 331 tower. Although these 12 datasets did not include driver data, we compared the mod-
 332 eled R_H flux (based on L4SM and MERRA-2 driver data) from those nearby FLUXNET
 333 sites, for each experiment, to the (partitioned) R_H flux from COSORE.

334 3 Results

335 Each modification to the R_H and/or SOC sub-models produced a meaningful im-
 336 provement in the estimated RECO and NEE seasonal cycles relative to the TCF NRv8.3
 337 model baseline with no modifications (Figure 2). The modification to the R_A model, via
 338 the Kok effect, produced no discernible improvement in the seasonal cycles (Tables 1,
 339 2). The mean day-of-year (DOY) of the NEE minimum (RECO maximum) for the high
 340 northern latitudes (≥ 40 degrees N latitude), based on filtering of tower data (Table S2),
 341 is estimated to be 181 (197). Depending on the method used to quantify the phase dif-
 342 ference (Tables S2, S3), in NRv8.3 the NEE minimum (RECO maximum) is delayed (ad-
 343 vanced) by 15-26 days (12-14 days). This aggregate seasonal cycle obscures underlying
 344 heterogeneity but is useful as a high-level diagnostic. Some PFTs show a stronger phase
 345 correction than others (Figure 3). Spatial variation in the timing of the NEE minimum
 346 due to PFT and climate can be observed if we apply the TCF model at global extent
 347 (Figure 4).

348 The Fourier regression (Table S3) and low-pass filter results (Table S2) agree broadly
 349 as to the effect of each modification on the overall fit to the seasonal cycle of the EC flux
 350 towers; i.e., each intervention, other than the Kok effect, produces a meaningful model
 351 improvement. However, they disagree substantially as to the length of the time lag for
 352 all PFTs except ENF (Tables 2 and S3). Some of this difference can be attributed to the
 353 lack of strong periodicity in NEE for some PFTs (e.g., SHB, GRS) which can confound
 354 the Fourier regression results; conversely, PFTs with broad seasonal peaks/ troughs (e.g.,
 355 CCR, BCR) may confound the low-pass filter. Differences in the TCF model fit param-
 356 eters (if re-calibrated) and other observations unique to each experiment are reported
 357 below.

Table 1: Difference (experiment minus Tower observations) in day-of-year (DOY) of NEE minimum (maximum net ecosystem carbon uptake), in days, for each experiment, based on the mean NEE seasonal cycle, smoothed with a low-pass filter using a 7-day moving window, for all sites above 40 degrees N latitude.

Product	ENF	DNF	DBF	SHB	GRS	CCR	BCR
NRv8.3	+26	+19	+16	+5	+4	+12	+15
NRv8.3 + Kok Effect	+26	+19	+16	+4	+4	+12	+15
NRv8.3 + O2 Limit	+14	+18	+3	-5	+4	+11	+1
NRv8.3 + Litterfall Phenology	+13	+18	+1	+3	+3	+10	-1
NRv8.3 + Soil Profile	+26	+17	+4	+3	+4	+10	+1
NRv8.3 + O2 Limit + Litterfall	+12	+18	+1	-6	-5	+10	+0
NRv8.3 + Soil Profile + O2 Limit	+28	+17	+4	+4	+6	+10	-1
NRv8.3 + Soil Profile + Litterfall	+13	+17	+2	+3	+4	+10	+0
NRv8.3 + Soil Profile + O2 Limit + Litterfall	+26	+17	+2	+4	+6	+10	-2

Table 2: Difference (experiment minus Tower observations) in day-of-year (DOY) of RECO maximum, in days, for each experiment, based on the mean RECO seasonal cycle, smoothed with a low-pass filter using a 7-day moving window, for all sites above 40 degrees N latitude.

Product	ENF	DNF	DBF	SHB	GRS	CCR	BCR
NRv8.3	-13	-34	-17	-2	-10	-13	-36
NRv8.3 + Kok Effect	-12	-34	-17	-2	-10	-13	-18
NRv8.3 + O2 Limit	-6	-34	-13	+0	+1	-9	-17
NRv8.3 + Litterfall Phenology	-5	-34	+3	+0	+19	+3	+32
NRv8.3 + Soil Profile	-12	-9	-17	+0	-9	-9	-17
NRv8.3 + O2 Limit + Litterfall	-4	-10	+0	+1	+4	-4	+9
NRv8.3 + Soil Profile + O2 Limit	-13	-9	-14	-2	+0	-8	-2
NRv8.3 + Soil Profile + Litterfall	-5	-9	-13	+0	+6	+3	+2
NRv8.3 + Soil Profile + O2 Limit + Litterfall	-12	-9	-13	-1	+0	+3	-1

3.1 Single-Factor Experiments

3.1.1 NRv8.3 + Litterfall Phenology

A seasonally varying litterfall scheme produced the best joint improvement in the NEE and RECO seasonal cycles (Table S2), relative to NRv8.3, particularly for DBF (Tables 1, 2). The NEE seasonal cycle of DBF, with the new litterfall scheme, is almost a perfect match to the tower record (despite a bias difference), including the autumn increase in CO₂ flux to the atmosphere. This autumnal increase is also shown in the modeled NEE results for the BCR PFT, but it is not apparent in the corresponding tower data. Conversely, NRv8.3 shows a spurious high NEE anomaly for BCR in spring that is eliminated by this experiment’s considerable shift in the BCR RECO seasonal cycle (Figure S3).

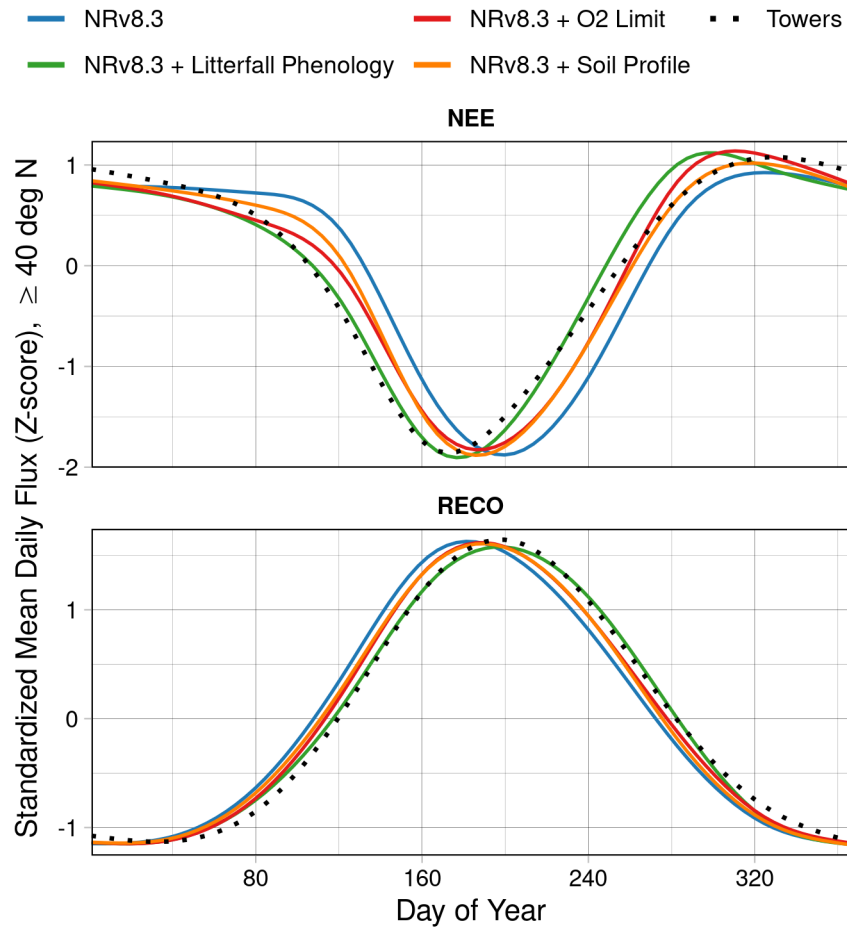


Figure 2. Mean seasonal RECO and NEE cycles for each experiment and for the EC flux towers (“Towers”), shown with smoothing b-splines, for all sites north of 40 degrees N latitude. The NRv8.3 + Kok Effect experiment is not shown because it overplots the NRv8.3 baseline almost exactly.

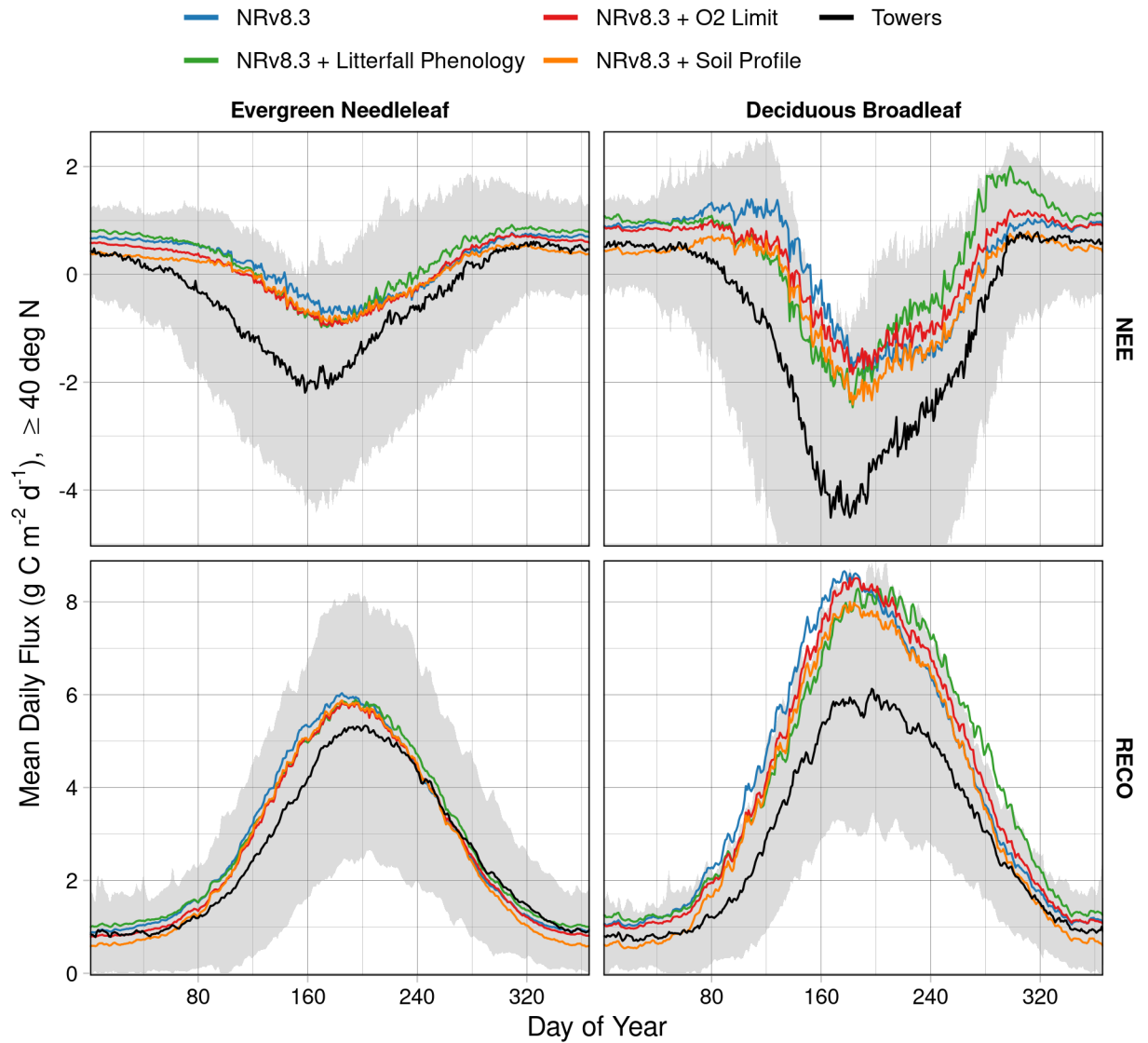


Figure 3. Mean seasonal RECO and NEE cycles for each experiment and for the EC flux towers (“Towers”) at tower sites north of 40 degrees N latitude for the ENF and DBF PFTs. The shaded area shows one spatial standard deviation for the Towers and is clipped for DBF NEE. Plots of the mean seasonal cycles for each PFT, separately, are available in the Supplement.

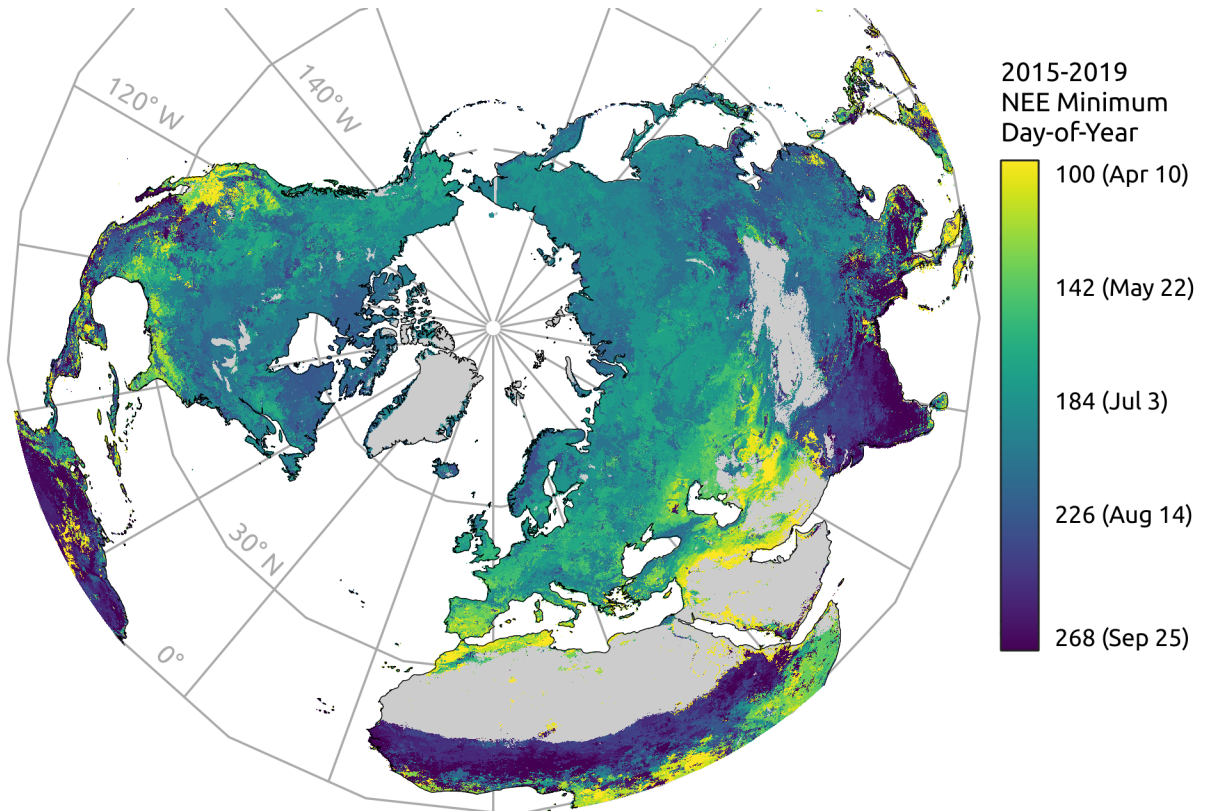


Figure 4. Map of the day-of-year on which the minimum net ecosystem exchange (NEE) occurs, based on the average 2015-2019 seasonal cycle of NEE from SMAP L4C Version 5 product, which incorporates the TCF model. Areas outside the model domain are shown in gray and white.

3.1.2 NRv8.3 + O₂ Limit

With the O₂ diffusion limit, all PFTs show reduced NEE magnitude and most show less RECO throughout most of the year, though increased RECO is observed in the fall for some PFTs, particularly DBF (Figure 3). The RECO seasonal cycle is improved for ENF, DBF, SHB, and cropland PFTs. As with the new litterfall scheme, the addition of an O₂ diffusion limit eliminated a spurious spring NEE anomaly for BCR in NRv8.3 (Figure S4). But unlike the new litterfall scheme, the O₂ diffusion limit did *not* introduce a spurious autumnal NEE anomaly for BCR (Figures S3 and S4). In general, the resulting phase correction in RECO is not as strong as in the NRv8.3 + Litterfall Phenology experiment (Figure S3). Looking at the residuals (compared to tower observations), NRv8.3 over-estimates RECO at high SM in ENF, GRS, and croplands. Adding an O₂ diffusion limit reduces that high bias; however, in the NRv8.3 + O₂ Limit experiment, GRS and DBF show a slight under-estimation of RECO at high SM.

3.1.3 NRv8.3 + Soil Profile

The NRv8.3 + Soil Profile experiment produced only a moderate correction to the NEE and RECO seasonal cycles. We experimented with different functional forms for the litterfall input distribution and R_H extinction function, $h(z)$ (Equation 7). For the litterfall inputs, as Koven et al. also suggested, we evaluated profiles based on the root profiles of Jackson et al., a root density profile based on the Community Land Model (Lawrence et al., 2019), and the normalized, median SOC profile from SoilGrids 250m (Hengl et al., 2017) (Figure S16). The negative exponential $h(z)$ better matched the shape of the median SoilGrids 250m profile and, in anticipation of a high RECO bias due to high SOC storage, we reduced the SOC storage magnitude by using a 9-cm e -folding depth (Figure S18), instead of 10-cm as suggested by Koven et al.. As expected, SOC storage increases with a multi-layer soil model (Figure S19).

3.1.4 NRv8.3 + Kok Effect

Plant CUE was much lower in the re-calibrated BPLUT when the Kok effect was applied, with values in the range [0.38, 0.70] across PFTs compared to [0.53, 0.78] in NRv8.3. Accordingly, RECO in the Kok effect experiment is partitioned very differently from NRv8.3, with a general decline in R_H but an increase in R_A . Despite this change, the overall RECO level is very similar to that of NRv8.3 and the seasonal cycles of NEE and RECO are unchanged. The apparent improvement for the BCR PFT (Table 2) is likely spurious due to a broad, flat minimum NEE for that PFT's seasonal cycle.

3.2 Factorial Combinations

In addition to single-factor experiments, we ran experiments in which multiple factors were combined, with the exception of the Kok effect implementation, as that experiment did not show improvement in the timing of the mean seasonal cycles. For the NRv8.3 + O₂ Limit + Litterfall multi-factor experiment, no re-calibration was necessary, as the NRv8.3 + O₂ Limit parameters were re-used. The NRv8.3 + Soil Profile + O₂ Limit experiment did require re-calibration. The experiment combining both an O₂ limit and litterfall phenology generally resembles an average of those single-factor experiments (Figure S8). Interestingly, the NRv8.3 + O₂ Limit + Litterfall experiment yields the most substantial correction of all multi-factor experiments and a substantial improvement in the RECO and NEE seasonal cycles for ENF compared to the single-factor experiments.

Where an O₂ limit and vertical soil profile were combined, the steady-state SOC storage was unreasonably high, with total-column SOC content exceeding 870 kg m⁻² and surface-layer (0-5 cm) SOC density of around 120 kg m⁻³. Non-exponential litterfall input functions combined with the power-law R_H extinction function yielded smaller,

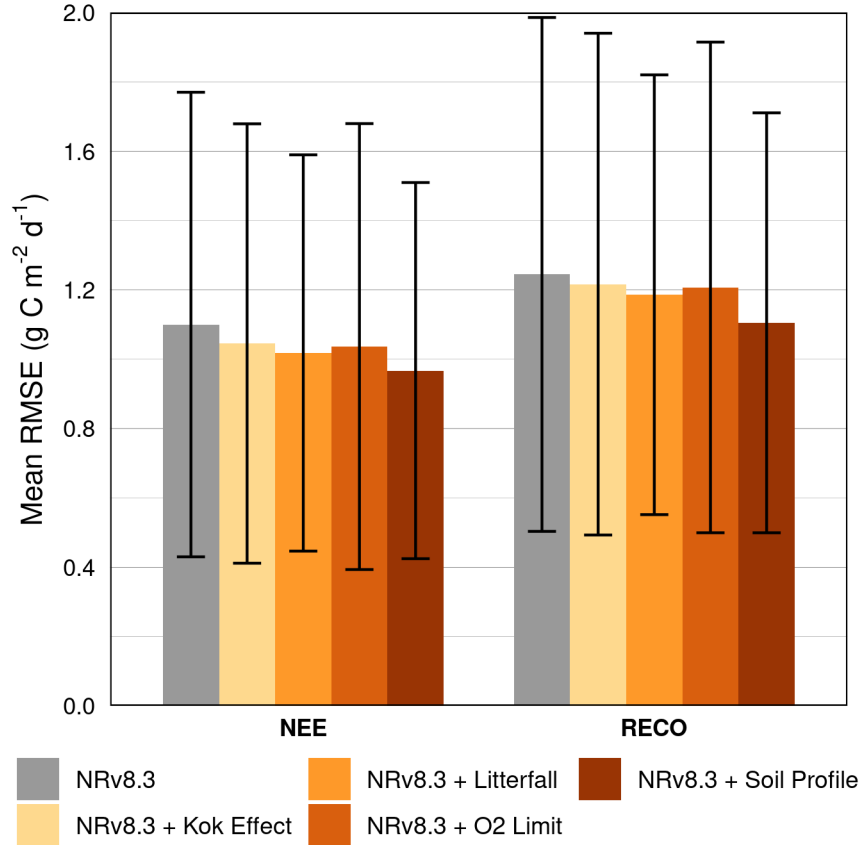


Figure 5. Root mean-squared error (RMSE) of modeled NEE, RECO fluxes versus observed fluxes at the 26 L4C Core Validation EC tower Sites (CVS) for the single-factor experiments. Error bars show one standard deviation across EC tower sites.

417 more realistic steady-state SOC pools, but failed to improve the RECO and NEE skill.
 418 The NRv8.3 + Soil Profile + Litterfall experiment, however, improved upon the base-
 419 line and the respective single-factor experiments; notably, an autumn high bias in the
 420 NEE cycles of DBF and BCR in the NRv8.3 + Litterfall experiment was much reduced
 421 (Figures S3, S7).

422 3.3 Validation against Tower and Chamber Datasets

423 Modeled fluxes from each single-factor experiment compared well to the observed
 424 NEE, RECO fluxes at the L4C CVS (Figure 5). Some of these sites are located below
 425 40 degrees N latitude, including the southern hemisphere, and therefore indicate that
 426 none of the new respiration mechanisms, as single factors, results in degraded NEE or
 427 RECO skill relative to the baseline NRv8.3. Conversely, in the combined experiments,
 428 the combination of an O₂ diffusion limit with other changes to the R_H model led to de-
 429 graded NEE and RECO skill (Figure 6).

430 Compared to FLUXCOM, the NRv8.3 + O₂ Limit showed the best agreement in
 431 the RECO and NEE seasonal cycles, though the NRv8.3 + Soil Profile and NRv8.3 +
 432 Soil Profile + Litterfall experiments also compare well (Tables 3, S5). Both phase esti-
 433 mation approaches agree that the single-factor experiments (other than NRv8.3 + Kok
 434 Effect) match the FLUXCOM seasonal cycles of RECO and NEE better than the base-

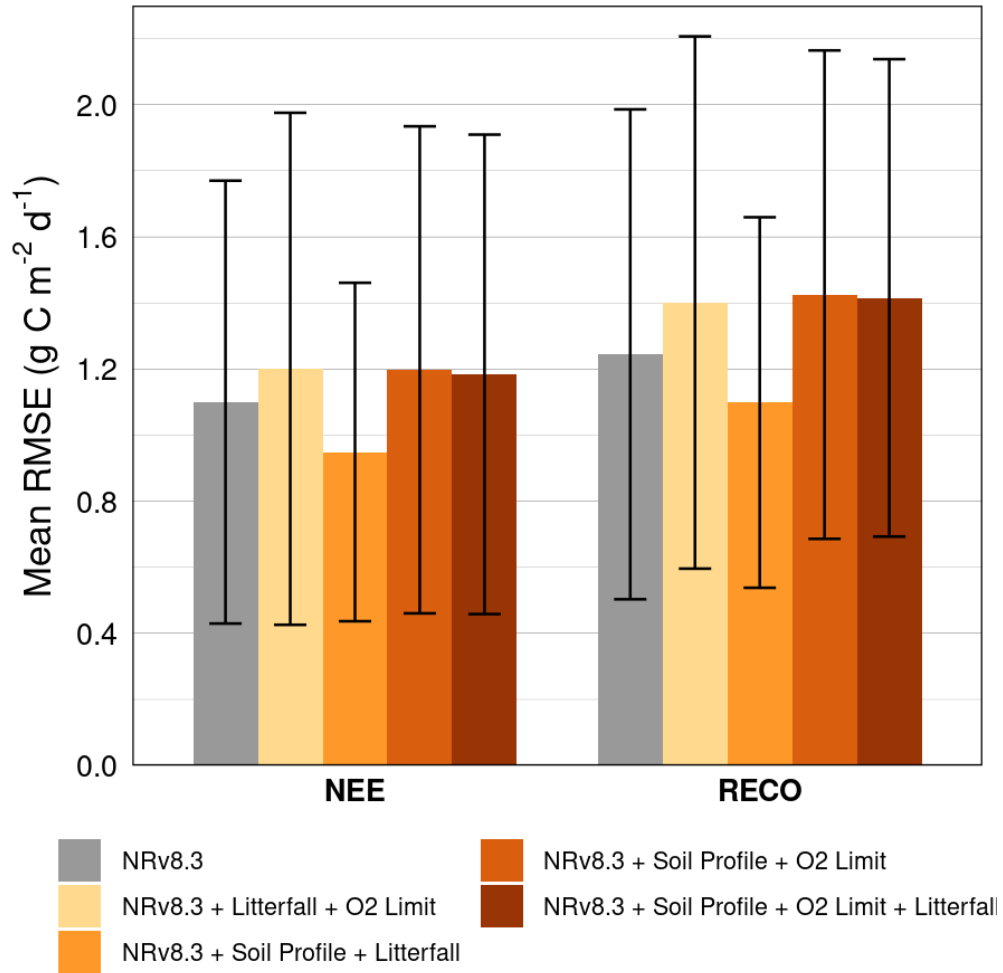


Figure 6. Root mean-squared error (RMSE) of modeled NEE, RECO fluxes versus observed fluxes at the 26 L4C Core Validation EC tower Sites (CVS) for the experiments with combinations of factors. Error bars show one standard deviation across EC tower sites.

line NRv8.3 product; however, they disagree considerably about the multi-factor experiments and the apparent residual lead in the RECO seasonal cycle (Table 3).

The modeled results at COSORE sites, combining those with independent driver data and those that are within an EC tower footprint, indicate that every experiment, other than NRv8.3 + Kok Effect, improved upon the NRv8.3 baseline in terms of R_H modeling skill (Table 4). The experiment with a vertical soil profile, with or without a litterfall phenology, produced an improvement in the R_H anomaly correlation and the greatest improvement in all skill metrics. The O₂ diffusion limitation, in particular, produced a substantial improvement in R_H RMSE and biased-adjusted RMSE (ubRMSE) that can be attributed primarily to the substantial reduction in high- R_H residuals at high SM (Figure S10). The improvement in the NRv8.3 + O₂ Limit experiment is notable at one moist, high-elevation ENF site (Chang et al., 2008); NRv8.3 and all other experiments fail to accurately simulate R_H dynamics at this site (median $r = 0.15$; median anomaly $r = 0.50$) but, with the O₂ limit, TCF simulates R_H with very high accuracy, including spikes in R_H during dry-downs ($r = 0.88$; anomaly $r = 0.85$; Figures S20 and S21).

4 Discussion

Three different modifications to the TCF soil decomposition model resulted in substantial corrections to the modeled seasonal carbon cycles in the NH and improved overall RECO and NEE modeling skill. Of the singular modifications tested, a seasonally varying litterfall scheme resulted in the greatest, consistent improvement in the RECO and NEE phase across PFTs. As that experiment involved no model re-calibration or new parameterization, we can attribute that improvement to the relative change in SOC substrate availability for R_H . In contrast, the moderate improvements in RECO and associated NEE phase under the O₂ diffusion limitation and vertical soil profile experiments seem to have resulted from an overall reduction in RECO, particularly during the NH spring (Figure 3). Seasonally varying litterfall was most effective at reducing the phase bias in DBF, while an O₂ limit was most effective in GRS; both were effective in ENF. The vertical soil profile was much less effective at reducing either RECO or NEE phase bias in most PFTs, though it did mitigate bias in croplands and improved overall modeling skill (Table 4).

It should be noted that the high NH RECO bias of TCF is a major contributing factor to the NEE phase bias; as the modeled GPP cycle is tied to satellite observations and fixed in each experiment, merely reducing the RECO magnitude would result in a phase shift of the NEE cycle. In the NH, the NEE cycle would be advanced (i.e., shifted earlier in time). We verified the role of RECO magnitude in the TCF simulations, by inflating tower RECO 25%, and then re-calculating NEE using NRv8.3 GPP. Consequently, while an NEE phase correction may result from the reduction of a bias in RECO magnitude, we can interpret a RECO phase correction as an improvement in the timing of respiration phenology. To verify the mechanisms tested here, we examined the change in the RECO residual (difference in residual between modeled and observed RECO) for each experiment compared to the baseline NRv8.3 (Figures S11-S14). The experiments that were successful at correcting the RECO seasonal cycle all showed substantially reduced RECO during the NH spring months (April, May, June), particularly for the DBF and cropland PFTs. With the exception of the NRv8.3 + Kok Effect experiment, which failed to mitigate RECO bias, each experiment reduced the spring RECO bias in a different way.

The O₂ diffusion limitation produced the greatest reduction in residual RECO at both low and high values of soil moisture (SM), particularly in spring (Figure S13), suggesting that an optimum SM exists for soil heterotrophs, at least when antecedent SM conditions are not taken into account (Ryan et al., 2015; Sihi et al., 2018). An upper limit

Table 3: Day-of-year (DOY) of NEE minimum, RECO maximum for FLUXCOM, EC flux towers (“Towers”), and experiments along with the difference in DOY (experiment/ Towers minus FLUXCOM), in days, for Towers, NRv8.3, and each experiment, identified using a low-pass filter, for the land domain above 40 degrees N latitude (FLUXCOM) or EC flux tower sites above 40 degrees N latitude.

Product	Peak RECO DOY	Peak NEE DOY	RECO Phase (days)	NEE Phase (days)
FLUXCOM	195	183	n.a.	n.a.
Towers	197	181	+2	-2
NRv8.3	183	196	-12	+13
NRv8.3 + Kok Effect	184	196	-11	+13
NRv8.3 + Litterfall Phenology	187	182	-8	-1
NRv8.3 + O2 Limit	186	186	-9	+3
NRv8.3 + Soil Profile	185	186	-10	+3
NRv8.3 + O2 Limit + Litterfall	187	182	-8	-1
NRv8.3 + Soil Profile + Litterfall	186	183	-9	+0
NRv8.3 + Soil Profile + O2 Limit	186	186	-9	+3
NRv8.3 + Soil Profile + O2 Limit + Litterfall	186	183	-9	+0

Table 4: For each experiment, the average root mean-squared error (RMSE), average unbiased RMSE (ubRMSE), median Pearson's correlation (r), and median r for demeaned anomalies, across sites, against the observed COSORE R_H flux. Standard deviation across sites is noted for RMSE, ubRMSE in parentheses. Significant improvements in correlation, relative to NRv8.3, are denoted: *** (p-value < 0.01), ** (p-value < 0.05), * (p-value < 0.1).

Product	Num. Sites	RMSE	ubRMSE	Correlation (r)	Anomaly r
NRv8.3	25	2.04 (± 0.99)	0.68 (± 0.42)	0.630	0.390
NRv8.3 + Kok Effect	25	1.77 (± 0.83)	0.65 (± 0.41)	0.631	0.389
NRv8.3 + Litterfall Phenology	25	1.99 (± 0.94)	0.69 (± 0.43)	***0.687	0.369
NRv8.3 + O2 Limit	25	1.58 (± 0.65)	0.65 (± 0.41)	***0.687	0.383
NRv8.3 + O2 Limit + Litterfall	25	1.87 (± 0.88)	0.66 (± 0.43)	***0.659	0.377
NRv8.3 + Soil Profile	25	1.31 (± 0.67)	0.62 (± 0.40)	***0.746	***0.438
NRv8.3 + Soil Profile + Litterfall	25	1.28 (± 0.67)	0.62 (± 0.40)	***0.750	***0.441
NRv8.3 + Soil Profile + O2 Limit	25	1.55 (± 0.93)	0.80 (± 0.49)	***0.655	0.369
NRv8.3 + Soil Profile + O2 Limit + Litterfall	25	1.55 (± 0.93)	0.80 (± 0.49)	***0.657	0.361

486 on the response of R_H to soil moisture has been shown to improve modeled RH estimates
 487 (Tůpek et al., 2019) and, as our results at COSORE sites indicate, specifically improves
 488 estimates at sites that experience high soil moisture conditions and at one alpine ENF
 489 site (Table 4 and Figure S10). When the O_2 diffusion limit is combined with a linear or
 490 sub-linear function that increases with soil moisture (i.e., representing greater substrate
 491 availability), the result is a triangular function with a fairly narrow range of optimum
 492 soil moisture, which agrees with the observation that SM is most limiting on R_H when
 493 soils are relatively dry or approaching saturation (Reichstein et al., 2003). At high north-
 494 ern latitudes, these conditions may predominate during spring thaw (Oikawa et al., 2014;
 495 Winnick et al., 2020), which underscores the key role of SM in accurately modeling the
 496 corresponding carbon cycle transitions.

497 The new litterfall allocation scheme shows a similar spring reduction in the RECO
 498 residual but it is not patterned by soil moisture or temperature (Figure S12). Instead,
 499 there is a temporal pattern: residual RECO is reduced in the first half of the year but
 500 is elevated during the second half, effectively reducing R_H and RECO in spring just as
 501 an O_2 diffusion limitation does when SM is high. The fall RECO increase then results
 502 from a release from substrate limitation (Leitner et al., 2016; Nielsen et al., 2019). The
 503 CASA model (Randerson et al., 1996), from which our litterfall scheme is derived, dis-
 504 plays RECO and NEE phase biases similar to TCF (Byrne et al., 2018, Figure 2). This
 505 is particularly interesting as the NRv8.3 + Litterfall Phenology experiment considerably
 506 improved the phase offset between TCF and the tower observations (Tables 1, 2) and
 507 perhaps over-corrected when compared to FLUXCOM (Table S4). Randerson et al. noted
 508 the CASA litterfall scheme led to an advanced R_H seasonal cycle (earlier peak), which
 509 was expected due to a build-up of fall substrate inputs and, in turn, a high substrate avail-
 510 ability in spring (Byrne et al., 2018). However, in our experiment, the same litterfall scheme
 511 only delayed the R_H cycle. This discrepancy depends on whether or not winter-time R_H
 512 is sufficiently reduced, relative to litterfall inputs, so as to allow substrate pools to in-
 513 crease before spring. Another key difference between CASA and TCF is the much coarser
 514 spatial resolution of CASA (and coarser temporal resolution in Randerson et al., 1996).

515 When we look at the difference in RECO residuals from the NRv8.3 + Kok Effect
 516 experiment, stratified by PAR, the RECO residual is still high at almost all levels of PAR
 517 but especially when PAR is high, indicating that a CUE response to PAR is not hav-
 518 ing the intended effect on the seasonal cycle (Figure S11). This may be due to TCF's
 519 high RECO bias in the NH (Figure 3), i.e., the R_A fraction increases to the extent that
 520 R_H is reduced, resulting in a similar level of RECO to NRv8.3. This intrinsic high bias
 521 in RECO may be due to the night-time partitioning of EC tower fluxes (Keenan et al.,
 522 2019). Alternatively, or in addition to this problem, there may be a problem with our
 523 implementation of a PAR scalar modulating CUE at daily time scale, as R_A is known
 524 to continue throughout the day and sub-daily co-variation of PAR and temperature is
 525 considerable (Heskel et al., 2013; Peng et al., 2013); TCF's use of daily average mete-
 526 orology that is more representative of daytime conditions may contribute to the high RECO
 527 bias (Wehr et al., 2016).

528 Despite its small effect on the mean seasonal cycles, the greatest improvement in
 529 both NEE and RECO modeling skill (Figure 5) came from the incorporation of a ver-
 530 tical soil profile into the TCF soil decomposition model. The small correction in phase
 531 bias seems to be due to the lagged R_H flux that arises from the slow diffusion of heat
 532 and, to a lesser extent, of moisture through the soil column. We verified this mechanism
 533 by plotting the standardized, modeled R_H flux in each soil layer from the NRv8.3 + Soil
 534 Profile experiment, along with the (single-layer) flux from NRv8.3 (Figure S15). The re-
 535 sults indicate that, with a vertically stratified soil decomposition model, the individual-
 536 layer R_H fluxes are lagged and decline in magnitude with increasing soil depth. Conse-
 537 quently, the whole-column, total R_H flux in the vertically resolved model approaches the
 538 magnitude of the single-layer model, though the multi-layer total is slightly smaller. The

539 result is that the NEE and RECO cycles both peak in early July (Table S2) but the RECO
 540 peak is broader, consistent with Yi et al.. In mid-to-late summer, the RECO flux at the
 541 NH sites is substantially reduced due to SM (i.e., substrate diffusion) limits (not shown).

542 This lag effect and corresponding improvement in the RECO seasonal cycle could
 543 be enhanced if deeper soil layers were modeled with higher SOC storage. In the NRv8.3
 544 + Soil Profile experiment, SOC storage diminishes to almost zero at 1.5 and 3-m depth.
 545 The exponentially declining input distribution of Koven et al. is a good match for the
 546 median, global SOC profile from SoilGrids 250m (Figure S16) as well as the distribution
 547 of carbon by age (Balesdent et al., 2018); however, TCF depletes deep SOC storage dur-
 548 ing model spin-up (Figure S18). This underscores that further improvements to effec-
 549 tively model SOC protection mechanisms are needed in order to accurately simulate R_H
 550 fluxes from a multi-layer soil decomposition model. The exponential litterfall distribu-
 551 tions that allocate very little SOC to deeper layers (Figure S16) are probably more re-
 552 alistic than distributions based on root fractions (Shi et al., 2020). However, an expo-
 553 nential extinction of R_H with depth may not be reasonable, as there is recent evidence
 554 that between 30-60% of CO₂ efflux originates below 1 m depth (Wan et al., 2018). For
 555 simplicity, our model varies neither the turnover times nor the environmental response
 556 functions with depth. Addressing these limitations will require improved data on the ver-
 557 tical distribution of R_H flux.

558 In TCF, calibrating SOC turnover is somewhat subjective, as the base decay rates
 559 are determined by comparing the inferred SOC storage from inverting the R_H flux with
 560 that indicated by the International Geosphere-Biosphere Data and Information System
 561 (IGBP-DIS) soil inventory record (Global Soil Data Task Group, 2000). However, the
 562 base rates likely should be modified when soil decomposition mechanisms are changed
 563 and should probably vary with soil layer depth; doing so might result in more favorable
 564 RECO, NEE skill metrics for the multi-factor experiments (Figure 6). Another limita-
 565 tion in this study is the neglect of GPP magnitude bias. Although the phase of GPP is
 566 expected to be constrained by the satellite-observed fPAR (Messerschmidt et al., 2013),
 567 a GPP magnitude bias also has the potential to introduce an NEE phase bias and re-
 568 quires further research along the same lines of this study.

569 The model enhancements produce similar phase corrections when results from dif-
 570 ferent PFTs are pooled. This equifinality suggests that the modifications to TCF assessed
 571 here may not be equally relevant to all PFTs. For instance, the new litterfall scheme re-
 572 sulted in a better match to autumnal NEE for DBF but also created a spurious high NEE
 573 anomaly in autumn for BCR. The combination of O₂ limit and vertical soil profile also
 574 further delayed (advanced) the mean NEE (RECO) seasonal cycle for ENF. The equi-
 575 finality among experiments also indicates that the NH seasonal cycle of NEE is an emer-
 576 gent property of terrestrial ecosystems (Birch et al., 2021) and that we are likely miss-
 577 ing some interactions between limiting factors and driving relationships of soil decom-
 578 position, e.g., microbial biomass and stabilization of SOC (Johnston & Sibly, 2018) or
 579 litter input traits (Hu et al., 2018). After all, there is some residual misfit in the mod-
 580 eled seasonal cycles (Tables 1, 2) and TCF still retains a high RECO bias. In addition
 581 to the high residual RECO bias, which may be due to the partitioning of EC tower fluxes,
 582 TCF also has a relatively large NEE magnitude bias, as its summer-time GPP and NEE
 583 amplitudes are smaller than tower observations (Figure 3). Future development of TCF
 584 and similar models—given their promise for global, operational terrestrial carbon bud-
 585 geting (e.g., SMAP L4C)—should focus on reducing RECO bias, starting with an as-
 586 sessment of different EC flux partitioning methods (Keenan et al., 2019) and SOC pro-
 587 tection mechanisms.

588 5 Conclusions

589 A seasonally varying adjustment of R_H model processes, including the litterfall al-
 590 location to SOC available for decomposition, resulted in major corrections to the mod-
 591 eled RECO and NEE seasonal cycles, as compared to EC flux tower observations, in a
 592 first-order soil decomposition model. An explicit litterfall phenology, with or without a
 593 vertically resolved SOC decomposition model, yields the best improvement in phase. The
 594 NEE phase bias in TCF for high northern latitude sites (≥ 40 N), was reduced from a
 595 lag of 15-26 days to between a 5-day lead or 15-day lag, depending on the experiment.
 596 Based on a comparison to the FLUXCOM seasonal cycle above 40 degrees N latitude,
 597 the model enhancements generally eliminated the NEE phase bias, though a smaller RECO
 598 phase bias remains. Comparison to independent, *in situ* chamber measurements indi-
 599 cates the proposed mechanisms can improve RECO and NEE modeling skill.

600 The RECO phase bias can result from a bias in RECO magnitude, i.e., from ex-
 601 cess modeled autotrophic (R_A) or heterotrophic respiration (R_H) at key seasonal inter-
 602 vals. Two model enhancements, adding a limit on O_2 diffusion for soil heterotrophs or
 603 a seasonally varying litterfall inputs scheme, reduced the phase biases in RECO and NEE
 604 by reducing R_H during the NH spring season. The O_2 limit restricts R_H as soil mois-
 605 ture increases, which is common in the NH spring in many regions due to snowmelt and
 606 increased rainfall. The new litterfall scheme directly shifts the R_H seasonal cycle later
 607 in time by enhancing substrate limitation in the spring. Although less effective at cor-
 608 recting RECO or NEE phase bias, a multi-layer soil decomposition model also reduced
 609 spring NH RECO. This is due to lagged R_H flux from deeper soil layers, effectively amor-
 610 tizing the whole-column R_H flux over a longer period.

611 Accurate timing of the terrestrial NEE cycle is key if such modeled estimates are
 612 to be used as priors in atmospheric inversion studies. Moreover, the NEE seasonal cy-
 613 cle, observed by EC flux towers or estimated in data-driven syntheses, can be used to
 614 diagnose missing or poorly represented model processes. Going forward, increased *in situ*
 615 monitoring of soil respiration fluxes—particularly vertically resolved fluxes—of soil or-
 616 ganic carbon, and of below-ground R_A will be essential for constraining modeled soil res-
 617 piration in terrestrial carbon flux models.

618 Acknowledgments

619 The authors would like to thank Randal D. Koster (Global Modeling and Assim-
 620 ilation Office, NASA Goddard Space Flight Center) for his feedback on the soil hydro-
 621 ology model and the paper. This study was supported with funding from NASA (NX14AI50G,
 622 80NSSC19M0114). The SMAP L4C operational product (Version 5) is publicly acces-
 623 sible through the National Snow and Ice Data Center (NSIDC) at [https://nsidc.org/
 624 data/SPL4CMDL/versions/5](https://nsidc.org/data/SPL4CMDL/versions/5). The TCF model code is available online at [https://github
 625 .com/arthur-e/pyl4c](https://github.com/arthur-e/pyl4c). The soil hydrology model code is available at [https://github
 626 .com/arthur-e/simsoil](https://github.com/arthur-e/simsoil).

627 References

- 628 Alexandrov, G. A. (2014). Explaining the seasonal cycle of the globally averaged
 629 CO_2 with a carbon-cycle model. *Earth System Dynamics*, 5(2), 345–354. doi: 10
 630 .5194/esd-5-345-2014
- 631 Ataka, M., Kominami, Y., Yoshimura, K., Miyama, T., Jomura, M., & Tani, M.
 632 (2014, oct). In Situ CO_2 Efflux from Leaf Litter Layer Showed Large Temporal
 633 Variation Induced by Rapid Wetting and Drying Cycle. *PLoS ONE*, 9(10),
 634 e108404. Retrieved from <https://dx.plos.org/10.1371/journal.pone.0108404>
 635 doi: 10.1371/journal.pone.0108404

- 636 Baldocchi, D. (2008). 'Breathing' of the terrestrial biosphere: lessons learned
637 from a global network of carbon dioxide flux measurement systems. *Australian*
638 *Journal of Botany*, 56(1), 1. Retrieved from [http://www.publish.csiro.au/](http://www.publish.csiro.au/?paper=BT07151)
639 [?paper=BT07151](http://www.publish.csiro.au/?paper=BT07151) doi: 10.1071/BT07151
- 640 Baldocchi, D., Tang, J., & Xu, L. (2006, jun). How switches and lags in biophysical
641 regulators affect spatial-temporal variation of soil respiration in an oak-grass
642 savanna. *Journal of Geophysical Research: Biogeosciences*, 111(G2), n/a–
643 n/a. Retrieved from <http://doi.wiley.com/10.1029/2005JG000063> doi:
644 10.1029/2005JG000063
- 645 Balesdent, J., Basile-Doelsch, I., Chadoeuf, J., Cornu, S., Derrien, D., Fekia-
646 cova, Z., & Hatté, C. (2018, jul). Atmosphere–soil carbon transfer as a func-
647 tion of soil depth. *Nature*, 559(7715), 599–602. Retrieved from [https://](https://www.cambridge.org/core/product/identifier/9781139029339/%23CN-bp-6/type/book%5Bpart%5Dhttp://www.nature.com/articles/s41586-018-0328-3)
648 [www.cambridge.org/core/product/identifier/9781139029339-%23CN-bp-6/](https://www.cambridge.org/core/product/identifier/9781139029339/%23CN-bp-6/type/book%5Bpart%5Dhttp://www.nature.com/articles/s41586-018-0328-3)
649 [type/book%5Bpart%5Dhttp://www.nature.com/articles/s41586-018-0328-3](https://www.cambridge.org/core/product/identifier/9781139029339/%23CN-bp-6/type/book%5Bpart%5Dhttp://www.nature.com/articles/s41586-018-0328-3) doi:
650 10.1038/s41586-018-0328-3
- 651 Barba, J., Cueva, A., Bahn, M., Barron-Gafford, G. A., Bond-Lamberty, B., Hanson,
652 P. J., ... Vargas, R. (2018). Comparing ecosystem and soil respiration: Review
653 and key challenges of tower-based and soil measurements. *Agricultural and Forest*
654 *Meteorology*, 249(March 2017), 434–443. doi: 10.1016/j.agrformet.2017.10.028
- 655 Birch, L., Schwalm, C. R., Natali, S., Lombardozzi, D., Keppel-Aleks, G., Watts,
656 J., ... Rogers, B. M. (2021, jun). Addressing biases in Arctic–boreal carbon cy-
657 cling in the Community Land Model Version 5. *Geoscientific Model Development*,
658 14(6), 3361–3382. Retrieved from [https://gmd.copernicus.org/articles/14/](https://gmd.copernicus.org/articles/14/3361/2021/)
659 [3361/2021/](https://gmd.copernicus.org/articles/14/3361/2021/) doi: 10.5194/gmd-14-3361-2021
- 660 Bond-Lamberty, B., Bailey, V. L., Chen, M., Gough, C. M., & Vargas, R. (2018).
661 Globally rising soil heterotrophic respiration over recent decades. *Nature*,
662 560(7716), 80–83. Retrieved from [http://dx.doi.org/10.1038/s41586-018-](http://dx.doi.org/10.1038/s41586-018-0358-x)
663 [0358-x](http://dx.doi.org/10.1038/s41586-018-0358-x) doi: 10.1038/s41586-018-0358-x
- 664 Bond-Lamberty, B., Epron, D., Harden, J., Harmon, M. E., Hoffman, F., Ku-
665 mar, J., ... Vargas, R. (2016). Estimating heterotrophic respiration at large
666 scales: Challenges, approaches, and next steps. *Ecosphere*, 7(6), 1–13. doi:
667 10.1002/ecs2.1380
- 668 Bond-Lamberty, B., Christianson, D. S., Malhotra, A., Pennington, S. C., Sihi,
669 D., AghaKouchak, A., ... Zou, J. (2020, dec). COSORE: A community
670 database for continuous soil respiration and other soil-atmosphere green-
671 house gas flux data. *Global Change Biology*, 26(12), 7268–7283. Retrieved
672 from <https://onlinelibrary.wiley.com/doi/10.1111/gcb.15353> doi:
673 10.1111/gcb.15353
- 674 Byrne, B., Wunch, D., Jones, D. B., Strong, K., Deng, F., Baker, I., ... Roehl,
675 C. M. (2018). Evaluating GPP and respiration estimates over northern midlati-
676 tude ecosystems using solar-induced fluorescence and atmospheric CO₂ measure-
677 ments. *Journal of Geophysical Research: Biogeosciences*, 123(9), 2976–2997. doi:
678 10.1029/2018JG004472
- 679 Carbone, M. S., Park Williams, A., Ambrose, A. R., Boot, C. M., Bradley, E. S.,
680 Dawson, T. E., ... Still, C. J. (2013, feb). Cloud shading and fog drip influ-
681 ence the metabolism of a coastal pine ecosystem. *Global Change Biology*, 19(2),
682 484–497. Retrieved from [https://onlinelibrary.wiley.com/doi/10.1111/](https://onlinelibrary.wiley.com/doi/10.1111/gcb.12054)
683 [gcb.12054](https://onlinelibrary.wiley.com/doi/10.1111/gcb.12054) doi: 10.1111/gcb.12054
- 684 Carbone, M. S., Still, C. J., Ambrose, A. R., Dawson, T. E., Williams, A. P., Boot,
685 C. M., ... Schimel, J. P. (2011, sep). Seasonal and episodic moisture controls on
686 plant and microbial contributions to soil respiration. *Oecologia*, 167(1), 265–278.
687 Retrieved from <http://link.springer.com/10.1007/s00442-011-1975-3> doi:
688 10.1007/s00442-011-1975-3
- 689 Chang, S.-C., Tseng, K.-H., Hsia, Y.-J., Wang, C.-P., & Wu, J.-T. (2008, may). Soil

- 690 respiration in a subtropical montane cloud forest in Taiwan. *Agricultural and For-*
 691 *est Meteorology*, 148(5), 788–798. Retrieved from [https://linkinghub.elsevier](https://linkinghub.elsevier.com/retrieve/pii/S0168192308000026)
 692 [.com/retrieve/pii/S0168192308000026](https://linkinghub.elsevier.com/retrieve/pii/S0168192308000026) doi: 10.1016/j.agrformet.2008.01.003
- 693 Chapin, F. S., Woodwell, G. M., Randerson, J. T., Rastetter, E. B., Lovett, G. M.,
 694 Baldocchi, D. D., ... Schulze, E. D. (2006, nov). Reconciling carbon-cycle
 695 concepts, terminology, and methods. *Ecosystems*, 9(7), 1041–1050. Re-
 696 trieved from <http://link.springer.com/10.1007/s10021-005-0105-7> doi:
 697 10.1007/s10021-005-0105-7
- 698 Ciais, P., Tan, J., Wang, X., Roedenbeck, C., Chevallier, F., Piao, S. L., ... Tans,
 699 P. (2019). Five decades of northern land carbon uptake revealed by the inter-
 700 hemispheric CO₂ gradient. *Nature*, 568(7751), 221–225. Retrieved from [http://](http://dx.doi.org/10.1038/s41586-019-1078-6)
 701 dx.doi.org/10.1038/s41586-019-1078-6 doi: 10.1038/s41586-019-1078-6
- 702 Curtis, P. S., Vogel, C. S., Gough, C. M., Schmid, H. P., Su, H.-B., & Bovard, B. D.
 703 (2005, aug). Respiratory carbon losses and the carbon-use efficiency of a northern
 704 hardwood forest, 1999–2003. *New Phytologist*, 167(2), 437–456. Retrieved from
 705 <https://onlinelibrary.wiley.com/doi/10.1111/j.1469-8137.2005.01438.x>
 706 doi: 10.1111/j.1469-8137.2005.01438.x
- 707 Davidson, E. A., Richardson, A. D., Savage, K. E., & Hollinger, D. Y. (2006). A
 708 distinct seasonal pattern of the ratio of soil respiration to total ecosystem respira-
 709 tion in a spruce-dominated forest. *Global Change Biology*, 12(2), 230–239. doi:
 710 10.1111/j.1365-2486.2005.01062.x
- 711 Davidson, E. A., Samanta, S., Caramori, S. S., & Savage, K. (2012). The Dual
 712 Arrhenius and Michaelis-Menten kinetics model for decomposition of soil organic
 713 matter at hourly to seasonal time scales. *Global Change Biology*, 18(1), 371–384.
 714 doi: 10.1111/j.1365-2486.2011.02546.x
- 715 Detto, M., Bohrer, G., Nietz, J., Maurer, K., Vogel, C., Gough, C., & Curtis, P.
 716 (2013, oct). Multivariate Conditional Granger Causality Analysis for Lagged
 717 Response of Soil Respiration in a Temperate Forest. *Entropy*, 15(12), 4266–
 718 4284. Retrieved from <http://www.mdpi.com/1099-4300/15/10/4266> doi:
 719 10.3390/e15104266
- 720 Diamond, H. J., Karl, T. R., Palecki, M. A., Baker, C. B., Bell, J. E., Leeper, R. D.,
 721 ... Thorne, P. W. (2013, apr). U.S. Climate Reference Network after One Decade
 722 of Operations: Status and Assessment. *Bulletin of the American Meteorological*
 723 *Society*, 94(4), 485–498. Retrieved from [https://journals.ametsoc.org/doi/](https://journals.ametsoc.org/doi/10.1175/BAMS-D-12-00170.1)
 724 [10.1175/BAMS-D-12-00170.1](https://journals.ametsoc.org/doi/10.1175/BAMS-D-12-00170.1) doi: 10.1175/BAMS-D-12-00170.1
- 725 dos Santos, T., Keppel-Aleks, G., De Roo, R., & Steiner, A. L. (2021). Can Land
 726 Surface Models Capture the Observed Soil Moisture Control of Water and Car-
 727 bon Fluxes in Temperate-To-Boreal Forests? *Journal of Geophysical Research:*
 728 *Biogeosciences*, 126(4), 1–18. doi: 10.1029/2020jg005999
- 729 Endsley, K. A. (2021a). *pyl4c (Version 0.12.0.dev)*. Retrieved from [https://github](https://github.com/arthur-e/pyl4c/)
 730 [.com/arthur-e/pyl4c/](https://github.com/arthur-e/pyl4c/) doi: <https://doi.org/10.5281/zenodo.5156231>
- 731 Endsley, K. A. (2021b). *simsoil: Very simple, point-scale soil hydrology model (Ver-*
 732 *sion 0.1.0)*. Zenodo. doi: <http://doi.org/10.5281/zenodo.4906830>
- 733 Endsley, K. A., Kimball, J. S., Reichle, R. H., & Watts, J. D. (2020, dec). Satellite
 734 monitoring of global surface soil organic carbon dynamics using the SMAP Level
 735 4 Carbon Product. *Journal of Geophysical Research: Biogeosciences*, 125(12).
 736 Retrieved from <https://onlinelibrary.wiley.com/doi/10.1029/2020JG006100>
 737 doi: 10.1029/2020JG006100
- 738 Entekhabi, D., Njoku, E. G., O’Neill, P. E., Kellogg, K. H., Crow, W. T., Edelstein,
 739 W. N., ... Van Zyl, J. (2010, may). The Soil Moisture Active Passive (SMAP)
 740 Mission. *Proceedings of the IEEE*, 98(5), 704–716. Retrieved from [http://](http://ieeexplore.ieee.org/document/5460980/)
 741 ieeexplore.ieee.org/document/5460980/ doi: 10.1109/JPROC.2010.2043918
- 742 Forkel, M., Carvalhais, N., Rödenbeck, C., Keeling, R., Heimann, M., Thonicke, K.,
 743 ... Reichstein, M. (2016). Enhanced seasonal CO₂ exchange caused by amplified

- 744 plant productivity in northern ecosystems. *Science*, *351*(6274), 696–699. doi:
745 10.1126/science.aac4971
- 746 Forkel, M., Carvalhais, N., Schaphoff, S., Bloh, W. V., Migliavacca, M., Thurner, M.,
747 & Thonicke, K. (2014). Identifying environmental controls on vegetation greenness
748 phenology through model-data integration. *Biogeosciences*, *11*(23), 7025–7050.
749 doi: 10.5194/bg-11-7025-2014
- 750 Friedl, M. A., Sulla-Menashe, D., Tan, B., Schneider, A., Ramankutty, N., Sibley, A.,
751 & Huang, X. (2010, jan). MODIS Collection 5 global land cover: Algorithm re-
752 finements and characterization of new datasets. *Remote Sensing of Environment*,
753 *114*(1), 168–182. Retrieved from [https://linkinghub.elsevier.com/retrieve/](https://linkinghub.elsevier.com/retrieve/pii/S0034425709002673)
754 [pii/S0034425709002673](https://linkinghub.elsevier.com/retrieve/pii/S0034425709002673) doi: 10.1016/j.rse.2009.08.016
- 755 Gaumont-Guay, D., Black, T. A., Barr, A. G., Griffis, T. J., Jassal, R. S., Krish-
756 nan, P., ... Nestic, Z. (2014, jan). Eight years of forest-floor CO₂ exchange
757 in a boreal black spruce forest: Spatial integration and long-term temporal
758 trends. *Agricultural and Forest Meteorology*, *184*, 25–35. Retrieved from
759 <https://linkinghub.elsevier.com/retrieve/pii/S0168192313002177> doi:
760 10.1016/j.agrformet.2013.08.010
- 761 Gelaro, R., McCarty, W., Suárez, M. J., Todling, R., Molod, A., Takacs, L., ...
762 Zhao, B. (2017, jul). The Modern-Era Retrospective Analysis for Research and
763 Applications, Version 2 (MERRA-2). *Journal of Climate*, *30*(14), 5419–5454.
764 Retrieved from <http://journals.ametsoc.org/doi/10.1175/JCLI-D-16-0758.1>
765 doi: 10.1175/JCLI-D-16-0758.1
- 766 Giasson, M. A., Ellison, A. M., Bowden, R. D., Crill, P. M., Davidson, E. A., Drake,
767 J. E., ... Finzi, A. C. (2013). Soil respiration in a northeastern US temperate
768 forest: A 22-year synthesis. *Ecosphere*, *4*(11). doi: 10.1890/ES13.00183.1
- 769 Global Soil Data Task Group. (2000). *Global Gridded Surfaces of Selected Soil Char-*
770 *acteristics (IGBP-DIS)* (Tech. Rep.). ORNL DAAC. doi: [https://doi.org/10.3334/](https://doi.org/10.3334/ORNLDAAC/569)
771 [ORNLDAAC/569](https://doi.org/10.3334/ORNLDAAC/569)
- 772 Graven, H. D., Keeling, R. F., Piper, S. C., Patra, P. K., Stephens, B. B.,
773 Wofsy, S. C., ... Bent, J. D. (2013). Enhanced seasonal exchange of CO₂
774 by Northern ecosystems since 1960. *Science*, *341*(6150), 1085–1089. doi:
775 10.1126/science.1239207
- 776 Hengl, T., De Jesus, J. M., Heuvelink, G. B. M., Gonzalez, M. R., Kilibarda,
777 M., Blagotić, A., ... Kempen, B. (2017). SoilGrids250m: Global gridded
778 soil information based on machine learning. *PLoS ONE*, *12*(2), 1–40. doi:
779 10.1371/journal.pone.0169748
- 780 Heskell, M. A., Atkin, O. K., Turnbull, M. H., & Griffin, K. L. (2013). Bringing the
781 Kok effect to light: A review on the integration of daytime respiration and net
782 ecosystem exchange. *Ecosphere*, *4*(8), 1–14. doi: 10.1890/ES13-00120.1
- 783 Hu, Z., Michaletz, S. T., Johnson, D. J., McDowell, N. G., Huang, Z., Zhou, X.,
784 & Xu, C. (2018, nov). Traits drive global wood decomposition rates more
785 than climate. *Global Change Biology*, *24*(11), 5259–5269. Retrieved from
786 <http://doi.wiley.com/10.1111/gcb.14357> doi: 10.1111/gcb.14357
- 787 Ito, A., Inatomi, M., Huntzinger, D. N., Schwalm, C., Michalak, A. M., Cook, R.,
788 ... Zhao, F. (2016). Decadal trends in the seasonal-cycle amplitude of terres-
789 trial CO₂ exchange resulting from the ensemble of terrestrial biosphere mod-
790 els. *Tellus, Series B: Chemical and Physical Meteorology*, *68*(1), 1–20. doi:
791 10.3402/tellusb.v68.28968
- 792 Jackson, R. B., Canadell, J., Ehleringer, J. R., Mooney, H. A., Sala, O. E., &
793 Schulze, E. D. (1996). A global analysis of root distributions for terrestrial
794 biomes. *Oecologia*, *108*, 389–411.
- 795 Järveoja, J., Nilsson, M. B., Gažovič, M., Crill, P. M., & Peichl, M. (2018). Par-
796 titioning of the net CO₂ exchange using an automated chamber system reveals
797 plant phenology as key control of production and respiration fluxes in a boreal

- 798 peatland. *Global Change Biology*, *24*(8), 3436–3451. doi: 10.1111/gcb.14292
- 799 Jassal, R. S., Black, T. A., Novak, M. D., Gaumont-Guay, D., & Nesic, Z. (2008,
800 jun). Effect of soil water stress on soil respiration and its temperature sensitivity
801 in an 18-year-old temperate Douglas-fir stand. *Global Change Biology*, *14*(6),
802 1305–1318. Retrieved from [https://onlinelibrary.wiley.com/doi/10.1111/
803 j.1365-2486.2008.01573.x](https://onlinelibrary.wiley.com/doi/10.1111/j.1365-2486.2008.01573.x) doi: 10.1111/j.1365-2486.2008.01573.x
- 804 Jian, J., Vargas, R., Anderson-Teixeira, K., Stell, E., Herrmann, V., Horn, M., ...
805 Bond-Lamberty, B. (2021). A restructured and updated global soil respira-
806 tion database (SRDB-V5). *Earth System Science Data*, *13*(2), 255–267. doi:
807 10.5194/essd-13-255-2021
- 808 Johnston, A. S. A., & Sibly, R. M. (2018, oct). The influence of soil communities on
809 the temperature sensitivity of soil respiration. *Nature Ecology & Evolution*, *2*(10),
810 1597–1602. Retrieved from [http://www.nature.com/articles/s41559-018-0648
811 -6](http://www.nature.com/articles/s41559-018-0648-6) doi: 10.1038/s41559-018-0648-6
- 812 Jones, L. A., Kimball, J. S., Reichle, R. H., Madani, N., Glassy, J., Ardizzone, J. V.,
813 ... Scott, R. L. (2017). The SMAP Level 4 Carbon Product for Monitoring
814 Ecosystem Land-Atmosphere CO₂ Exchange. *IEEE Transactions on Geoscience
815 and Remote Sensing*, *55*(11), 6517–6532. doi: 10.1109/TGRS.2017.2729343
- 816 Jung, M., Schwalm, C., Migliavacca, M., Walther, S., Camps-Valls, G., Koirala, S.,
817 ... Reichstein, M. (2020). Scaling carbon fluxes from eddy covariance sites to
818 globe: Synthesis and evaluation of the FLUXCOM approach. *Biogeosciences*,
819 *17*(5), 1343–1365. doi: 10.5194/bg-17-1343-2020
- 820 Keenan, T. F., Gray, J., Friedl, M. A., Toomey, M., Bohrer, G., Hollinger, D. Y., ...
821 Richardson, A. D. (2014, jul). Net carbon uptake has increased through warming-
822 induced changes in temperate forest phenology. *Nature Climate Change*, *4*(7),
823 598–604. Retrieved from <http://www.nature.com/articles/nclimate2253> doi:
824 10.1038/nclimate2253
- 825 Keenan, T. F., Migliavacca, M., Papale, D., Baldocchi, D., Reichstein, M., Torn,
826 M., & Wutzler, T. (2019). Widespread inhibition of daytime ecosystem respi-
827 ration. *Nature Ecology and Evolution*, *3*(3), 407–415. Retrieved from [http://
828 dx.doi.org/10.1038/s41559-019-0809-2](http://dx.doi.org/10.1038/s41559-019-0809-2) doi: 10.1038/s41559-019-0809-2
- 829 Kimball, J. S., Jones, L. A., Zhang, K., Heinsch, F. A., McDonald, K. C., &
830 Oechel, W. C. (2009). A satellite approach to estimate land-atmosphere
831 CO₂ exchange for boreal and Arctic biomes using MODIS and AMSR-E.
832 *IEEE Transactions on Geoscience and Remote Sensing*, *47*(2), 569–587. doi:
833 10.1109/TGRS.2008.2003248
- 834 Koster, R. D., Guo, Z., Yang, R., Dirmeyer, P. A., Mitchell, K., & Puma, M. J.
835 (2009, aug). On the nature of soil moisture in land surface models. *Journal of
836 Climate*, *22*(16), 4322–4335. Retrieved from [http://journals.ametsoc.org/
837 doi/abs/10.1175/2009JCLI2832.1](http://journals.ametsoc.org/doi/abs/10.1175/2009JCLI2832.1) doi: 10.1175/2009JCLI2832.1
- 838 Koster, R. D., Suarez, M. J., Ducharne, A., Stieglitz, M., & Kumar, P. (2000, oct).
839 A catchment-based approach to modeling land surface processes in a general
840 circulation model: 1. Model structure. *Journal of Geophysical Research: At-
841 mospheres*, *105*(D20), 24809–24822. Retrieved from [http://doi.wiley.com/
842 10.1029/2000JD900328](http://doi.wiley.com/10.1029/2000JD900328) <http://doi.wiley.com/10.1029/2000JD900327> doi:
843 10.1029/2000JD900327
- 844 Koven, C. D., Hugelius, G., Lawrence, D. M., & Wieder, W. R. (2017, nov).
845 Higher climatological temperature sensitivity of soil carbon in cold than
846 warm climates. *Nature Climate Change*, *7*(11), 817–822. Retrieved from
847 <http://www.nature.com/articles/nclimate3421> doi: 10.1038/nclimate3421
- 848 Koven, C. D., Riley, W. J., Subin, Z. M., Tang, J. Y., Torn, M. S., Collins, W. D.,
849 ... Swenson, S. C. (2013). The effect of vertically resolved soil biogeochemistry
850 and alternate soil C and N models on C dynamics of CLM4. *Biogeosciences*,
851 *10*(11), 7109–7131. doi: 10.5194/bg-10-7109-2013

- 852 Lawrence, D. M., Fisher, R. A., Koven, C. D., Oleson, K. W., Swenson, S. C., Bo-
 853 nan, G. B., ... (2019, dec). The Community Land Model version 5: Descrip-
 854 tion of new features, benchmarking, and impact of forcing uncertainty. *Journal*
 855 *of Advances in Modeling Earth Systems*, *11*(12), 4245–4287. Retrieved from
 856 <https://onlinelibrary.wiley.com/doi/abs/10.1029/2018MS001583> doi:
 857 10.1029/2018MS001583
- 858 Leitner, S., Sae-Tun, O., Kranzinger, L., Zechmeister-Boltenstern, S., & Zimmer-
 859 mann, M. (2016, jun). Contribution of litter layer to soil greenhouse gas
 860 emissions in a temperate beech forest. *Plant and Soil*, *403*(1-2), 455–469. Re-
 861 trieved from <http://link.springer.com/10.1007/s11104-015-2771-3> doi:
 862 10.1007/s11104-015-2771-3
- 863 Messerschmidt, J., Parazoo, N. C., Wunch, D., Deutscher, N. M., Roehl, C.,
 864 Warneke, T., & Wennberg, P. O. (2013). Evaluation of seasonal atmosphere-
 865 biosphere exchange estimations with TCCON measurements. *Atmospheric Chem-*
 866 *istry and Physics*, *13*(10), 5103–5115. doi: 10.5194/acp-13-5103-2013
- 867 Migliavacca, M., Reichstein, M., Richardson, A. D., Mahecha, M. D., Cremonese,
 868 E., Delpierre, N., ... Cescatti, A. (2015). Influence of physiological phenology on
 869 the seasonal pattern of ecosystem respiration in deciduous forests. *Global Change*
 870 *Biology*, *21*(1), 363–376. doi: 10.1111/gcb.12671
- 871 Myneni, R. B., Knyazikhin, Y., & Park, T. (2015). *MCD15A2H*
 872 *MODIS/Terra+ Aqua Leaf Area Index/FPAR 8-day L4 Global 500m SIN Grid*
 873 *V006 [Data set]*. Retrieved 2021-07-02, from [https://doi.org/10.5067/MODIS/](https://doi.org/10.5067/MODIS/MCD15A2H.006)
 874 [MCD15A2H.006](https://doi.org/10.5067/MODIS/MCD15A2H.006) doi: <https://doi.org/10.5067/MODIS/MCD15A2H.006>
- 875 Nielsen, T. F., Ravn, N. R., & Michelsen, A. (2019, nov). Increased CO₂ efflux
 876 due to long-term experimental summer warming and litter input in subarctic
 877 tundra – CO₂ fluxes at snowmelt, in growing season, fall and winter. *Plant and*
 878 *Soil*, *444*(1-2), 365–382. Retrieved from [http://link.springer.com/10.1007/](http://link.springer.com/10.1007/s11104-019-04282-9)
 879 [s11104-019-04282-9](http://link.springer.com/10.1007/s11104-019-04282-9) doi: 10.1007/s11104-019-04282-9
- 880 Noormets, A., Chen, J., Gu, L., & Desai, A. (2009). The phenology of gross ecosys-
 881 tem productivity and ecosystem respiration in temperate hardwood and conifer
 882 chronosequences. *Phenology of Ecosystem Processes: Applications in Global*
 883 *Change Research*, 1–275. doi: 10.1007/978-1-4419-0026-5
- 884 Noormets, A., Gavazzi, M. J., McNulty, S. G., Domec, J.-C., Sun, G., King, J. S.,
 885 & Chen, J. (2010, jan). Response of carbon fluxes to drought in a coastal plain
 886 loblolly pine forest. *Global Change Biology*, *16*(1), 272–287. Retrieved from
 887 <https://onlinelibrary.wiley.com/doi/10.1111/j.1365-2486.2009.01928.x>
 888 doi: 10.1111/j.1365-2486.2009.01928.x
- 889 Oikawa, P. Y., Grantz, D. A., Chatterjee, A., Eberwein, J. E., Allsman, L. A., &
 890 Jenerette, G. D. (2014, apr). Unifying soil respiration pulses, inhibition, and
 891 temperature hysteresis through dynamics of labile soil carbon and O₂. *Jour-*
 892 *nal of Geophysical Research: Biogeosciences*, *119*(4), 521–536. Retrieved from
 893 <http://doi.wiley.com/10.1002/2013JG002434> doi: 10.1002/2013JG002434
- 894 Papale, D., & Valentini, R. (2003). A new assessment of European forests carbon ex-
 895 changes by eddy fluxes and artificial neural network spatialization. *Global Change*
 896 *Biology*, *9*(4), 525–535. doi: 10.1046/j.1365-2486.2003.00609.x
- 897 Parazoo, N. C., Arneeth, A., Pugh, T. A. M., Smith, B., Steiner, N., Luus, K., ...
 898 Miller, C. (2018). Spring photosynthetic onset and net CO₂ uptake in Alaska
 899 triggered by landscape thawing. *Global Change Biology*, *24*(8), 3416–3435. doi:
 900 10.1111/gcb.14283
- 901 Peng, S., Ciais, P., Chevallier, F., Peylin, P., Cadule, P., Sitch, S., ... Wang, X.
 902 (2014). Global biogeochemical cycles simulated by terrestrial ecosystem models.
 903 *Global Biogeochemical Cycles*, *29*, 46–64. doi: 10.1002/2014GB004931. Received
- 904 Peng, S., Ciais, P., Chevallier, F., Peylin, P., Cadule, P., Sitch, S., ... Zhao,
 905 H. (2015, jan). Benchmarking the seasonal cycle of CO₂ fluxes simulated

- 906 by terrestrial ecosystem models. *Global Biogeochemical Cycles*, 29(1), 46–
 907 64. Retrieved from <http://doi.wiley.com/10.1002/2014GB004931> doi:
 908 10.1002/2014GB004931
- 909 Peng, S., Piao, S., Ciais, P., Myneni, R. B., Chen, A., Chevallier, F., . . . Zeng, H.
 910 (2013). Asymmetric effects of daytime and night-time warming on Northern
 911 Hemisphere vegetation. *Nature*, 501(7465), 88–92. doi: 10.1038/nature12434
- 912 Randerson, J. T., Thompson, M. V., Malmstrom, C. M., Field, C. B., & Fung, I. Y.
 913 (1996). Substrate limitations for heterotrophs: Implications for models that esti-
 914 mate the seasonal cycle of atmospheric CO₂. *Global Biogeochemical Cycles*, 10(4),
 915 585–602. doi: 10.1029/96GB01981
- 916 Reichle, R. H., De Lannoy, G., Koster, R. D., Crow, W. T., Kimball, J. S., & Liu,
 917 Q. (2019). *SMAP L4 Global 3-hourly 9 km EASE-Grid Surface and Root*
 918 *Zone Soil Moisture Geophysical Data, Version 4*. Boulder, Colorado, U.S.A.:
 919 NASA National Snow and Ice Data Center Distributed Active Archive Cen-
 920 ter. Retrieved 2019-08-01, from <https://nsidc.org/data/SPL4SMGP> doi:
 921 10.5067/KPJNN2GI1DQR
- 922 Reichle, R. H., De Lannoy, G. J. M., Liu, Q., Koster, R. D., Kimball, J. S.,
 923 Crow, W. T., . . . Smith, E. B. (2017, dec). Global Assessment of the SMAP
 924 Level-4 Surface and Root-Zone Soil Moisture Product Using Assimilation
 925 Diagnostics. *Journal of Hydrometeorology*, 18(12), 3217–3237. Retrieved
 926 from <http://journals.ametsoc.org/doi/10.1175/JHM-D-17-0130.1> doi:
 927 10.1175/JHM-D-17-0130.1
- 928 Reichstein, M., Rey, A., Freibauer, A., Tenhunen, J., Valentini, R., Banza, J., . . .
 929 Yakir, D. (2003). Modeling temporal and large-scale spatial variability of soil
 930 respiration from soil water availability, temperature and vegetation productivity
 931 indices. *Global Biogeochemical Cycles*, 17(4). doi: 10.1029/2003gb002035
- 932 Richardson, A. D., Andy Black, T., Ciais, P., Delbart, N., Friedl, M. A., Gobron,
 933 N., . . . Varlagin, A. (2010, oct). Influence of spring and autumn phenological
 934 transitions on forest ecosystem productivity. *Philosophical Transactions of the*
 935 *Royal Society B: Biological Sciences*, 365(1555), 3227–3246. Retrieved from
 936 <https://royalsocietypublishing.org/doi/10.1098/rstb.2010.0102> doi:
 937 10.1098/rstb.2010.0102
- 938 Ryan, E. M., Ogle, K., Zelikova, T. J., Lecain, D. R., Williams, D. G., Morgan,
 939 J. A., & Pendall, E. (2015). Antecedent moisture and temperature conditions
 940 modulate the response of ecosystem respiration to elevated CO₂ and warming.
 941 *Global Change Biology*, 21(7), 2588–2602. doi: 10.1111/gcb.12910
- 942 Sánchez-Cañete, E. P., Oyonarte, C., Serrano-Ortiz, P., Curiel Yuste, J., Pérez-
 943 Priego, O., Domingo, F., & Kowalski, A. S. (2016, aug). Winds induce
 944 CO₂ exchange with the atmosphere and vadose zone transport in a karstic
 945 ecosystem. *Journal of Geophysical Research: Biogeosciences*, 121(8), 2049–
 946 2063. Retrieved from <http://doi.wiley.com/10.1002/2016JG003500> doi:
 947 10.1002/2016JG003500
- 948 Schaefer, G. L., Cosh, M. H., & Jackson, T. J. (2007, dec). The USDA Natural
 949 Resources Conservation Service Soil Climate Analysis Network (SCAN). *Journal*
 950 *of Atmospheric and Oceanic Technology*, 24(12), 2073–2077. Retrieved
 951 from <http://journals.ametsoc.org/doi/10.1175/2007JTECHA930.1> doi:
 952 10.1175/2007JTECHA930.1
- 953 Shi, M., Parazoo, N. C., Jeong, S. J., Birch, L., Lawrence, P., Euskirchen, E. S., &
 954 Miller, C. E. (2020). Exposure to cold temperature affects the spring phenology of
 955 Alaskan deciduous vegetation types. *Environmental Research Letters*, 15(2). doi:
 956 10.1088/1748-9326/ab6502
- 957 Sihi, D., Davidson, E. A., Chen, M., Savage, K. E., Richardson, A. D., Keenan,
 958 T. F., & Hollinger, D. Y. (2018). Merging a mechanistic enzymatic model of
 959 soil heterotrophic respiration into an ecosystem model in two AmeriFlux sites of

- 960 northeastern USA. *Agricultural and Forest Meteorology*, 252(May 2017), 155–166.
 961 Retrieved from <https://doi.org/10.1016/j.agrformet.2018.01.026> doi:
 962 10.1016/j.agrformet.2018.01.026
- 963 Sulman, B. N., Desai, A. R., Schroeder, N. M., Ricciuto, D., Barr, A., Richardson,
 964 A. D., ... Weng, E. (2012). Impact of hydrological variations on modeling of
 965 peatland CO₂ fluxes: Results from the North American Carbon Program site
 966 synthesis. *Journal of Geophysical Research: Biogeosciences*, 117(1), 1–21. doi:
 967 10.1029/2011JG001862
- 968 Tao, J., Reichle, R. H., Koster, R. D., Forman, B. A., & Xue, Y. (2017). Evalua-
 969 tion and Enhancement of Permafrost Modeling With the NASA Catchment Land
 970 Surface Model. *Journal of Advances in Modeling Earth Systems*, 9(7), 2771–2795.
 971 doi: 10.1002/2017MS001019
- 972 Thum, T., Nabel, J. E. M. S., Tsuruta, A., Aalto, T., Dlugokencky, E. J., Liski,
 973 J., ... Zaehle, S. (2020, nov). Evaluating two soil carbon models within
 974 the global land surface model JSBACH using surface and spaceborne ob-
 975 servations of atmospheric CO₂. *Biogeosciences*, 17(22), 5721–5743. Re-
 976 trieved from <https://bg.copernicus.org/articles/17/5721/2020/> doi:
 977 10.5194/bg-17-5721-2020
- 978 Turner, D. P., Ritts, W. D., Cohen, W. B., Gower, S. T., Running, S. W., Zhao, M.,
 979 ... Ahl, D. E. (2006, jun). Evaluation of MODIS NPP and GPP products across
 980 multiple biomes. *Remote Sensing of Environment*, 102(3-4), 282–292. Retrieved
 981 from <https://linkinghub.elsevier.com/retrieve/pii/S0034425706000873>
 982 doi: 10.1016/j.rse.2006.02.017
- 983 Ueyama, M., Yoshikawa, K., & Takagi, K. (2018, jul). A cool-temperate young
 984 larch plantation as a net methane source - A 4-year continuous hyperbolic relaxed
 985 eddy accumulation and chamber measurements. *Atmospheric Environment*, 184,
 986 110–120. Retrieved from [https://linkinghub.elsevier.com/retrieve/pii/](https://linkinghub.elsevier.com/retrieve/pii/S1352231018302565)
 987 [S1352231018302565](https://linkinghub.elsevier.com/retrieve/pii/S1352231018302565) doi: 10.1016/j.atmosenv.2018.04.025
- 988 Vargas, R., Sánchez-Cañete P, E., Serrano-Ortiz, P., Curiel Yuste, J., Domingo, F.,
 989 López-Ballesteros, A., & Oyonarte, C. (2018, aug). Hot-Moments of Soil CO₂
 990 Efflux in a Water-Limited Grassland. *Soil Systems*, 2(3), 47. Retrieved from
 991 <http://www.mdpi.com/2571-8789/2/3/47> doi: 10.3390/soilsystems2030047
- 992 Wan, J., Tokunaga, T. K., Dong, W., Williams, K. H., Kim, Y., Conrad, M. E., ...
 993 Hubbard, S. S. (2018, sep). Deep Unsaturated Zone Contributions to Carbon Cy-
 994 cling in Semiarid Environments. *Journal of Geophysical Research: Biogeosciences*,
 995 123(9), 3045–3054. Retrieved from [https://onlinelibrary.wiley.com/doi/](https://onlinelibrary.wiley.com/doi/10.1029/2018JG004669)
 996 [10.1029/2018JG004669](https://onlinelibrary.wiley.com/doi/10.1029/2018JG004669) doi: 10.1029/2018JG004669
- 997 Watts, J. D., Kimball, J. S., Parmentier, F. J. W., Sachs, T., Rinne, J., Zona, D.,
 998 ... Aurela, M. (2014, apr). A satellite data driven biophysical modeling ap-
 999 proach for estimating northern peatland and tundra CO₂ and CH₄ fluxes. *Biogeosciences*, 11(7), 1961–1980. Re-
 1000 trieved from <https://bg.copernicus.org/articles/11/1961/2014/> doi:
 1001 10.5194/bg-11-1961-2014
- 1002
- 1003 Wehr, R., Munger, J. W., McManus, J. B., Nelson, D. D., Zahniser, M. S., David-
 1004 son, E. A., ... Saleska, S. R. (2016). Seasonality of temperate forest photosyn-
 1005 thesis and daytime respiration. *Nature*, 534(7609), 680–683. Retrieved from
 1006 <http://dx.doi.org/10.1038/nature17966> doi: 10.1038/nature17966
- 1007 Winnick, M. J., Lawrence, C. R., McCormick, M., Druhan, J. L., & Maher, K.
 1008 (2020). Soil respiration response to rainfall modulated by plant phenology in a
 1009 montane meadow, East River, Colorado, USA. *Journal of Geophysical Research:*
 1010 *Biogeosciences*, 125(10), 1–20. doi: 10.1029/2020JG005924
- 1011 Wohlfahrt, G., Bahn, M., Haslwanter, A., Newsely, C., & Cernusca, A. (2005). Es-
 1012 timation of daytime ecosystem respiration to determine gross primary production
 1013 of a mountain meadow. *Agricultural and Forest Meteorology*, 130(1-2), 13–25. doi:

- 1014 10.1016/j.agrformet.2005.02.001
 1015 Wu, C., Chen, J. M., Black, T. A., Price, D. T., Kurz, W. A., Desai, A. R., ...
 1016 Blanken, P. D. (2013). Interannual variability of net ecosystem productivity
 1017 in forests is explained by carbon flux phenology in autumn. *Global Ecology and*
 1018 *Biogeography*, 22(8), 994–1006. doi: 10.1111/geb.12044
- 1019 Yi, Y., Kimball, J. S., Jones, L. A., Reichle, R. H., Nemani, R., & Margolis, H. A.
 1020 (2013, jun). Recent climate and fire disturbance impacts on boreal and arc-
 1021 tic ecosystem productivity estimated using a satellite-based terrestrial carbon
 1022 flux model. *Journal of Geophysical Research: Biogeosciences*, 118(2), 606–
 1023 622. Retrieved from <http://doi.wiley.com/10.1002/jgrg.20053> doi:
 1024 10.1002/jgrg.20053
- 1025 Yi, Y., Kimball, J. S., Watts, J. D., Natali, S. M., Zona, D., Liu, J., ... Miller, C. E.
 1026 (2020, nov). Investigating the sensitivity of soil heterotrophic respiration to recent
 1027 snow cover changes in Alaska using a satellite-based permafrost carbon model.
 1028 *Biogeosciences*, 17(22), 5861–5882. Retrieved from [https://bg.copernicus.org/](https://bg.copernicus.org/articles/17/5861/2020/)
 1029 [articles/17/5861/2020/](https://bg.copernicus.org/articles/17/5861/2020/) doi: 10.5194/bg-17-5861-2020
- 1030 Zhang, Q., Phillips, R. P., Manzoni, S., Scott, R. L., Oishi, A. C., Finzi, A., ...
 1031 Novick, K. A. (2018, sep). Changes in photosynthesis and soil moisture drive the
 1032 seasonal soil respiration-temperature hysteresis relationship. *Agricultural and For-*
 1033 *est Meteorology*, 259, 184–195. Retrieved from [https://linkinghub.elsevier](https://linkinghub.elsevier.com/retrieve/pii/S0168192318301515)
 1034 [.com/retrieve/pii/S0168192318301515](https://linkinghub.elsevier.com/retrieve/pii/S0168192318301515) doi: 10.1016/j.agrformet.2018.05.005
- 1035 Zhao, F., & Zeng, N. (2014, dec). Continued increase in atmospheric CO2 sea-
 1036 sonal amplitude in the 21st century projected by the CMIP5 Earth system
 1037 models. *Earth System Dynamics*, 5(2), 423–439. Retrieved from [https://](https://esd.copernicus.org/articles/5/423/2014/)
 1038 esd.copernicus.org/articles/5/423/2014/ doi: 10.5194/esd-5-423-2014
- 1039 Zhao, F., Zeng, N., Asrar, G., Friedlingstein, P., Ito, A., Jain, A., ... Zaehle, S.
 1040 (2016). Role of CO2, climate and land use in regulating the seasonal amplitude
 1041 increase of carbon fluxes in terrestrial ecosystems: A multimodel analysis. *Biogeo-*
 1042 *sciences*, 13(17), 5121–5137. doi: 10.5194/bg-13-5121-2016
- 1043 Āupek, B., Launiainen, S., Peltoniemi, M., Sievänen, R., Perttunen, J., Kulmala, L.,
 1044 ... Lehtonen, A. (2019). Evaluating CENTURY and Yasso soil carbon models
 1045 for CO2 emissions and organic carbon stocks of boreal forest soil with Bayesian
 1046 multi-model inference. *European Journal of Soil Science*, 70(4), 847–858. doi:
 1047 10.1111/ejss.12805

Supplemental Materials for “Soil respiration phenology improves modeled phase of terrestrial net ecosystem exchange in northern hemisphere”

K. Arthur Endsley¹, John S. Kimball¹, and Rolf H. Reichle²

¹Numerical Terradynamic Simulation Group (NTSG), W.A. Franke College of Forestry and Conservation, University of Montana, Missoula, MT

²Global Modeling and Assimilation Office, NASA Goddard Space Flight Center, Greenbelt, Maryland, USA

Appendix A: Soil Hydrology Model

The soil hydrology model developed for this study proceeds in four main steps that are repeated for each daily time step. First, the maximum soil water infiltration rate, based on soil ice content and the land surface saturation fraction, is calculated. Second, soil water loss through potential transpiration is calculated based on the Priestly-Taylor method [Mu et al., 2011] and this is converted to actual transpiration in each soil layer based on the root distributions of Jackson et al. [1996] and soil water stress, based on the wilting point and field capacity estimates of Balland et al. [2008]. Third, the change in soil water content, $\Delta \theta$, is calculated based on Darcy’s Law and the Richards equation. Finally, lateral drainage due to sub-surface saturation is removed and the soil water content in each layer is rebalanced so as to maintain physical limits.

The model uses daily average estimates of surface infiltration and potential transpiration rates to estimate daily changes in volumetric soil moisture, θ , using sub-daily (e.g., hourly) time steps. Hydraulic conductivity, soil matric potential, and soil water diffusion (based on the Richards equation) are calculated as in CLM 5.0 [Lawrence et al., 2018], based on empirical equations from Clapp and Hornberger [1978] and Cosby et al. [1984]. Saturated hydraulic conductivity and saturated matric potential, both functions of soil texture, are calculated as in CLM 4.0. Soil texture, porosity, and daily surface infiltration (mm s^{-1}) are taken from the Catchment land model and SMAP L4SM. The fraction of the land surface that is saturated was calculated based on relative humidity [Mu et al., 2011], which was calculated from VPD and the saturation vapor pressure [Allen et al., 1998, Chapter 3]. Topographic slope was computed at each site based on the L4SM global 9-km elevation model.

The maximum surface infiltration rate is calculated as in CLM 5.0:

$$q_{max} = (1 - f_{sat})\Theta_{ice}k_{sat} \quad (1)$$

Where f_{sat} is the fraction of the land surface that is saturated, Θ_{ice} is the impedance due to soil ice content, and k_{sat} is the saturated hydraulic conductivity. The actual surface infiltration rate is taken to be the minimum of q_{max} and the daily average rate from L4SM. The impedance due to ice is also calculated as in CLM 5.0:

$$\Theta_{ice} = 10^{-\Omega F_{ice}} \quad \text{where} \quad F_{ice} = \theta \frac{f_{ice}}{\theta_{sat}} = \frac{\theta_{ice}}{\theta_{sat}}; \Omega = 6 \quad (2)$$

Where f_{ice} is the ice fraction of the combined liquid and ice water volumes, after the empirical formulation by Decker and Zeng [2006, Equation 4]. For simplicity, explicit phase changes and ice content are not tracked; instead, f_{ice} is used as an instantaneous estimate of ice content as a fraction of total soilmoisture.

Daily potential transpiration is calculated using the Priestly-Taylor method [Mu et al., 2011] and is reduced by a factor, β , representing plant water stress:

$$\beta = \left(\frac{\theta_{liq} - \theta_{WP}}{\theta_{FC} - \theta_{WP}} \right)^q \quad (3)$$

Where θ_{liq} is the liquid soil volumetric water content; θ_{FC} and θ_{WP} are the soil moisture at field capacity and at wilting point, respectively; and q is an empirical coefficient describing the curvature of the relationship between transpiration and available soil water [Verhoef and Egea, 2014]. We set $q = 1$ for this study. Field capacity and wilting point were defined based on soil texture using the empirical relationships of Balland et al. [2008]. Actual transpiration (potential transpiration reduced by β) is partitioned across the soil layers using the empirical root profiles of Jackson et al. [1996, Table 1], based on matching PFTs; the Evergreen Needleleaf PFT is the average of the boreal forest and temperate coniferous types of Jackson et al. [1996].

The surface infiltration rate and the transpiration from each layer represent two key source and sink terms, respectively, in the water balance equation, which is identical to that used in CLM 5.0 [Lawrence et al., 2018]:

$$\Delta z_i \frac{\partial \theta_{liq,i}}{\partial t} = -q_{i-1} + q_i - e_i$$

Where Δz_i is the thickness (mm) of soil layer i , q_{i-1} is the flow into layer i from above (layers are enumerated downward from the surface), q_i is the flow out of layer i to the layer below, and e_i is the hydraulic sink of transpiration loss. For the surface layer, q_{i-1} is equal to the surface infiltration rate. Equation , applied to each soil layer, forms a sparse, tridiagonal system of equations where the change in liquid soil moisture in each layer, $\Delta \theta_{liq}$, is solved for simultaneously.

There are two additional, potential hydraulic sinks that are computed separately: free drainage from the bottom layer and lateral drainage in the presence of sub-surface saturation, including from perched, saturated zones. The free drainage condition is equivalent to the “flux” boundary condition of CLM 5.0 [UCAR, 2020] and is based on the hydraulic conductivity, k , and derivative of k of the bottom layer:

$$q_{drain} = k_i + \left[\frac{\partial k}{\partial \theta_{liq}} \times \Delta \theta_{liq} \right]_i \quad (4)$$

When the soil column is saturated from the bottom-up, lateral drainage from the saturated layer(s) is calculated after CLM 4.5 [Oleson et al., 2013]:

$$q_{drain} = \Theta_{ice} 10 \sin(\gamma) \exp(-f_{drain} z_{\nabla}) \quad \text{where} \quad f_{drain} = 2.5 \text{ m}^{-1} \quad (5)$$

Where γ is the topographic slope and z_{∇} is the depth to the water table (top of saturated zone). Lateral drainage from a perched, saturated zone is also calculated after CLM 4.5:

$$q_{perch} = 10^{-5} \sin(\gamma) \left(\frac{\sum_{i=j}^{i=k} \Theta_{ice,i} k_{sat}(z_i) \Delta z_i}{\sum_{i=j}^{i=k} \Delta z_i} \right) (z_{frost} - z_{\nabla,perch}) \quad (6)$$

Where j and k are the soil layers that are perched and frozen (first such layer counting down from the surface), respectively, and z_{frost} and $z_{\nabla,perch}$ are the depths to the frozen and perched layers.

After the change in liquid soil moisture is applied and lateral drainage is removed, soil moisture is manually re-balanced so as to maintain each layer within physical limits of $1 \text{ mm} \leq \theta_{liq,i} \Delta z_i \leq (\phi - \theta_{ice,i}) \Delta z_i$, as described in Lawrence et al. [2018]. While the maximum surface infiltration rate and the actual transpiration rate are calculated once per day, the remaining steps are taken using sub-daily time intervals, usually less than 1 hour, and the soil moisture of the time final step is recorded as a daily snapshot and used as the initial conditions for the next day. The sub-daily time step varies according to the adaptive time-stepping scheme of CLM 5.0 [Lawrence et al., 2019]. All modeled sites are spun-up over a 20-year period to equilibrium soil moisture using a 365-day climatology of driver datasets.

Supplemental Tables

Table S1: The 25 COSORE datasets used in this study. *These sites provided concurrent, daily soil moisture and temperature measurements along with CO₂ flux. **This site was reported as “Open shrubland” and was mapped to the MOD12Q1 PFT “Shrubland.” ***This “wetland” site is a northern peatland and was mapped to MOD12Q1 PFT “Grassland.”

Dataset	PFT	Citation
d20190424_ZHANG_maple	DBF	[Zhang et al., 2018]
d20190424_ZHANG_oak	DBF	[Zhang et al., 2018]
d20200212_ATAKA*	DBF	[Ataka et al., 2014]
d20200212_KAYE_LNE*	DBF	n.a.
d20200212_KAYE_LNW*	DBF	n.a.
d20200212_KAYE_LSE*	DBF	n.a.
d20200212_KAYE_LSW*	DBF	n.a.
d20200212_KAYE_UNE*	DBF	n.a.
d20200212_KAYE_USE*	DBF	n.a.
d20200212_KAYE_USW*	DBF	n.a.
d20200221_MATHES	DBF	[Curtis et al., 2005]
d20200224_MATHES	DBF	[Detto et al., 2013]
d20200328_UEYAMA_TESHIO	DNF	[Ueyama et al., 2018]
d20200228_RENCHON	EBF	n.a.
d20200108_JASSAL	ENF	[Jassal et al., 2008]
d20200114_CARBONE_SC_EMBUDO*	ENF	[Carbone et al., 2011]
d20200114_CARBONE_SC_SAUCE*	ENF	[Carbone et al., 2013]
d20200120_CHANG*	ENF	[Chang et al., 2008]
d20200122_BLACK	ENF	[Gaumont-Guay et al., 2014]
d20200220_GAVAZZI	ENF	[Noormets et al., 2010]
d20200417_ARAIN_TP39	ENF	[Arain, 2018]
d20200331_PEICHL	GRS***	[Järveoja et al., 2018]
d20200423_OYONARTE*	GRS	[Vargas et al., 2018]
d20191017_BALDOCCHI	SHB	[Baldocchi et al., 2006]
d20200423_SANCHEZ-CANETE*	SHB**	[Sánchez-Cañete et al., 2016]

Table S2: Day-of-year (DOY) of NEE minimum, RECO maximum for EC flux towers (“Towers”) and mean difference in DOY (experiment minus Towers), in days, for each experiment, based on the mean NEE seasonal cycle, identified using a low-pass filter, for all sites above 40 degrees N latitude.

Product	Peak RECO DOY	Peak NEE DOY	RECO Phase (days)	NEE Phase (days)
Towers	197	181	n.a.	n.a.
NRv8.3	183	196	-14	+15
NRv8.3 + Kok Effect	184	196	-13	+15
NRv8.3 + Litterfall Phenology	187	182	-10	+1
NRv8.3 + O2 Limit	186	186	-11	+5
NRv8.3 + Soil Profile	185	186	-12	+5
NRv8.3 + O2 Limit + Litterfall	187	182	-10	+1
NRv8.3 + Soil Profile + Litterfall	186	183	-11	+2
NRv8.3 + Soil Profile + O2 Limit	186	186	-11	+5
NRv8.3 + Soil Profile + O2 Limit + Litterfall	186	183	-11	+2

Table S3: Mean difference in day-of-year (DOY) of NEE minimum, RECO maximum for each experiment compared to that of EC flux towers (experiment minus Towers), based on the seasonal cycle north of 40 degrees N latitude using Fourier regression. Standard deviation across PFTs is shown in parentheses.

Product	RECO Phase (days)	NEE Phase (days)
Towers	n.a. (4.7)	n.a. (14.6)
NRv8.3	-12.0 (4.7)	26.2 (17.6)
NRv8.3 + Kok Effect	-11.9 (5.1)	22.8 (15.4)
NRv8.3 + O2 Limit	-7.4 (4.5)	11.0 (13.4)
NRv8.3 + Litterfall Phenology	-1.6 (7.3)	-4.7 (9.3)
NRv8.3 + Soil Profile	-9.4 (3.4)	15.6 (13.1)
NRv8.3 + O2 Limit + Litterfall	-0.6 (6.2)	-17.9 (21.1)
NRv8.3 + Soil Profile + O2 Limit	-4.4 (5.5)	-7.2 (21.1)
NRv8.3 + Soil Profile + Litterfall	-4.8 (4.6)	4.2 (9.6)
NRv8.3 + Soil Profile + O2 Limit + Litterfall	-2.3 (6.2)	-13.5 (18.4)

Table S4: Day-of-year (DOY) of RECO maximum for EC flux towers (“Towers”) and difference in DOY (experiment minus Towers), in days, for each experiment, based on the mean RECO seasonal cycle, identified using Fourier regression, for all sites above 40 degrees N latitude.

Product	ENF	DNF	DBF	SHB	GRS	CCR	BCR
NRv8.3	-11.9	-20.2	-10.9	-6.2	-4.8	-10.5	-19.6
NRv8.3 + Kok Effect	-11.5	-20.8	-10.7	-6.0	-4.0	-11.0	-19.3
NRv8.3 + O2 Limit	-8.8	-18.8	-5.0	-3.1	-2.4	-4.4	-9.0
NRv8.3 + Litterfall Phenology	-8.0	-11.3	2.7	-1.6	0.9	-1.4	7.7
NRv8.3 + Soil Profile	-10.3	-18.2	-6.1	-7.2	-3.7	-6.6	-14.0
NRv8.3 + O2 Limit + Litterfall	-5.9	-10.3	2.1	1.0	1.1	1.5	6.1
NRv8.3 + Soil Profile + O2 Limit	-8.4	-15.5	-1.4	-4.7	-2.9	0.7	1.3
NRv8.3 + Soil Profile + Litterfall	-9.0	-12.3	-0.9	-5.7	-1.9	-2.4	-1.0
NRv8.3 + Soil Profile + O2 Limit + Litterfall	-7.4	-12.6	1.0	-3.7	-1.2	2.2	5.6

Table S5: Difference in day-of-year (DOY) of NEE minimum and RECO maximum for each experiment and for the EC flux towers (“Towers”) compared to that of FLUXCOM (experiment/ Towers minus FLUXCOM), based on the seasonal cycle north of 40 degrees N latitude using Fourier regression.

Product	RECO Phase (days)	NEE Phase (days)
Towers	+5.7	-2.2
NRv8.3	-5.9	+16.1
NRv8.3 + Kok Effect	-5.8	+16.2
NRv8.3 + Litterfall Phenology	+3.4	-8.2
NRv8.3 + O2 Limit	-0.9	+1.3
NRv8.3 + Soil Profile	-2.7	+6.5
NRv8.3 + O2 Limit + Litterfall	+4.7	-20.5
NRv8.3 + Soil Profile + Litterfall	+1.0	-3.3
NRv8.3 + Soil Profile + O2 Limit	+2.1	-24.6
NRv8.3 + Soil Profile + O2 Limit + Litterfall	+3.9	-28.2

Table S6: The mean $R_H:R_S$ ratios, and standard deviation in ratio across studies, from the Soil Respiration Database (SRDB) version 5, based on inferring Plant Functional Types from reported biome, ecosystem type, and leaf habit.

PFT	Rh:Rs Ratio	Std. Dev.
DBF	0.581	0.192
EBF	0.597	0.172
ENF	0.599	0.198
GRS	0.584	0.192
SHB	0.637	0.230
Cropland	0.642	0.210
Other	0.634	0.198

Supplemental Figures

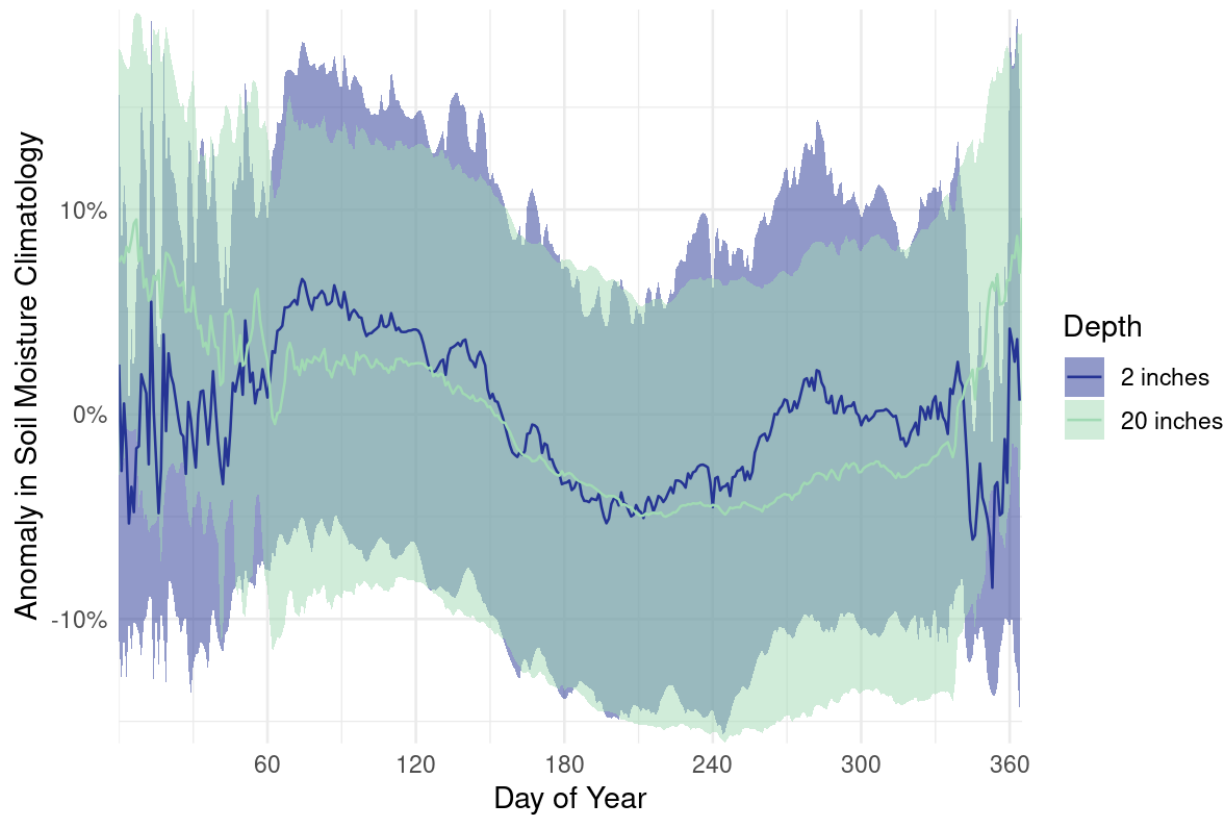


Figure S1: The mean seasonal cycle of soil moisture (SM) across USCRN and SCAN sites at the same depth north of 40 degrees N latitude. Very high variability is seen in the winter months, when *in situ* soil moisture measurement is less reliable, but a clear increase in surface soil moisture can be seen in spring. SM data were first cleaned, removing spikes and measurements during freezing conditions. SM measurements are unreliable at near or below freezing, which is the cause of the high variability seen in winter months.

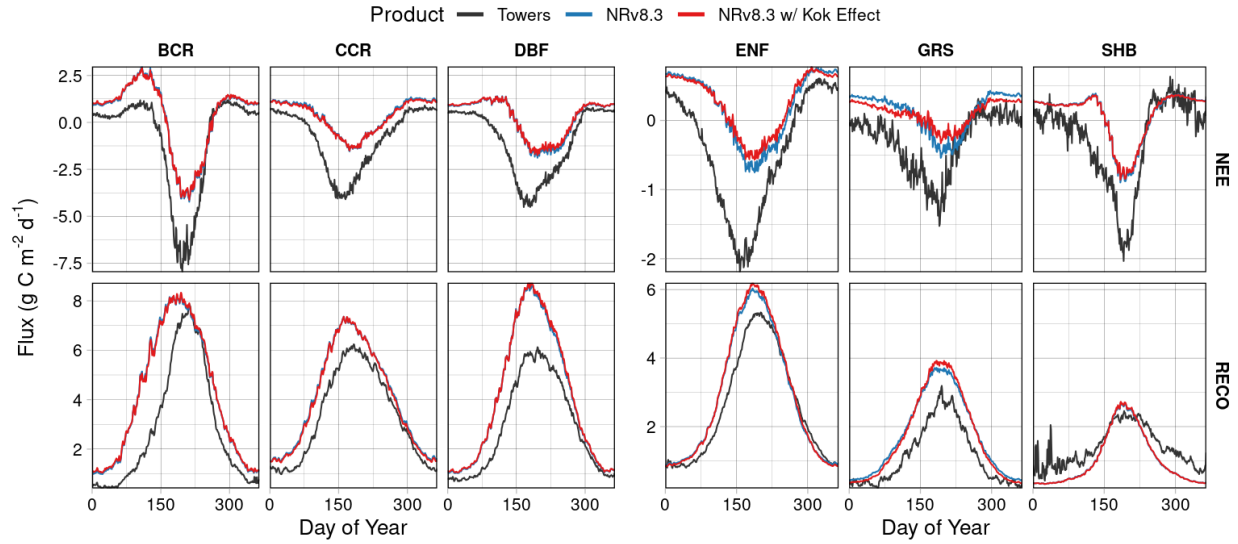


Figure S2: NEE and RECO seasonal cycles at each EC flux tower site in each PFT group, as modeled in the NRv8.3 + Kok Effect experiment.

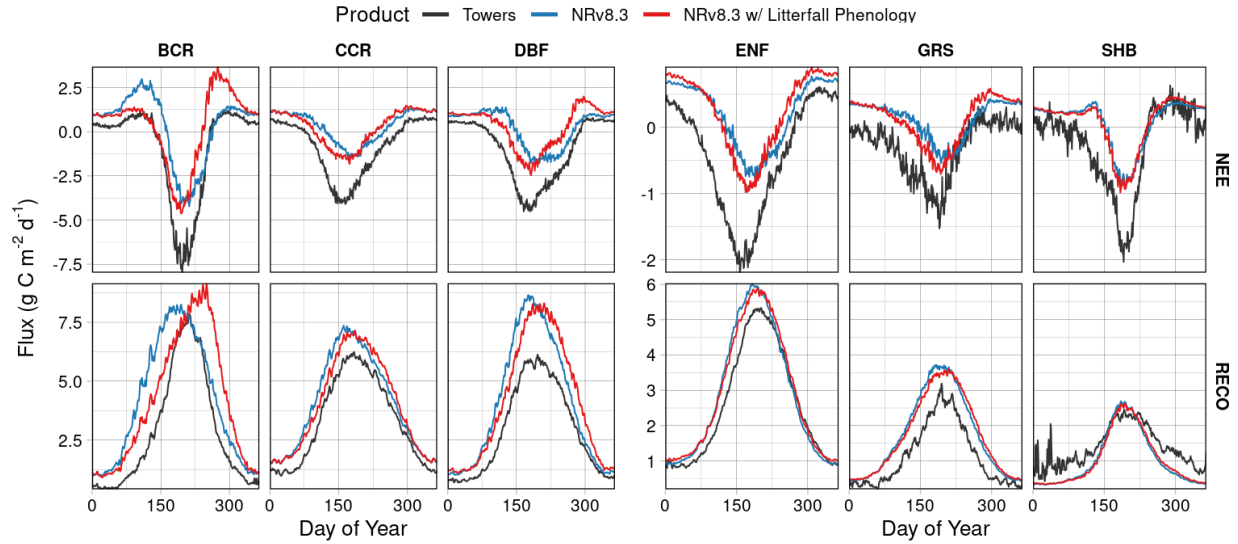


Figure S3: NEE and RECO seasonal cycles at each EC flux tower site in each PFT group, as modeled in the NRv8.3 + Litterfall Phenology experiment.

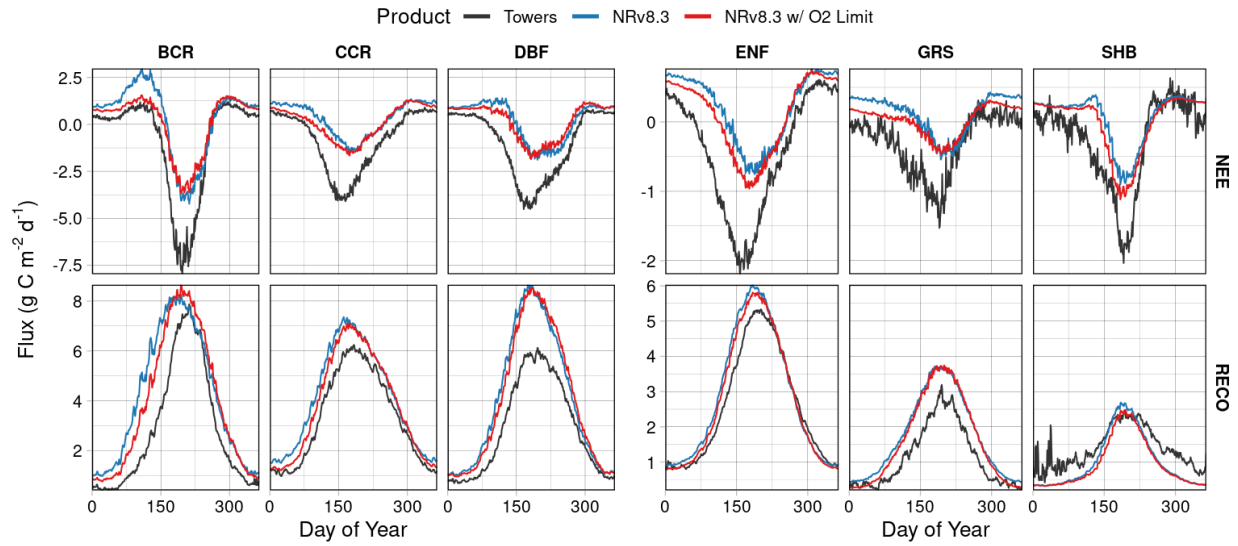


Figure S4: NEE and RECO seasonal cycles at each EC flux tower site in each PFT group, as modeled in the NRv8.3 + O2 Limit experiment.

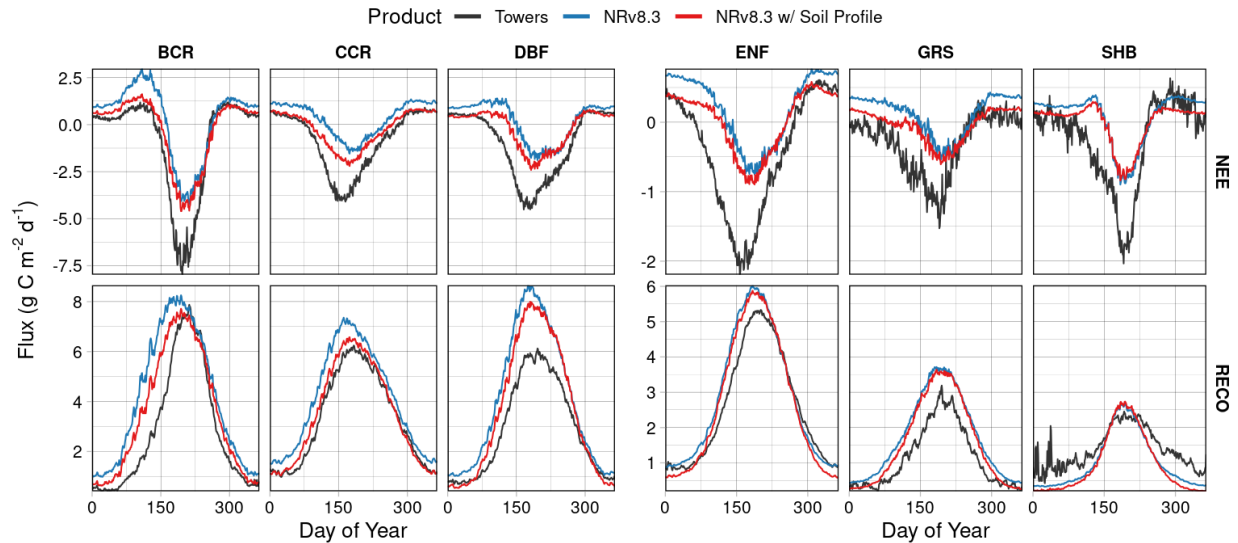


Figure S5: NEE and RECO seasonal cycles at each EC flux tower site in each PFT group, as modeled in the NRv8.3 + Soil Profile experiment.

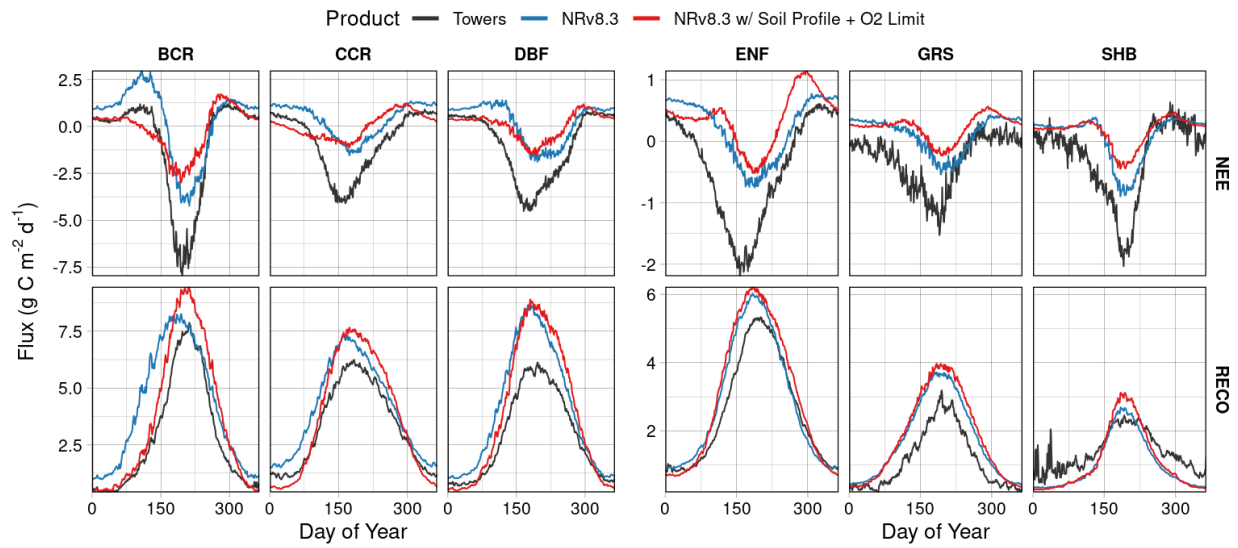


Figure S6: NEE and RECO seasonal cycles at each EC flux tower site in each PFT group, as modeled in the NRv8.3 + Soil Profile + O₂ Limit experiment.

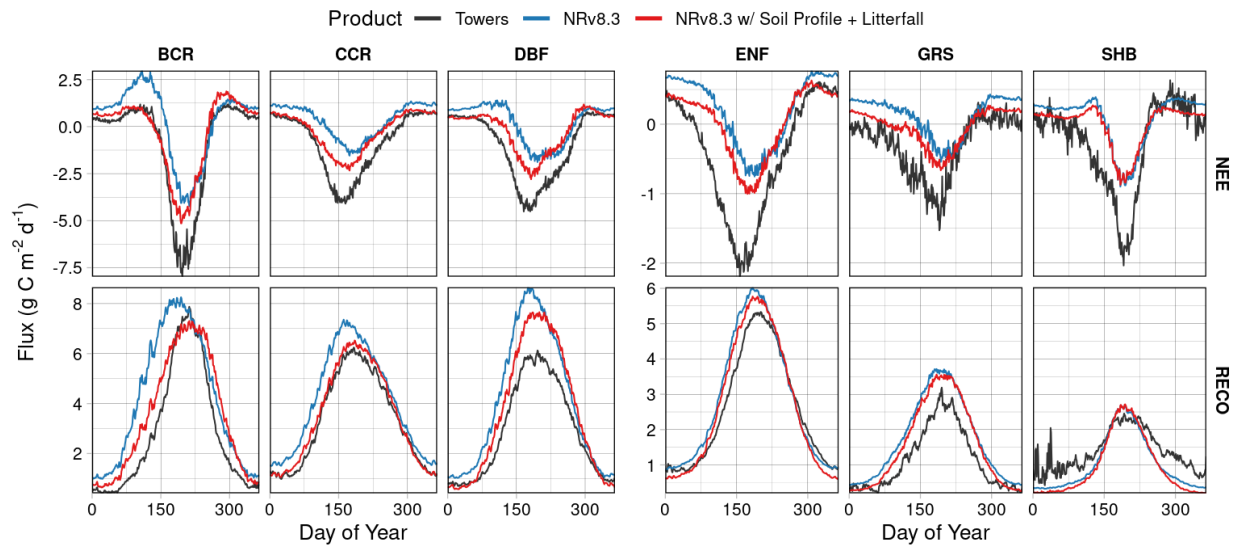


Figure S7: NEE and RECO seasonal cycles at each EC flux tower site in each PFT group, as modeled in the NRv8.3 + Soil Profile + Litterfall experiment.

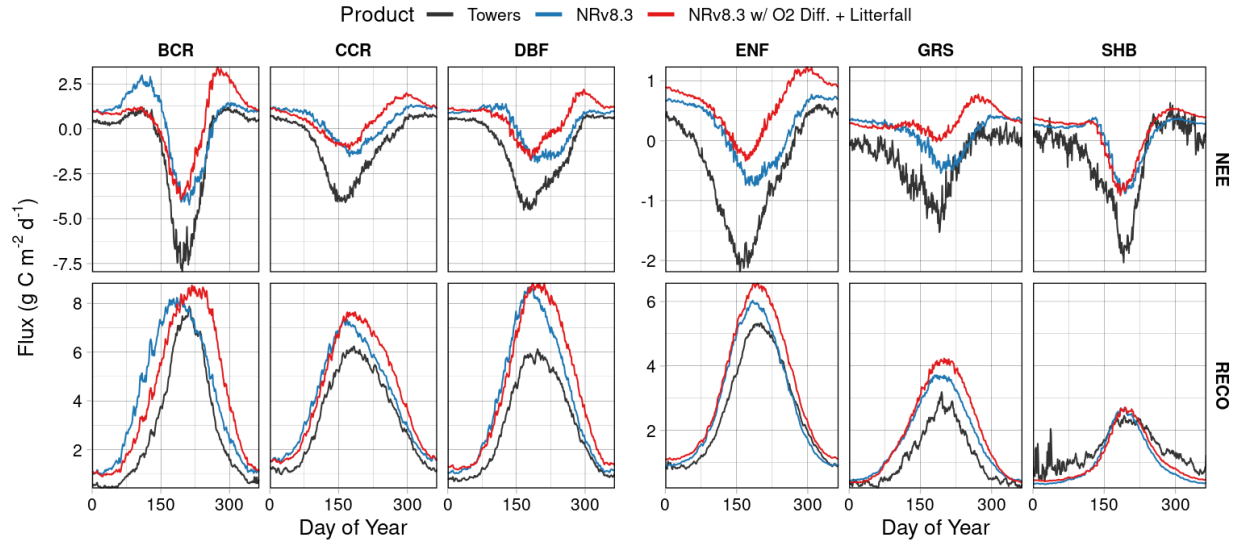


Figure S8: NEE and RECO seasonal cycles at each EC flux tower site in each PFT group, as modeled in the NRv8.3 + O2 Limit + Litterfall experiment.

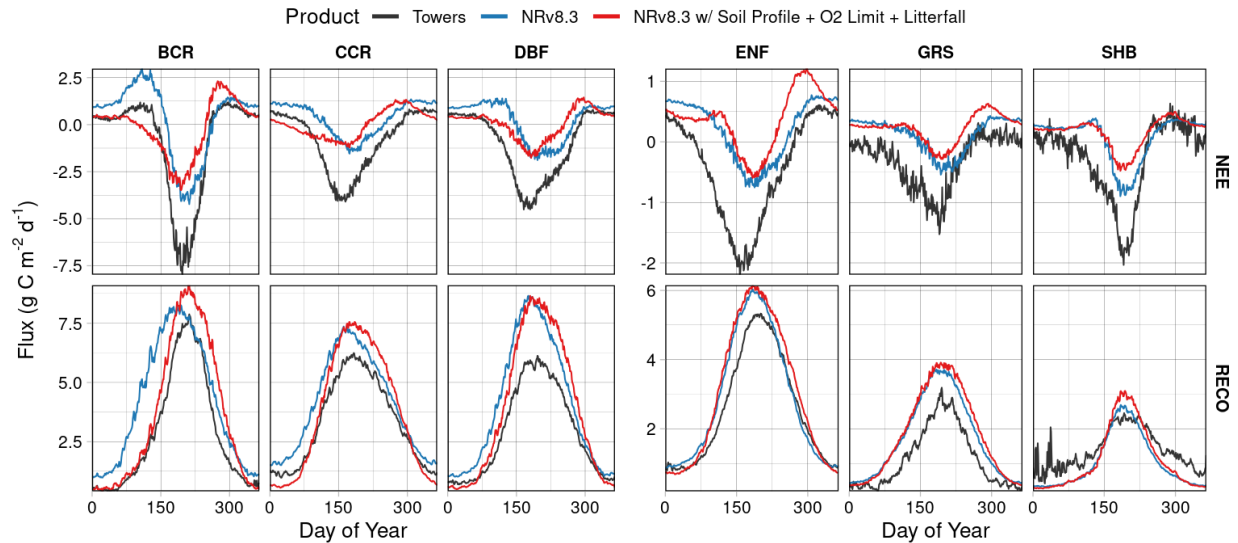


Figure S9: NEE and RECO seasonal cycles at each EC flux tower site in each PFT group, as modeled in the NRv8.3 + Soil Profile + O2 Limit + Litterfall experiment.

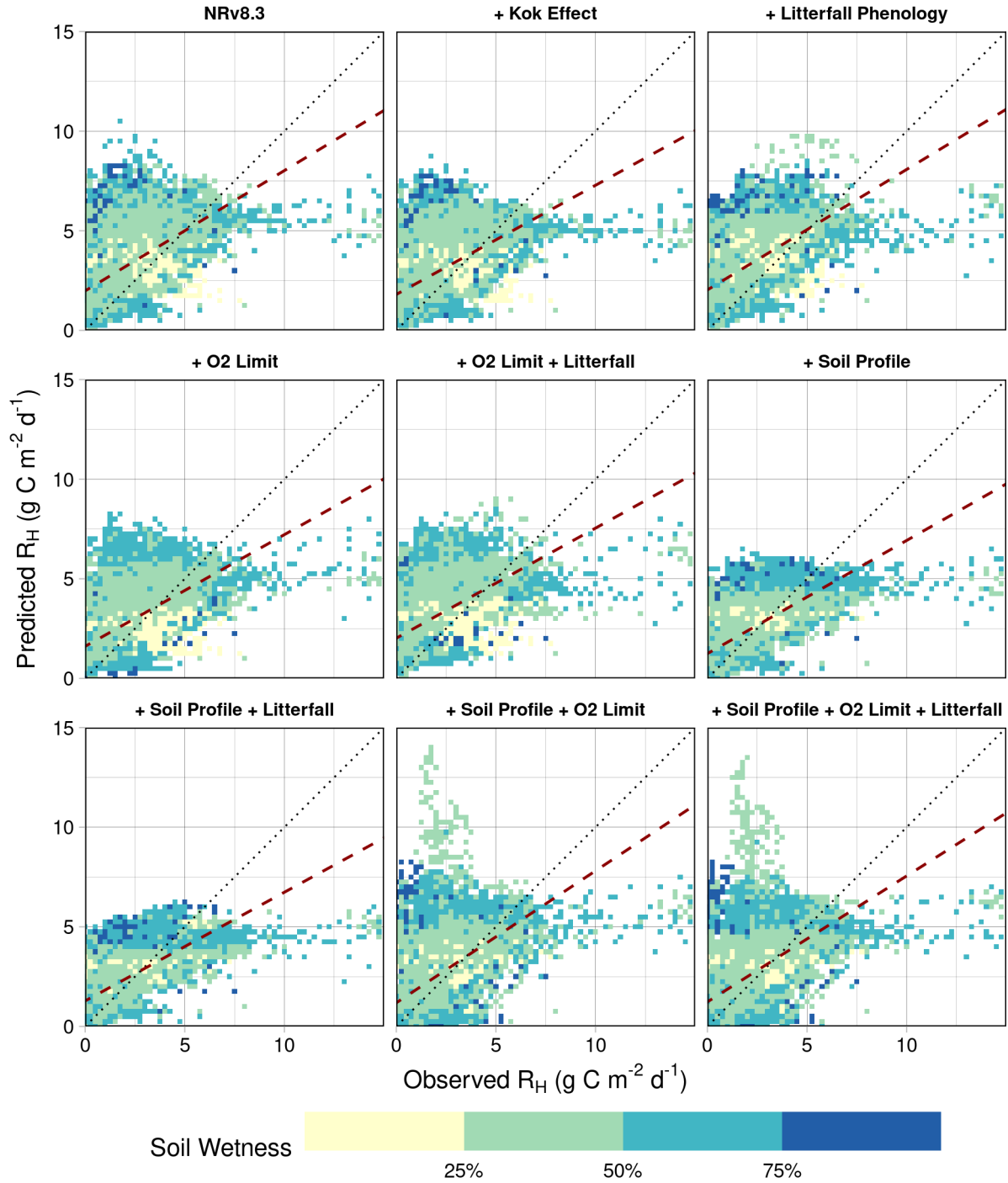


Figure S10: Predicted (modeled) RECO versus observed RECO at COSORE sites for each experiment, for all COSORE sites within an eddy covariance tower footprint or with independent driver data. Soil wetness and R_H are averaged within bins of $0.25\ g\ C\ m^{-2}\ d^{-1}$. Dotted line is the 1:1 line; red dashed line is the line of best fit.

Change in residual RECO versus NRv8.3: NRv8.3 + Kok Effect

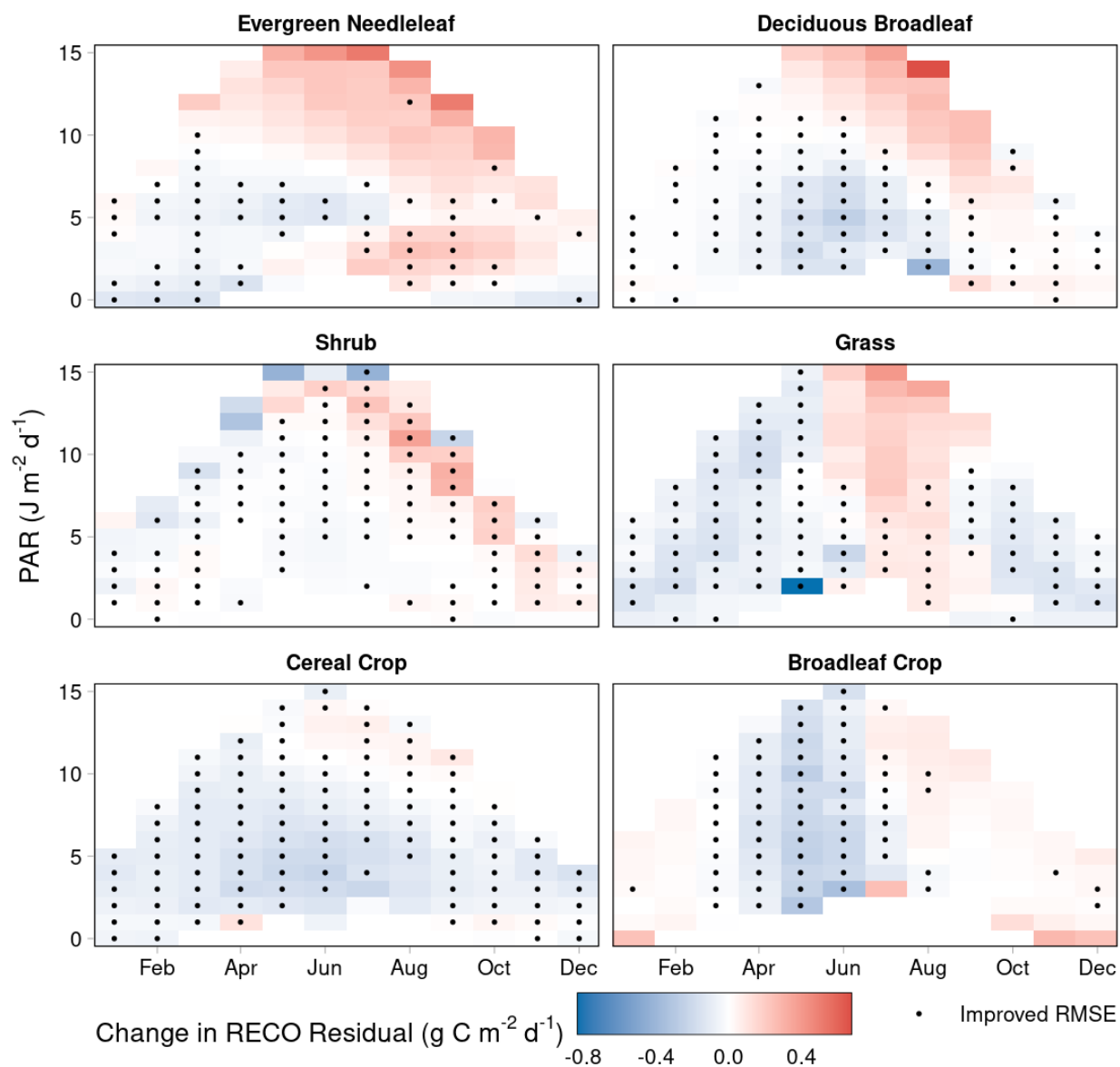


Figure S11: Change in modeled RECO residuals between NRv8.3 and the NRv8.3 + Kok Effect experiment (NRv8.3 minus experiment) for each PFT; shown as mean change in residual for each bin of PAR values by month. A black dot indicates that the change in RECO residual represents an improvement; i.e., a decrease in a high-biased RECO residual or an increase in a low-biased RECO residual.

Change in residual RECO versus NRv8.3: NRv8.3 + Litterfall Phenology

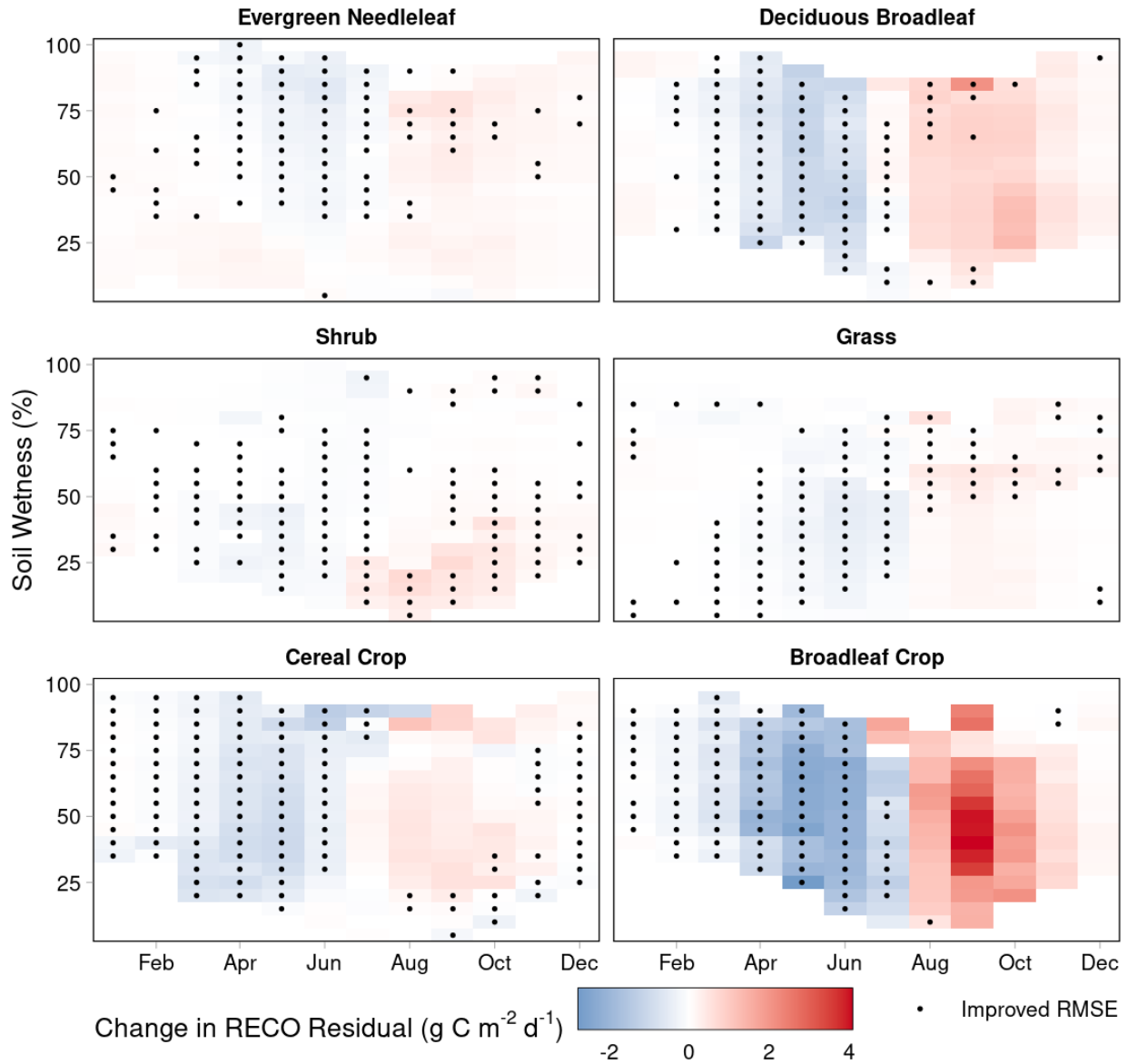


Figure S12: Change in modeled RECO residuals between NRv8.3 and the NRv8.3 + Litterfall Phenology experiment (NRv8.3 minus experiment) for each PFT; shown as mean change in residual for each bin of soil moisture values by month. A black dot indicates that the change in RECO residual represents an improvement; i.e., a decrease in a high-biased RECO residual or an increase in a low-biased RECO residual.

Change in residual RECO versus NRv8.3: NRv8.3 + O2 Limit

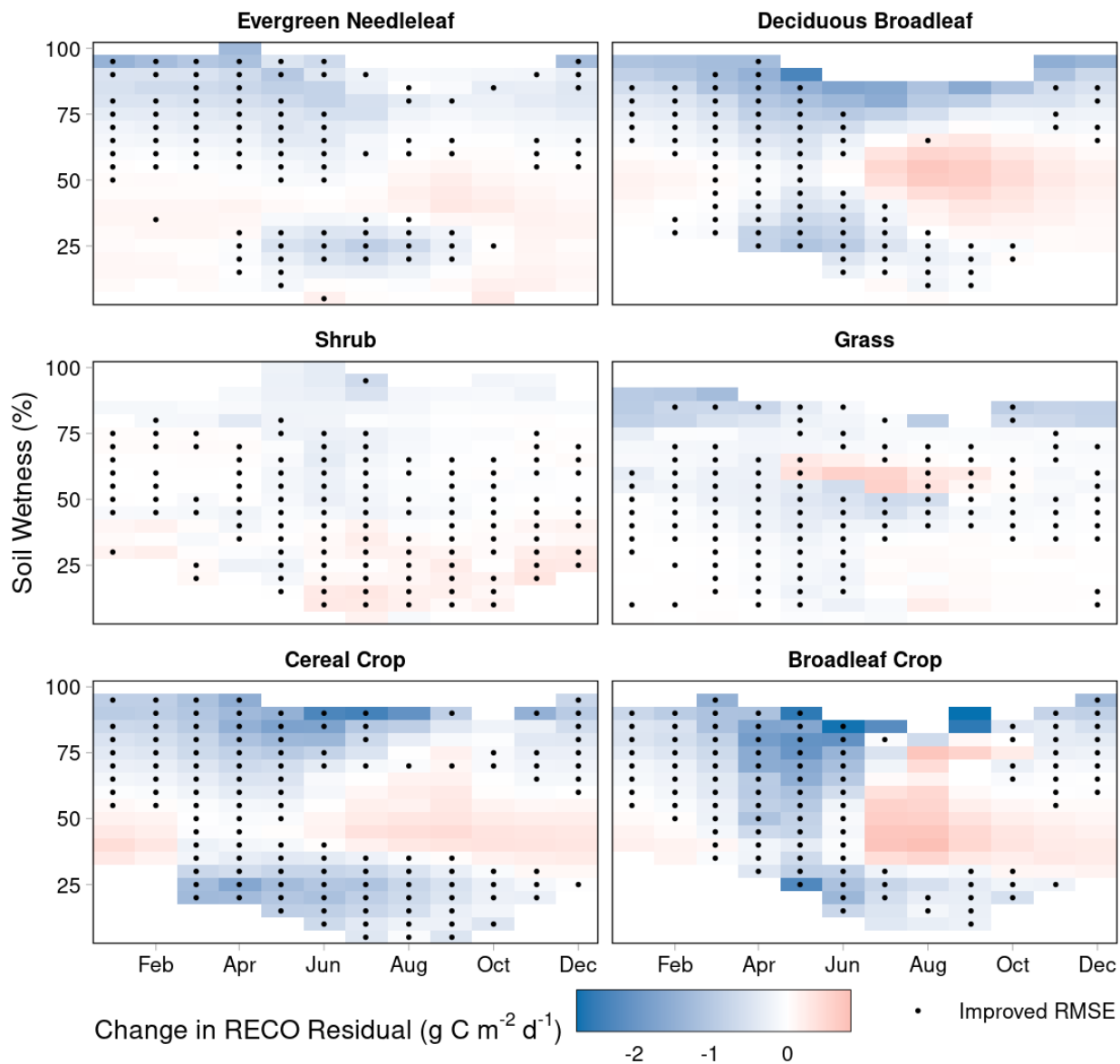


Figure S13: Change in modeled RECO residuals between NRv8.3 and the NRv8.3 + O2 Limit experiment (NRv8.3 minus experiment) for each PFT; shown as mean change in residual for each bin of soil moisture values by month. A black dot indicates that the change in RECO residual represents an improvement; i.e., a decrease in a high-biased RECO residual or an increase in a low-biased RECO residual.

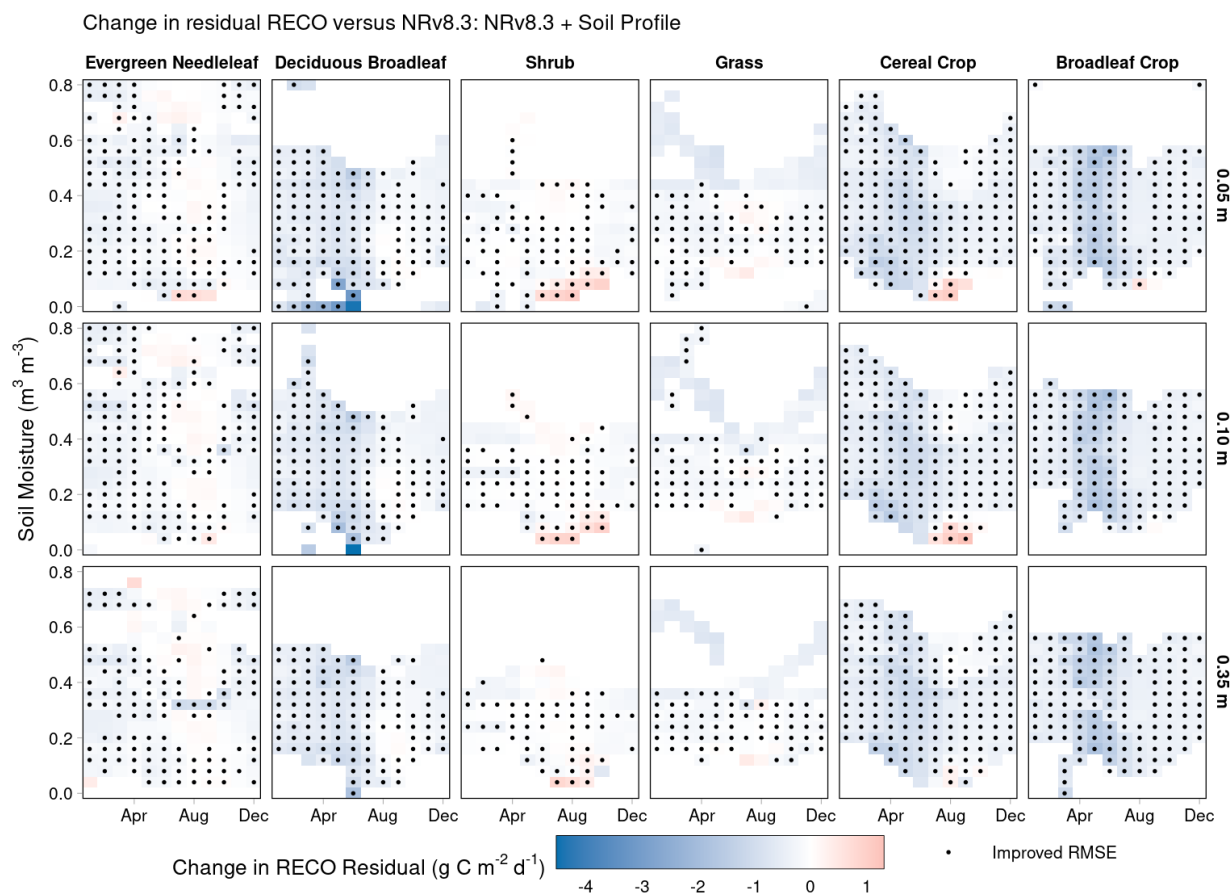


Figure S14: Change in modeled RECO residuals between NRv8.3 and the NRv8.3 + Soil Profile (NRv8.3 minus experiment) for each PFT and each soil layer; shown as mean change in residual for each bin of soil moisture values by month. A black dot indicates that the change in RECO residual represents an improvement; i.e., a decrease in a high-biased RECO residual or an increase in a low-biased RECO residual.

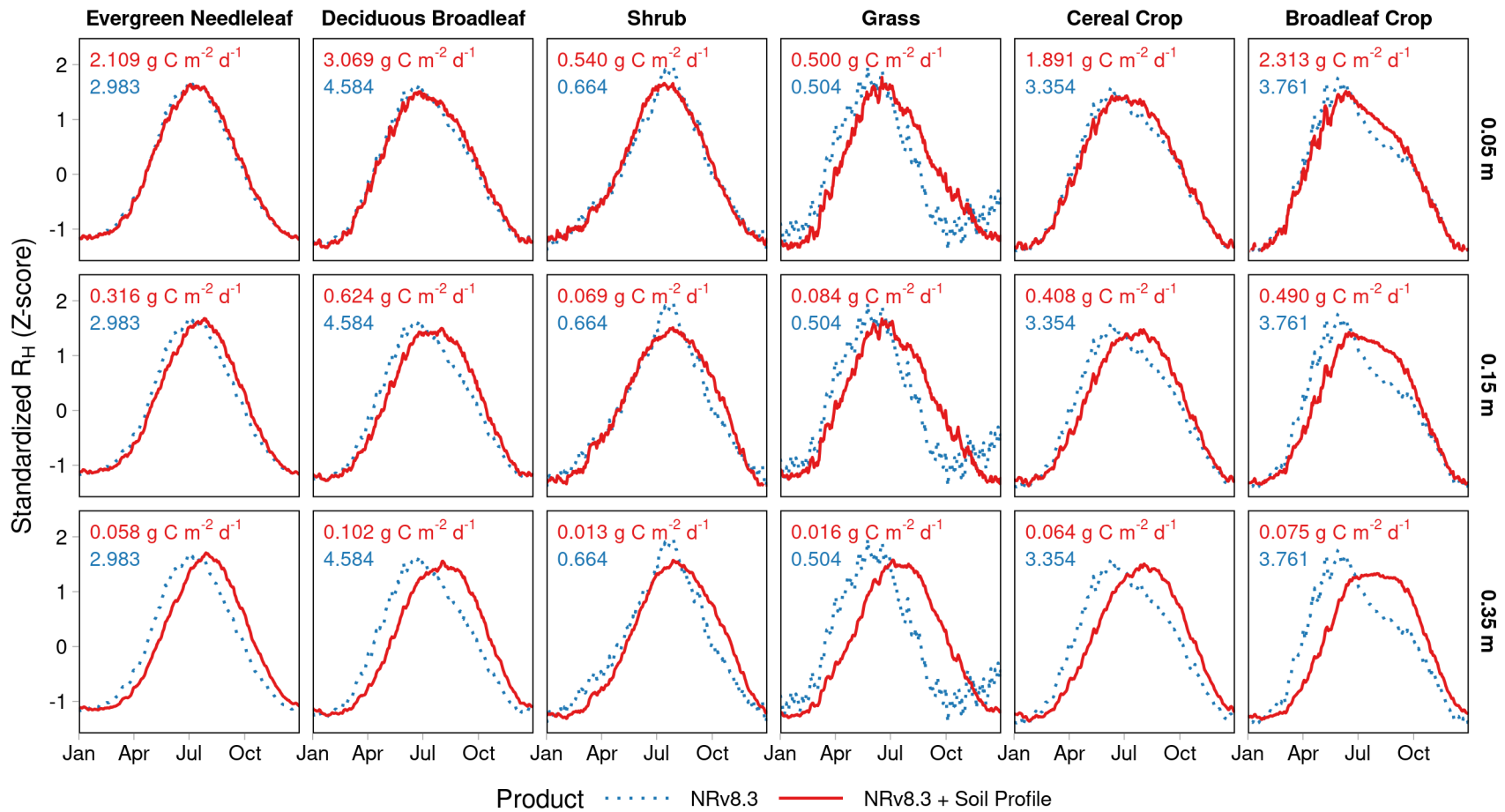


Figure S15: For each PFT, the normalized, mean seasonal cycle of R_H for NRv8.3 and mean seasonal cycle of R_H by depth for the NRv8.3 + Soil Profile experiment. The seasonal amplitude, in carbon units, for both NRv8.3 (blue, dotted line) and NRv8.3 + Soil Profile (red, solid line) are shown in the upper-left of each subplot. Note that the NRv8.3 results are not vertically stratified and therefore do not change across the rows, i.e., they are shown for reference in each soil layer but do not correspond to any single soil layer.

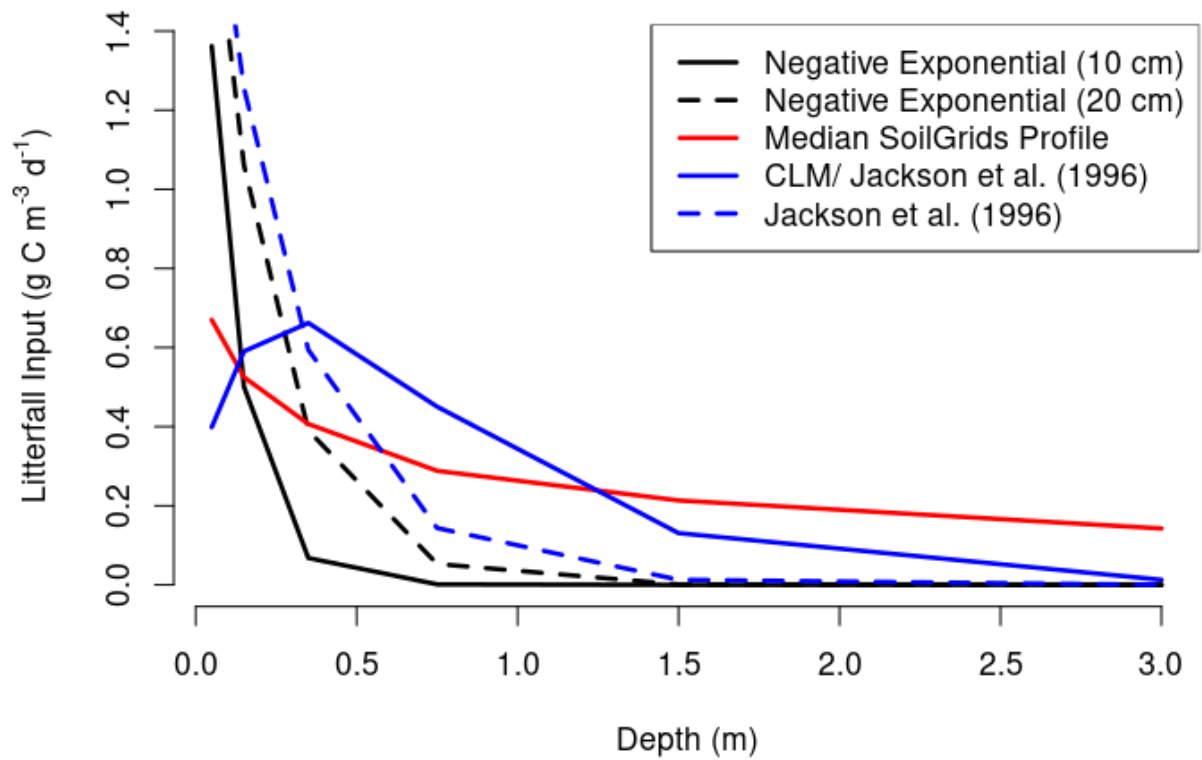


Figure S16: Litterfall input distribution functions, based on the NRv8.3 average daily litterfall (fraction of annual NPP sum). The median SoilGrids profile is from the global SoilGrids 250m product. The CLM/ Jackson et al. (1996) function is described in Lawrence et al. [2018], Equation 2.11.1.

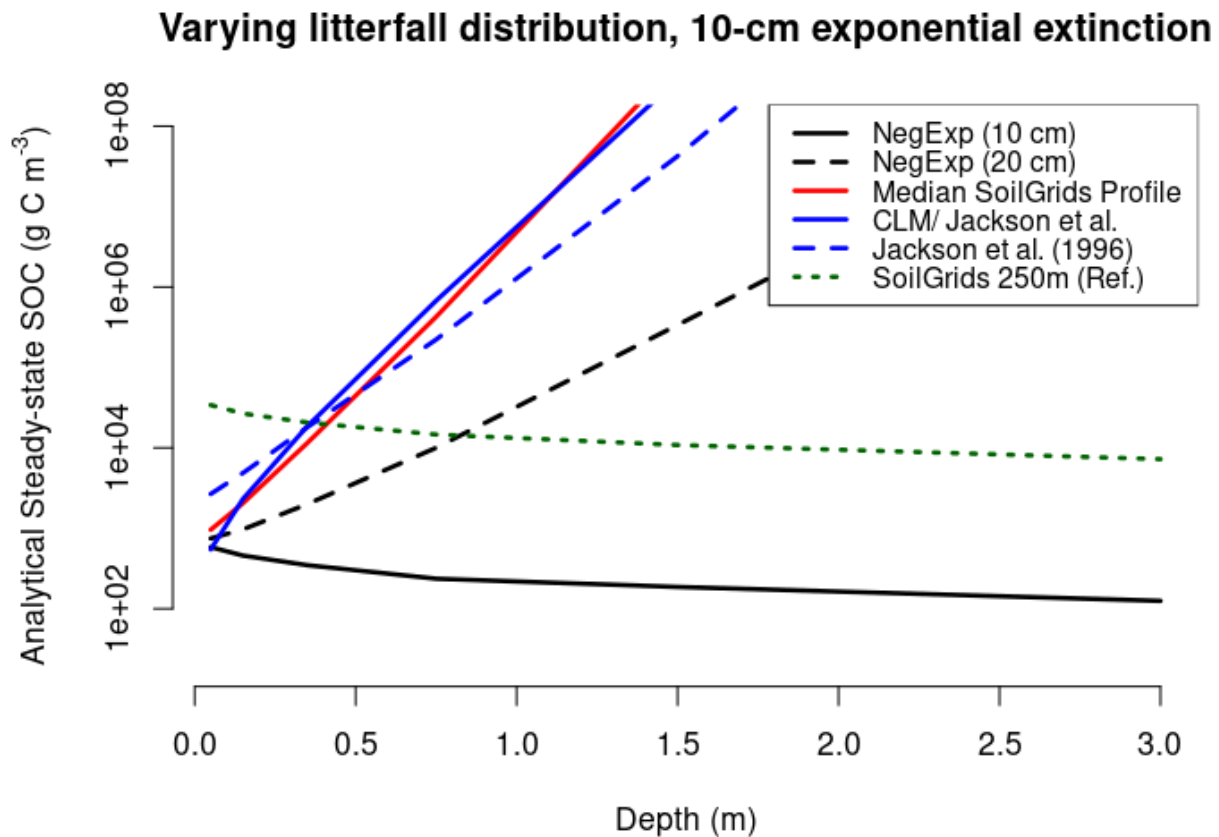


Figure S17: The analytical steady-state soil organic carbon (SOC) distribution, by depth, based on different litterfall input distribution functions and using a negative-exponential extinction function for heterotrophic respiration. The dotted, green line shows the reference SoilGrids 250m SOC profile.

Varying litterfall distribution, exponential extinction

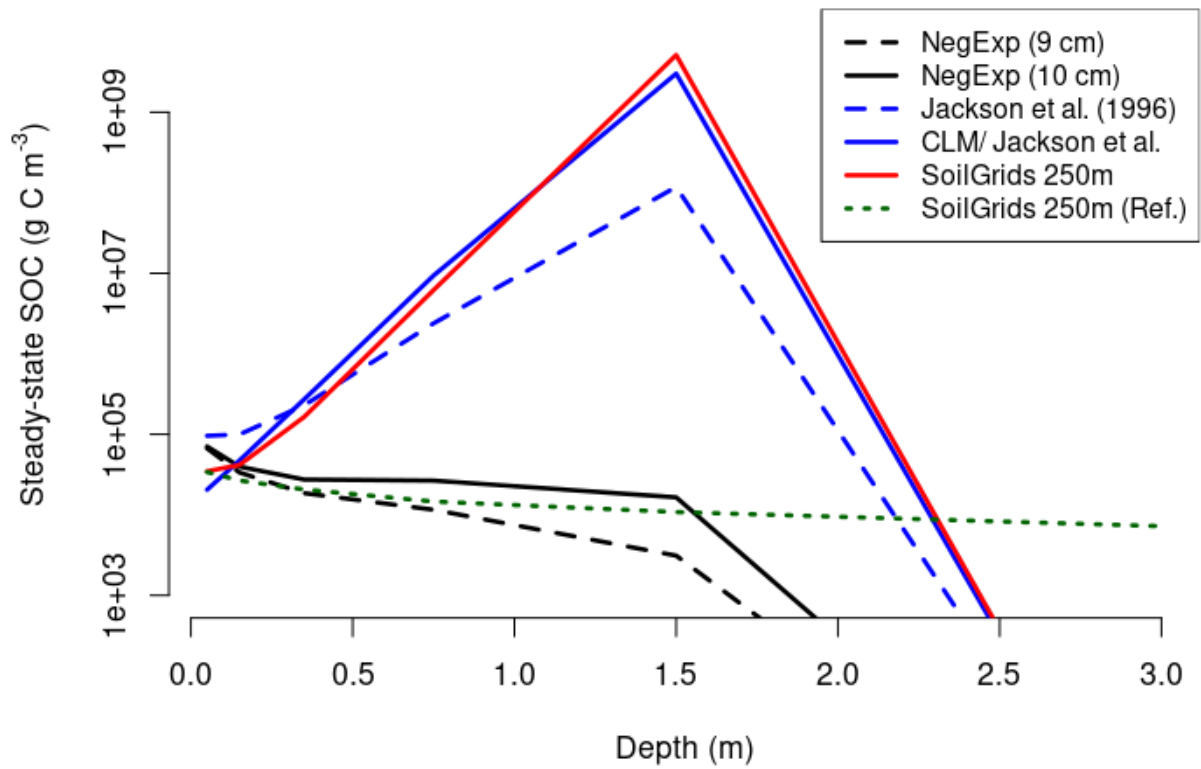


Figure S18: The numerical (final) steady-state soil organic carbon (SOC) distribution, by depth, based on different litterfall input distribution functions and using a negative-exponential extinction function for heterotrophic respiration. The dotted, green line shows the reference SoilGrids 250m SOC profile.

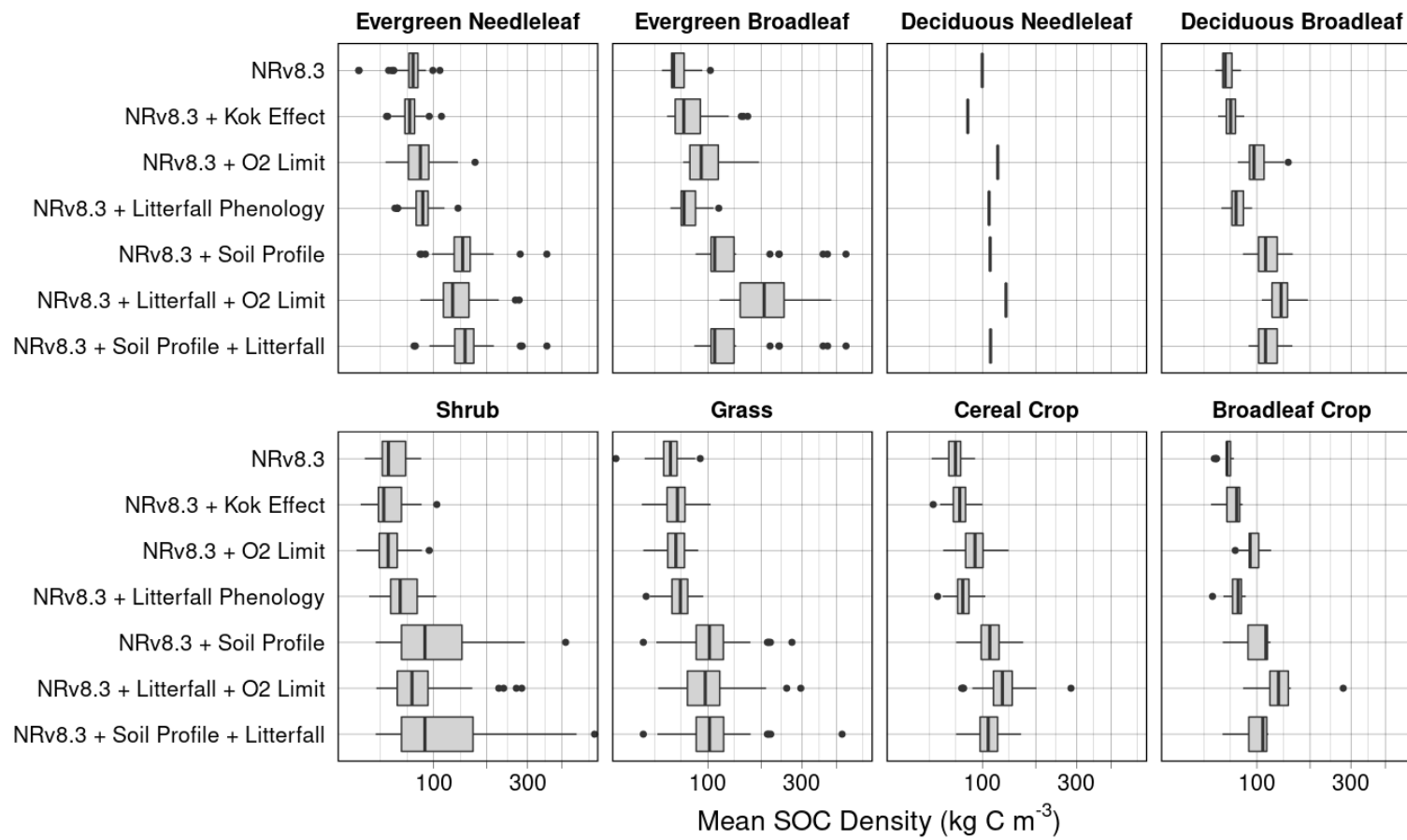


Figure S19: Total soil organic carbon (SOC) content distribution for each experiment, across all sites and all dates.

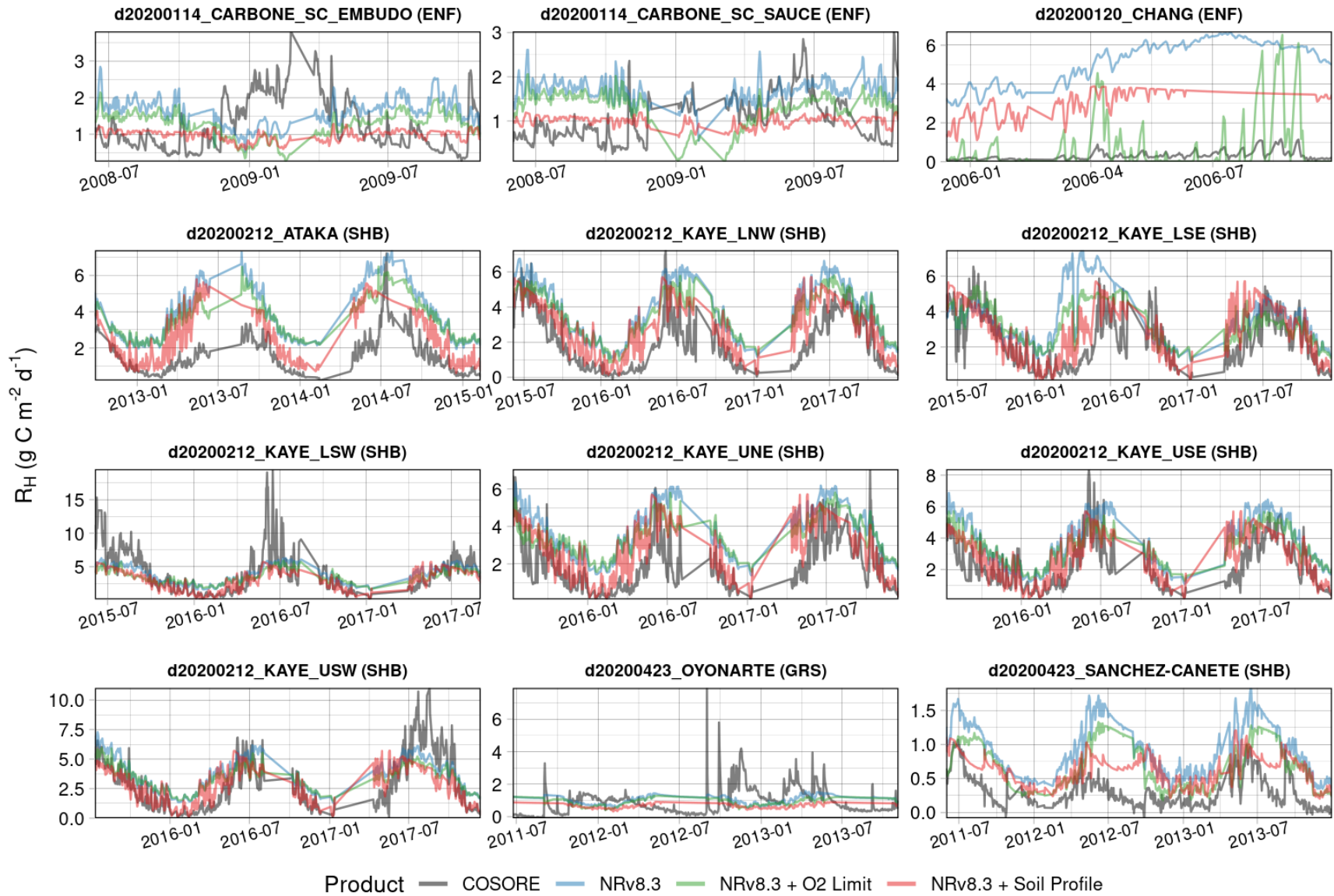


Figure S20: Observed (COSORE) or modeled R_H flux for select experiments, showing only those date ranges wherein COSORE data are available. Of the single-factor experiments, NRv8.3 + Litterfall Phenology is not shown because its dynamics are very similar to NRv8.3.

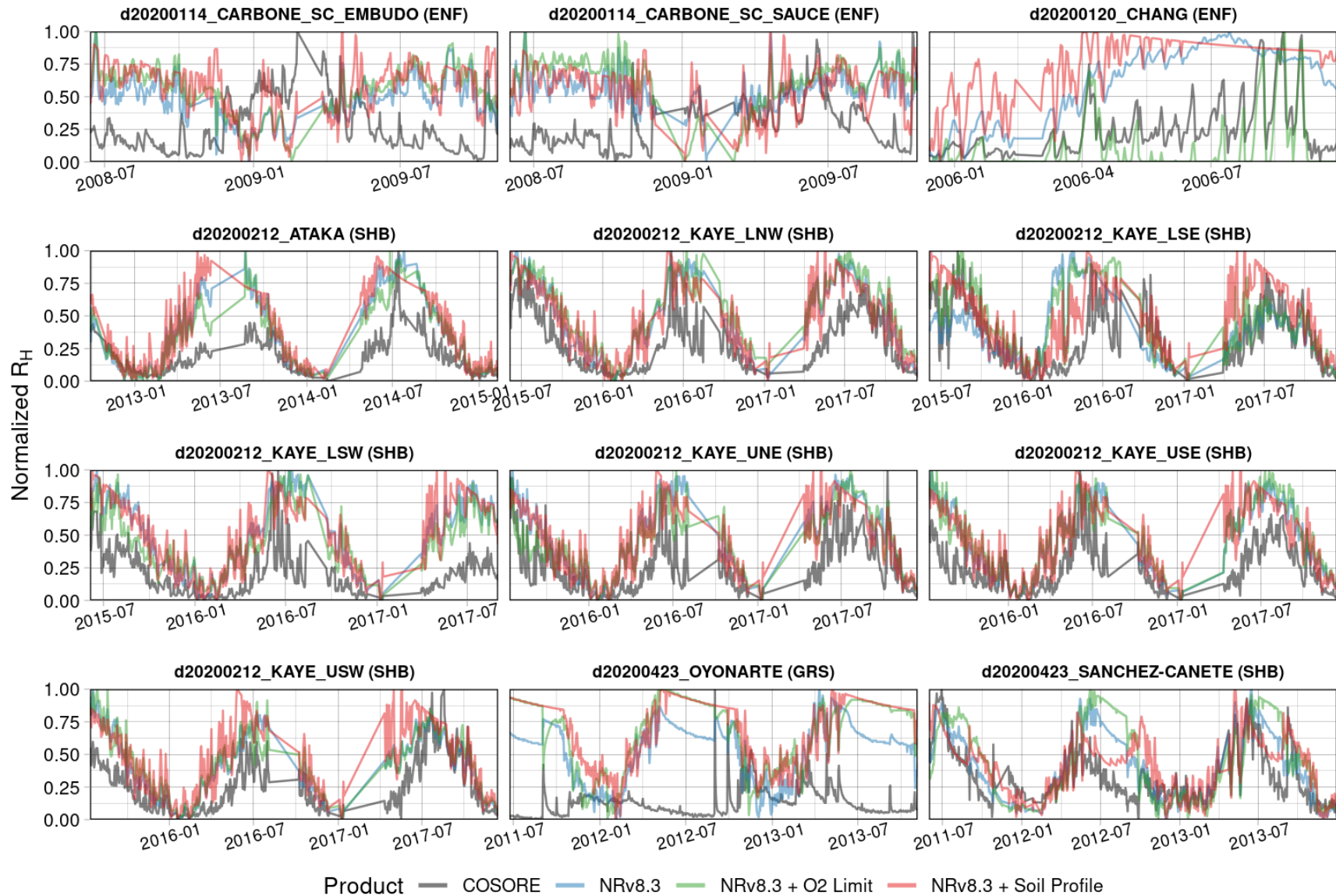


Figure S21: Observed (COSORE) or modeled R_H flux, normalized by each site and product's range in values, for select experiments, showing only those date ranges wherein COSORE data are available. Of the single-factor experiments, NRv8.3 + Litterfall Phenology is not shown because its dynamics are very similar to NRv8.3.

References

- R. G. Allen, L. S. Pereira, D. Raes, and M. Smith. Crop evapotranspiration - Guidelines for computing crop water requirements. Technical report, FAO - Food and Agriculture Organization of the United Nations, Rome, Italy, 1998.
- M. A. Arain. AmeriFlux CA-TP3 Ontario - Turkey Point 1974 Plantation White Pine, 2018.
- M. Ataka, Y. Kominami, K. Yoshimura, T. Miyama, M. Jomura, and M. Tani. In Situ CO₂ Efflux from Leaf Litter Layer Showed Large Temporal Variation Induced by Rapid Wetting and Drying Cycle. *PLoS ONE*, 9(10):e108404, oct 2014. ISSN 1932-6203. doi: 10.1371/journal.pone.0108404. URL <https://dx.plos.org/10.1371/journal.pone.0108404>.
- D. Baldocchi, J. Tang, and L. Xu. How switches and lags in biophysical regulators affect spatial-temporal variation of soil respiration in an oak-grass savanna. *Journal of Geophysical Research: Biogeosciences*, 111(G2):n/a–n/a, jun 2006. ISSN 01480227. doi: 10.1029/2005JG000063. URL <http://doi.wiley.com/10.1029/2005JG000063>.
- V. Balland, J. A. P. Pollacco, and P. A. Arp. Modeling soil hydraulic properties for a wide range of soil conditions. *Ecological Modelling*, 219(3-4):300–316, dec 2008. ISSN 03043800. doi: 10.1016/j.ecolmodel.2008.07.009. URL <https://linkinghub.elsevier.com/retrieve/pii/S0304380008003505>.
- M. S. Carbone, C. J. Still, A. R. Ambrose, T. E. Dawson, A. P. Williams, C. M. Boot, S. M. Schaeffer, and J. P. Schimel. Seasonal and episodic moisture controls on plant and microbial contributions to soil respiration. *Oecologia*, 167(1):265–278, sep 2011. ISSN 0029-8549. doi: 10.1007/s00442-011-1975-3. URL <http://link.springer.com/10.1007/s00442-011-1975-3>.
- M. S. Carbone, A. Park Williams, A. R. Ambrose, C. M. Boot, E. S. Bradley, T. E. Dawson, S. M. Schaeffer, J. P. Schimel, and C. J. Still. Cloud shading and fog drip influence the metabolism of a coastal pine ecosystem. *Global Change Biology*, 19(2):484–497, feb 2013. ISSN 13541013. doi: 10.1111/gcb.12054. URL <https://onlinelibrary.wiley.com/doi/10.1111/gcb.12054>.
- S.-C. Chang, K.-H. Tseng, Y.-J. Hsia, C.-P. Wang, and J.-T. Wu. Soil respiration in a subtropical montane cloud forest in Taiwan. *Agricultural and Forest Meteorology*, 148(5):788–798, may 2008. ISSN 01681923. doi: 10.1016/j.agrformet.2008.01.003. URL <https://linkinghub.elsevier.com/retrieve/pii/S0168192308000026>.
- R. B. Clapp and G. M. Hornberger. Empirical equations for some soil hydraulic properties. *Water Resources Research*, 14(4):601–604, 1978. ISSN 19447973. doi: 10.1029/WR014i004p00601.
- B. J. Cosby, G. M. Hornberger, R. B. Clapp, and T. R. Ginn. A statistical exploration of the relationships of soil moisture characteristics to the physical properties of soils. *Water Resources Research*, 20(6):682–690, 1984. ISSN 19447973. doi: 10.1029/WR020i006p00682.

- P. S. Curtis, C. S. Vogel, C. M. Gough, H. P. Schmid, H.-B. Su, and B. D. Bovard. Respiratory carbon losses and the carbon-use efficiency of a northern hardwood forest, 1999–2003. *New Phytologist*, 167(2):437–456, aug 2005. ISSN 0028-646X. doi: 10.1111/j.1469-8137.2005.01438.x. URL <https://onlinelibrary.wiley.com/doi/10.1111/j.1469-8137.2005.01438.x>.
- M. Decker and X. Zeng. An empirical formulation of soil ice fraction based on in situ observations. *Geophysical Research Letters*, 33(5):2–5, 2006. ISSN 00948276. doi: 10.1029/2005GL024914.
- M. Detto, G. Bohrer, J. Nietz, K. Maurer, C. Vogel, C. Gough, and P. Curtis. Multivariate Conditional Granger Causality Analysis for Lagged Response of Soil Respiration in a Temperate Forest. *Entropy*, 15(12):4266–4284, oct 2013. ISSN 1099-4300. doi: 10.3390/e15104266. URL <http://www.mdpi.com/1099-4300/15/10/4266>.
- D. Gaumont-Guay, T. A. Black, A. G. Barr, T. J. Griffis, R. S. Jassal, P. Krishnan, N. Grant, and Z. Nestic. Eight years of forest-floor CO₂ exchange in a boreal black spruce forest: Spatial integration and long-term temporal trends. *Agricultural and Forest Meteorology*, 184:25–35, jan 2014. ISSN 01681923. doi: 10.1016/j.agrformet.2013.08.010. URL <https://linkinghub.elsevier.com/retrieve/pii/S0168192313002177>.
- R. B. Jackson, J. Canadell, J. R. Ehleringer, H. A. Mooney, O. E. Sala, and E. D. Schulze. A global analysis of root distributions for terrestrial biomes. *Oecologia*, 108:389–411, 1996.
- J. Järveoja, M. B. Nilsson, M. Gažovič, P. M. Crill, and M. Peichl. Partitioning of the net CO₂ exchange using an automated chamber system reveals plant phenology as key control of production and respiration fluxes in a boreal peatland. *Global Change Biology*, 24(8):3436–3451, 2018. ISSN 13652486. doi: 10.1111/gcb.14292.
- R. S. Jassal, T. A. Black, M. D. Novak, D. Gaumont-Guay, and Z. Nestic. Effect of soil water stress on soil respiration and its temperature sensitivity in an 18-year-old temperate Douglas-fir stand. *Global Change Biology*, 14(6):1305–1318, jun 2008. ISSN 13541013. doi: 10.1111/j.1365-2486.2008.01573.x. URL <https://onlinelibrary.wiley.com/doi/10.1111/j.1365-2486.2008.01573.x>.
- D. Lawrence, R. Fisher, C. Koven, K. Oleson, S. Swenson, M. Vertenstein, B. Andre, G. Bonan, B. Ghimire, L. van Kampenhout, D. Kennedy, E. Kluzek, P. L. Ryan Knox, F. Li, H. Li, D. Lombardozzi, Y. Lu, J. Perket, W. Riley, WilliamSacks, M. Shi, W. Wieder, and C. Xu. Technical Description of version 5.0 of the Community Land Model (CLM). Technical report, University Corporation for Atmospheric Research (UCAR), 2018. URL <https://escomp.github.io/ctsm-docs/versions/release-clm5.0/html/tech{ }note/index.html>.
- D. M. Lawrence, R. A. Fisher, C. D. Koven, K. W. Oleson, S. C. Swenson, G. B. Bonan, N. Collier, B. Ghimire, L. Kampenhout, D. Kennedy, E. Kluzek, P. J. Lawrence, F. Li, H. Li, D. Lombardozzi, W. J. Riley, W. J. Sacks, M. Shi, M. Vertenstein, W. R. Wieder, C. Xu, A. A. Ali, A. M. Badger, G. Bisht, M. Broeke, M. A. Brunke, S. P. Burns, J. Buzan, M. Clark, A. Craig, K. Dahlin, B. Drewniak, J. B. Fisher, M. Flanner, A. M. Fox, P. Gentine, F. Hoffman, G. Keppel-Aleks, R. Knox, S. Kumar, J. Lenaerts, L. R. Leung,

- W. H. Lipscomb, Y. Lu, A. Pandey, J. D. Pelletier, J. Perket, J. T. Randerson, D. M. Ricciuto, B. M. Sanderson, A. Slater, Z. M. Subin, J. Tang, R. Q. Thomas, M. Val Martin, X. Zeng, and ... The Community Land Model version 5: Description of new features, benchmarking, and impact of forcing uncertainty. *Journal of Advances in Modeling Earth Systems*, 11(12):4245–4287, dec 2019. ISSN 1942-2466. doi: 10.1029/2018MS001583. URL <https://onlinelibrary.wiley.com/doi/abs/10.1029/2018MS001583>.
- Q. Mu, M. Zhao, and S. W. Running. Improvements to a MODIS global terrestrial evapotranspiration algorithm. *Remote Sensing of Environment*, 115(8):1781–1800, 2011. ISSN 00344257. doi: 10.1016/j.rse.2011.02.019. URL <http://dx.doi.org/10.1016/j.rse.2011.02.019>.
- A. Noormets, M. J. Gavazzi, S. G. McNulty, J.-C. Domec, G. Sun, J. S. King, and J. Chen. Response of carbon fluxes to drought in a coastal plain loblolly pine forest. *Global Change Biology*, 16(1):272–287, jan 2010. ISSN 13541013. doi: 10.1111/j.1365-2486.2009.01928.x. URL <https://onlinelibrary.wiley.com/doi/10.1111/j.1365-2486.2009.01928.x>.
- K. Oleson, D. M. Lawrence, G. B. Bonan, B. Drewniak, M. Huang, C. D. Koven, S. Levis, F. Li, W. J. Riley, Z. M. Subin, S. Swenson, P. E. Thornton, A. Bozbiyik, R. Fisher, C. L. Heald, E. Kluzek, J.-F. Lamarque, P. J. Lawrence, L. R. Leung, W. Lipscomb, S. P. Muszala, D. M. Ricciuto, W. J. Sacks, Y. Sun, J. Tang, and Z.-L. Yang. Technical description of version 4.5 of the Community Land Model (CLM). Technical report, 2013.
- E. P. Sánchez-Cañete, C. Oyonarte, P. Serrano-Ortiz, J. Curiel Yuste, O. Pérez-Priego, F. Domingo, and A. S. Kowalski. Winds induce CO₂ exchange with the atmosphere and vadose zone transport in a karstic ecosystem. *Journal of Geophysical Research: Biogeosciences*, 121(8):2049–2063, aug 2016. ISSN 21698953. doi: 10.1002/2016JG003500. URL <http://doi.wiley.com/10.1002/2016JG003500>.
- UCAR. The Community Terrestrial Systems Model, 2020. URL <https://github.com/ESCOMP/CTSM>.
- M. Ueyama, K. Yoshikawa, and K. Takagi. A cool-temperate young larch plantation as a net methane source - A 4-year continuous hyperbolic relaxed eddy accumulation and chamber measurements. *Atmospheric Environment*, 184:110–120, jul 2018. ISSN 13522310. doi: 10.1016/j.atmosenv.2018.04.025. URL <https://linkinghub.elsevier.com/retrieve/pii/S1352231018302565>.
- R. Vargas, E. Sánchez-Cañete P, P. Serrano-Ortiz, J. Curiel Yuste, F. Domingo, A. López-Ballesteros, and C. Oyonarte. Hot-Moments of Soil CO₂ Efflux in a Water-Limited Grassland. *Soil Systems*, 2(3):47, aug 2018. ISSN 2571-8789. doi: 10.3390/soilsystems2030047. URL <http://www.mdpi.com/2571-8789/2/3/47>.
- A. Verhoef and G. Egea. Modeling plant transpiration under limited soil water: Comparison of different plant and soil hydraulic parameterizations and preliminary implications for their use in land surface models. *Agricultural and Forest Meteorology*, 191:22–32, 2014. ISSN 01681923. doi: 10.1016/j.agrformet.2014.02.009. URL <http://dx.doi.org/10.1016/j.agrformet.2014.02.009>.

Q. Zhang, R. P. Phillips, S. Manzoni, R. L. Scott, A. C. Oishi, A. Finzi, E. Daly, R. Vargas, and K. A. Novick. Changes in photosynthesis and soil moisture drive the seasonal soil respiration-temperature hysteresis relationship. *Agricultural and Forest Meteorology*, 259: 184–195, sep 2018. ISSN 01681923. doi: 10.1016/j.agrformet.2018.05.005. URL <https://linkinghub.elsevier.com/retrieve/pii/S0168192318301515>.